# On the Coupling of Orbit and Attitude Determination of Satellite Formations from Atmospheric Drag

## Observability and Estimation Performance

Chaves Jimenez, Adolfo

**DOI**
10.4233/uuid:c333497d-05ac-422f-9688-31246a6fa7b1

**Publication date**
2020

**Document Version**
Final published version

**Citation (APA)**
Chaves Jimenez, A. (2020). *On the Coupling of Orbit and Attitude Determination of Satellite Formations from Atmospheric Drag: Observability and Estimation Performance*. [Dissertation (TU Delft), Delft University of Technology]. https://doi.org/10.4233/uuid:c333497d-05ac-422f-9688-31246a6fa7b1

# On the Coupling of Orbit and Attitude Determination of Satellite Formations from Atmospheric Drag

Observability and Estimation Performance

544941-L-bw-Jimenez
Processed on: 16-6-2020

# On the Coupling of Orbit and Attitude Determination of Satellite Formations from Atmospheric Drag

Observability and Estimation Performance

## Dissertation

for the purpose of obtaining the degree of doctor
at Delft University of Technology
by the authority of the Rector Magnificus Prof.dr.ir. T.H.J.J. van der Hagen,
chair of the Board of Doctorates
to be defended publicly on
Friday 26 of June 2020 at 10:00 o'clock

by


**Adolfo CHAVES JIMÉNEZ**

Licenciado en Ingeniería Electrónica,
Instituto Tecnológico de Costa Rica, Cartago, Costa Rica,
born in San Ramón, Costa Rica.

This dissertation has been approved by the promotor[s]

Promotor: Prof. Dr. E.K.A. Gill
Copromotor: Dr. J. Guo

Composition of the doctoral committee:

| | |
|---|---|
| Rector Magnificus, | chairperson |
| Prof. Dr. E.K.A. Gill | Delft University of Technology, promotor |
| Dr. J. Guo | Delft University of Technology, copromotor |
| | |
| *Independent members:* | |
| Prof. dr. A. Guerman | U. of Beira Interior, Portugal |
| Prof. dr. G. Zhu | York University, Canada |
| Prof. dr. M. Lavagna | Politecnico di Milano, Italy |
| Prof. dr. ir. H.A.P. Blom | Delft University of Technology |
| Prof. dr. L.L.A. Vermeersen | Delft University of Technology |

*Keywords:* Orbit attitude coupling, estimation, spacecraft relative dynamics, Observability Gramian, Extended Kalman Filter

*Printed by:* Ipskamp Printing, Enschede

*Front & Back:* Ipskamp Printing, Enschede



ISBN 978-94-028-2095-9

An electronic version of this dissertation is available at
http://repository.tudelft.nl

*Science is a wonderful thing*
*if one does not have to earn one's living at it.*

Albert Einstein

# Contents

# Summary

Spacecraft orbit and attitude dynamics have been classically seen as two separated subjects, since the effect of attitude in orbit dynamics was deemed too small to be considered, or simply, modeled as noise in the estimation process for most satellites.

In the eighties, a study by [1] showed that for a very large spacecraft, approximately the size of the International Space Station, the effect of the attitude in the orbit dynamics should be considered.

The advancement in miniaturization, communications, estimation, and control has created a new tendency: groups of small spacecraft achieving a mission that before was only possible with a large spacecraft, or even, enabling new possibilities that were not viable with a single spacecraft, such as constellations of more than a hundred spacecraft that monitor the Earth faster than ever before. In this case, the Planet Labs constellation is one of the best known examples, with the possibility of photographing any specific place on Earth within hours [2], something not possible with current single satellites. There are many examples of proposed distributed space systems (DSS) missions for technology demonstration with objectives ranging from Earth, planetary, solar or astrophysics science.

The increasing performance requirements had led engineers and scientist to apply Precise Orbit Determination (POD) approaches to comply with more rigorous mission requirements. However, despite the advancement in spacecraft relative dynamics (SRD) estimation methods, classically the assumption that relative spacecraft orbital and attitude dynamics are not coupled has been deemed accurate enough for most estimation and control purposes, due to the fact that the coupling effect is too small to affect the required accuracy of most missions.

Nevertheless, recent works are taking into account the joint representation of attitude and orbital dynamics for improved guidance, navigation and control performance, in order to use dynamics models that better represent the physical world.

This PhD research has the objective to establish and characterize an integrated approach to the estimation of orbit and attitude for satellite formations. Here, the impact of a sophisticated spacecraft relative dynamics model is treated theoretically and applied, taking into account the coupling between orbit and attitude dynamics on observability. As source of the dynamic coupling we consider the atmospheric drag, the largest non-gravitational effect affecting spacecraft trajectories in Low-Earth Orbit (LEO).

This thesis work aims to solve the question of whether the coupling influences the estimation of relative dynamics of spacecraft, by determining the effect of this phenomenon in a simulated scenario of two spacecraft flying in an along-track configuration, with an initial separation of 1000 km. Here, while the magnitude of the external areas of both spacecraft remains the same, the size of the spacecraft is changed ranging from volumes of 30x10x10 cm (3 units Cubesats) up to 240x40x40

cm. Orbit altitudes are changed from 300 km up to 700 km. Circular, equatorial orbits are used in the propagations.

Despite this limited scenario, this work provides a methodological framework that allows the application of this analysis to any formation flying scenario.

This is achieved first by using the Observability Gramian (OG). The OG is a method that determines the level of observability of linear time-variant systems. Using a linearization of the space-state equations describing the orbit and attitude absolute and relative states of two spacecraft, it is possible to determine the level of observability of different scenarios. Here it is shown that the coupling created by the atmospheric drag perturbation for spacecraft in low-Earth Orbit (LEO) enables full observability of the states which is not possible without such coupling, with the level of observability changing when the altitude or the spacecraft mechanical characteristics are changed. It is shown that full observability is achieved even for limited observability cases when only the relative position or the relative attitude of the spacecraft is known. These effects have been present in previous works, but the OG method enables the possibility to rank numerically different measurement scenarios. For this reason, the OG is a tool that may help spacecraft designers take decisions regarding type or location of sensors, for example, that may improve the performance of the selected estimation method.

Secondly, an Extended Kalman Filter (EKF) is used to show how the coupling between orbit and attitude dynamics caused by the atmospheric drag force and torque improves the estimation of relative dynamics of spacecraft, even when full observable scenarios are used. For this, an EKF that considers this coupling is applied. A second estimator, where the perturbation was simulated using only white-Gaussian noise, is used for comparison purposes, a common practice to simulate non-considered perturbations. In order to show that the ”coupled” estimator is better in any case that the ”uncoupled” estimator, the uncoupled estimator noise was varied up to the point of achieving the best possible estimation performance.

At a 300 km altitude orbit, the coupled estimator shows an improvement of 6.9 m in the average position estimation compared to the so called ”uncoupled” estimator for two 3-unit Cubesats flying in an along-track configuration. Even for altitudes up to 650 km, with two 240x40x40 cm Cubesats, the coupled estimator showed an improvement of 3.5 m in the average position estimation. At altitudes above 700 km, the differences between the two estimators are negligible.

The research methodologies used in this work make direct use of the nonlinear equations that describe the orbit and attitude absolute and relative dynamics of the system. For this reason, the methodology presented here may be expanded for the evaluation of any measurement scenario, any kind of orbit, from circular to highly elliptical, and any number of spacecraft. Therefore, there is a large area of future research in the subject of the evaluation of coupled orbit and attitude spacecraft dynamics for estimation purposes.

# Samenvatting

De baan- en attitude dynamica van ruimtevaartuigen worden normaal gesproken als afzonderlijke thema's gezien, omdat het effect van attitude in baandynamica te gering werd geacht om in overweging te nemen, of simpelweg als ruis werd gemodelleerd in het schattingsproces voor de meeste satellieten.

In de jaren tachtig liet onderzoek door [1] zien dat voor zeer grote ruimtevaartuigen, van grofweg het formaat van het International Space Station (ISS), het effect van attitude in baandynamica meegenomen zou moeten worden.

De vooruitgang in miniaturisering, communicatie, schatting en regelsystemen heeft tot een nieuwe tendens geleid: groepen van kleine ruimtevaartuigen die een missie volbrengen die voorheen alleen mogelijk was met een groot ruimtevaartuig, of sterker nog, nieuwe mogelijkheden creëren die niet haalbaar waren met één enkel ruimtevaartuig, zoals constellaties van meer dan honderd ruimtevaartuigen die sneller dan ooit de aarde monitoren. In dit geval is de Planet Labs constellatie één van de bekendste voorbeelden, met de mogelijkheid om binnen enkele uren [2] elke gewenste plek op aarde te fotograferen, iets dat niet mogelijk is met de huidige alleenstaande satellieten. Er zijn veel voorbeelden van voorgestelde Distributed Space Systems (DSS) missies voor technologiedemonstraties met variërende doelen; van aard- en zonnewetenschappen, planetaire wetenschappen tot astrofysica.

De toenemende prestatie-eisen heeft ingenieurs en wetenschapers geleid tot het toepassen van Precise Orbit Determination (POD) benaderingen om te voldoen aan meer rigoureuze missie-eisen. Echter, ondanks de vooruitgang in Spacecraft Relative Dynamics (SRD) schattingsmethodes, wordt de aanname dat de baan- en attitude dynamica niet gekoppeld zijn nauwkeurig genoeg geacht voor de meeste schattings- en regeldoeleinden. Reden voor deze aanname is dat het effect van de koppeling te gering is om de vereiste nauwkeurigheid bij een groot deel van de missies te beïnvloeden.

Desalniettemin wordt in recente studies de gezamenlijke representatie van baan- en attitude dynamica in beschouwing genomen als verbeterde besturing, navigatie en regelprestaties, om zo dynamische modellen te gebruiken die een betere afspiegeling vormen van de fysieke wereld.

Dit doctoraal onderzoek heeft als doel het vaststellen en karakteriseren van een geïntegreerde aanpak van de schatting van baan en attitude van sattelietformaties. Hier wordt de impact behandeld, zowel theoretisch als toegepast, van een verfijnd ruimtevaartuigmodel van relatieve dynamiek, met in acht neming van de koppeling tussen baan- en attitude dynamica in waarneembaarheid. Als bron van de dynamische koppeling wordt de luchtweerstand genomen, het grootste niet-gravitationele effect dat ruimtevaartuigen beïnvloedt in Low-Earh-Orbit (LEO).

Dit proefschrift heeft als doel de vraag te beantwoorden of de koppeling de schatting van relatieve dynamica in ruimtevaartuigen beïnvloedt, door het effect van dit fenomeen te bepalen in een gesimuleerd scenario van twee ruimtevaartuigen vliegend in een along-track configuratie met een initiële afstand van 1000 km. Terwijl het oppervlakte van beide ruimtevaartuigen hetzelfde blijft, wordt hier de grootte van de ruimtevaartuigen veranderd variërend van oppervlaktes van 30x10x10 cm (3-unit Cubesats) tot 240x40x40 cm. De hoogte varieert van 300 km tot 700 km. Circulaire, equatoriale banen worden in de propagatie gebruikt.

Ondanks het gelimiteerde scenario levert dit werk een methodologisch framework dat de toepassing van deze analyse toestaat op elk scenario van formatievlucht.

Dit wordt in eerste instantie bereikt door het gebruik van de Observability Gramian (OG). De OG is een methode die het niveau van waarneembaarheid van lineaire tijdsvariante systemen bepaalt. Door gebruik te maken van een linearisatie van de ruimtetoestandvergelijkingen waarmee de absolute en relatieve staat van baan en attitude van twee ruimtevaartuigen worden beschreven, is het mogelijk om het niveau van waarneembaarheid van verschillende scenario's te bepalen. Hier wordt aangetoond dat de koppeling gecreëerd door een stoornis in de luchtweerstand voor ruimtevaartuigen in LEO volledige waarneming van de toestand mogelijk maakt - iets dat niet mogelijk is zonder deze koppeling - met een veranderend niveau van waarneembaarheid als de hoogte of de mechanische karakteristieken van het ruimtevaartuig worden gewijzigd. Er wordt aangetoond dat zelfs bij gevallen met gelimiteerde waarneembaarheid een volledige waarneembaarheid wordt bereikt als alleen de relatieve positie of de relatieve attitude van het ruimtevaartuig bekend zijn. Deze effecten zijn in eerdere studies aanwezig geweest, maar de OG-methode maakt het mogelijk verschillende meetscenario's numeriek te rangschikken. Dit maakt dat de OG een instrument is dat ruimtevaartontwerpers zou kunnen helpen bij het nemen van beslissingen, over bijvoorbeeld het type of de locatie van sensoren, die de uitvoering van de geselecteerde schattingsmethode zouden kunnen verbeteren.

Ten tweede wordt een Extended Kalman Filter (EKF) gebruikt om te laten zien hoe de koppeling tussen baan- en attitude dynamica, veroorzaakt door luchtweerstand en krachtmoment, de schatting van relatieve dynamica van ruimtevaartuigen verbetert. Zelfs gebruikmakend van volledig waarneembare scenario's. Hiervoor wordt een EKF toegepast die met deze koppeling rekening houdt. Er wordt een andere schatter gebruikt voor vergelijkingsdoeleinden, waarbij de verstoring alleen door Gaussische witte ruis is gesimuleerd. Het is gebruikelijk dit soort ruis in te zetten om niet beschouwde verstoringen te stimuleren. Om te laten zien dat de "gekoppelde" schatter in elk geval beter is dan de "niet-gekoppelde" schatter, is de ruis van de niet-gekoppelde schatter gevarieerd tot de best mogelijke schattingsuitvoering is bereikt.

Bij een 300 km hoge baan laat de gekoppelde schatter voor twee 3-unit Cubesats vliegend in een along-track configuratie een verbetering zien van 6.9 m in de gemiddelde positieschatting ten opzichte van de zogeheten "niet-gekoppelde" schatter. Zelfs op hoogtes van 650 km, met twee 240x40x40 cm Cubesats, laat

de gekoppelde schatter een verbetering van 3.5 m zien in de gemiddelde positieschatting. Bij hoogtes van meer dan 700 km is het verschil tussen beide schatters verwaarloosbaar.

De onderzoeksmethodologieën die in deze studie zijn toegepast, maken direct gebruik van niet-lineaire vergelijkingen die de absolute en relatieve baan- en attitude dynamica van het systeem beschrijven. Hierdoor is het mogelijk de hier gepresenteerde methodologie uit te breiden naar de evaluatie van elk soort meetscenario, baan (van circulair tot zeer elliptisch) en elk aantal ruimtevaartuigen. Er is nog veel ruimte voor toekomstig onderzoek naar de evaluatie van gekoppelde baan- en attitude ruimtevaartdynamica voor schattingsdoeleinden.

# Preface

I believe every single PhD research is a great adventure. Mine has been life changing, without a doubt.

I come from a country where space engineering development did not exist when I was a child. I watched on television in my childhood astronaut Franklin Chang-Díaz, a Costarrican-born going to space. It was the hero of all Costarrican children in the eighties and nineties. I believe his accomplishments influenced a generation. I can say, for sure, they had a deep impact in me.

I do not even remember when I became in love with space. I may even say I was born loving space. But, nevertheless, I was born in a non-space fairing nation. When I was a child, I believed it was not fair that because I was Costarrican, I could not even dream with developing spacecraft unless I left the country.

I was a lucky child. My house was full of books. But not only that. My parents always helped me to learn whatever I wanted to learn the most, with no pressure, just for the joy of learning. I had an amazing childhood surrounded by Lego (which I used to create spacecraft, of course), books and freedom.

When I was about to decide what to study, I always said that I studied electronic engineering because it was not possible to study aerospace engineering in Costa Rica. It is still not possible, but I know that dream will become a reality soon. I loved becoming an electronic engineer, and I knew it was a path to pursue space. I was not wrong.

When I was working in industry, Luis Paulino Méndez, then the director of the electronic engineering school at the Costa Rica Institute of Technology (TEC) asked me to join them as a lecturer. He told me his intention was for me to pursuit a graduate degree. At that time, it was clear to me that I wanted to become a researcher, so there I was, with an offer to follow the path to pursue what I felt was my destiny. That one call became one of the fundamental moments of my life. I said yes (of course). Today, with Prof Méndez as the current president of TEC and I am about to defend my thesis, the only one thing that I can say to him is thank you for believing in me.

I came to the Netherlands because I wanted to learn to be a researcher. As a lecturer at the Costa Rica Institute of Technology, it was clear to me that my favorite area when I studied electronic engineering was systems and control. It was at that moment that Carlos Meza, who is now my colleague at TEC help us contact Prof Jacqueline Scherpen and Dr. Dimitri Jeltsema. They offered my friend Mauricio Muõz and myself the possibility to come to the Netherlands to specialize in systems and control at the Dutch Institute of Systems and Control, and later start our PhD studies. They opened the doors of the Netherlands to us. For that, thank you Carlos, Jacqueline and Dimitri.



544941-L-bw-Jimenez
Processed on: 16-6-2020

I started pursuing my PhD studies at the ”Applied Mathematics” group of EMI at TU Delft. I still remember how Shah helped me getting my first bicycle in the Netherlands, how much he helped me and how much I learned from him, from mathematics to sharing Ramadan with people from Pakistan and India. Also, how Katerina took me to Delftians and introduce me to the first group of friends that I had, all they way to the point that my only social day was Thursdays every two weeks. There I met Joe, Tom, Vera, Dana, Thomas, Dhiradj, Gian Luca, Alicja and so many other people. Those were wonderful and fruitful times.

It was in 2011 when my space adventure began: the Central American Association for Aeronautics and Space (ACAE) proposed in Costa Rica the idea to create the first Central American satellite. I joined ACAE remotely as the first director of ”Project Irazú”. Together, ACAE and TEC started the dream of making Costa Rica a space faring nation via the construction of the first Central American Satellite, a CubeSat.

Yes, it was crazy. I did not know a thing about satellites! But, lucky me, I was at TU Delft. I knew that because I was there, I could study whatever I wanted if offered as a course. In the pursue of the perfect course to learn about space projects development, I found the course ”Introduction to Space Engineering” by Prof Eberhard Gill. That was it! That was the course I had to join. But I did not only joined the course, I asked the people in charge if I could talk to them to explain them why I wanted to be there.

It was then when I met Dr. Jian Guo and Jasper Bouwmeester. They asked me ”why don’t you join our current satellite project, Delfi-n3Xt?”. Of course, I said yes. There I was, officially, part of a satellite project, in my free time and as a voluntary. It was that opportunity the chance that I always wanted to have, and for that, thank you Jian and Jasper.

While I was pursuing my PhD in Applied Mathematics, the group there realized that I was more attracted to space engineering than applied mathematics. For this reason, they asked me if I wanted to change my PhD research to Prof Gill’s group, Space Systems Engineering (SSE). It was at that time that I realized how the Dutch culture of openness was working in my favor. I asked Prof Gill, of course, if I could join.

I still remember as if it happened yesterday, when an email by Prof. Gill said that I was accepted to pursue my PhD in Space Systems Engineering with his group. There, I cried of happiness. I was about to learn about space engineering at TU Delft, while cooperating to create the first Costarrican satellite. There are no words to express how privileged I still feel to have this opportunity.

Of course, this is not the end of the story. It was just the beginning of the learning process to become a researcher. A space researcher. At the SSE group, I met some of the most important people in my life. The PhD students, Arash, Jing, Rui, and Prem welcomed me from day one there. I felt home. Prem, from that day on, became like my big brother, and all the way until today, he has always been there for me, specially on the difficult times. For that, I will be greatful for life.

Then, more PhD students and friends also came to SSE: Dadui, Minhe, Marsil, Dennis, Fiona, Linyu and my old good friend Johan. Together, having lunch and

walking after work, I learned about the world, and our joint dreams about space. I will miss them for life. Thank you for everything.

Of course, faculty members were always there for us, both at the faculty and sometimes in amazing discussions outside the office with a couple of beers in between. There, sharing with Angelo, Hans, Stefano, Barry, Trevor, Tatiana, was amazing.

Special thanks should go, without doubt to Debby. She should win "best Management Assistant" of TU Delft, every single year. You were always there for me Debby, thank you.

I meet many students at De Atmosfeer, the bar at the faculty. There, I had some of the best discussions and celebrations of my life, including the launch of Delfi-n3Xt, the first satellite where I ever worked. The master students and the Astrodynamics groups of the faculty became our friends.

Also, my adventures at Delft cannot be narrated without special attention to the Costarrican group there at the Netherlands, who kept Costa Rica "close" to me. Carmen, Johan, Andres, Andrea, Sebastian, Carlos, Laura, Jose, Edgar, Juan, Katherin, Julian, Marcos, Miguel, Daniel, Maricruz and Michael (yes, we were a lot), I miss you all!

Studies, of course, were not only beer and fun. Very hard times came, and the difficulties of learning about space engineering, and astrodynamics given my background, was quite an experience. Other difficulties arose. And I must say, the patience and help of Prof Gill and specially Dr. Jian Guo, saved my thesis.

I have to leave Delft three years ago now because my father became ill. On those hard times, it was not only my family in Costa Rica who were there for ey, but my friends in the Netherlands.

When I came to Costa Rica, I had the opportunity to be part of the final technical group who developed and operated the satellite of Project Irazú. Thanks to the effort of many people, and the contributions of even more Costarricans, the satellite was released in orbit in May 11th, 2018, from the International Space Station, and remained operational for around two years.

Today, after all the difficulties of finishing my thesis remotely, and even when the Covid-19 pandemic helped me from being in Delft defending my thesis, I cannot be but grateful for all the opportunities and friends I have. I know when this emergency finishes, space will become again a source of dreams for humanity. I believe this is the last decade in history when humans are only present in one celestial body.

Even when mentioned before, in my heart, a special recognition should go to Jian, Prem, Prof. Gill, Mauricio, and my mother Mirna and father Adolfo. I will definitely not be here today if it weren't for you. Please know I will be grateful for life. This thesis is also yours.

This thesis is dedicated to Adolfo Chaves-Campos, my dad. His legacy will always live on.

*Adolfo CHAVES JIMÉNEZ*
*Delft, June 26th, 2020*

# 1

# Introduction

*If you want to make an apple pie from scratch,*
*you must first create the universe.*

Carl Sagan

*The first principle is that you must not fool yourself and you are the easiest person to fool.*

Richard Feynman

## 1.1. Background

Since humankind was able to reach space for the first time in 1957 with the Sputnik satellite, an aluminum sphere of 58 cm-diameter aluminum and just 84 kg of mass [3], science, technology, and in general all kind of disciplines have benefited significantly from having a platform flying in space. The advancement in technology, driven significantly in the 50's and 60's by the space engineering development of the "Cold War" enabled more capabilities: from meteorological observations, telecommunication, to navigation systems such as the GPS, GLONASS, Galileo and BeiDou.

In order to support this advancement, satellites were, in the early decades of spaceflight, typically growing in size, to support their increasingly complex tasks. At the same time, often, a mission was associated with a single satellite.

Nevertheless, despite the advancement in launching technologies, the cost of using a rocket to place its payload in orbit was, and still is, very expensive. However, the advancement of launching technologies is currently reducing this cost dramatically. For example, Jones compares the cost of the NASA's space shuttle of

1

about $ 1.5 billion to launch 27500 kg to Low Earth Orbit (LEO) ($ 54500/kg) to the advertised cost of $62 million to launch 22,800 kg to LEO by SpaceX's Falcon 9 ($ 2720/kg). This reduction in cost illustrate that, in general, commercial launch has reduced the cost to LEO by a factor of 20 [4].

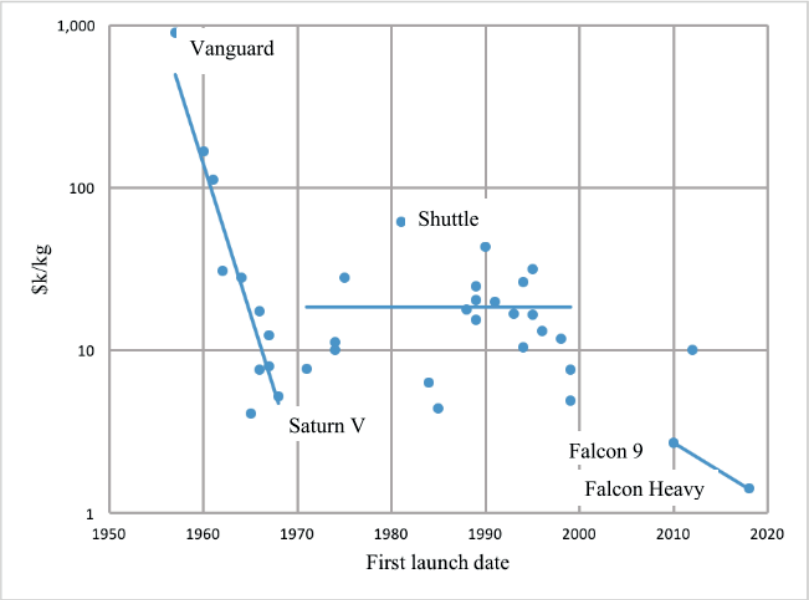


Figure 1.1: Launch cost per kilogram to LEO in current dollars for various launch systems shown against the first system launch date. [4].

At the same time, the advancement in electronics fabrication techniques has led to an exponential increase in performance of integrated circuits. This phenomenon has been reflected in the empirical observation made by Moore that "component density and performance of integrated circuits doubles every two years" [5]. This statement is commonly known as the "Moore Law" which has correctly predicted this increasing trend since it was stated in 1975.

This increase in density and performance of integrated circuits has enabled engineers to implement solutions that increase the capabilities of satellites, for example, by designing more capable spacecraft with less power and mass requirements than what would have been possible a few years ago. At the same time, using miniaturized spacecraft in groups instead of a single spacecraft to realize a mission provides for certain applications benefits in terms of efficiency or capabilities.

The trend of miniaturization is reflected, specially, in the growing use of small satellites called "CubeSats". These satellites are build in units of 10x10x10 cm cubes, where 1 cube is called 1U. Then, two cubes together form a 2U Cubesats and so on. They started as teaching tools and for technology demonstration, but the technology has matured enough to be used as platforms for space and earth sience mission within agencies like NASA [6].

Figure 1.2: ESA Sentinel 3 Satellite, an example of a satellite using Precise Orbit Determination (POD) techniques (source [10]).

In this framework, missions and spacecraft design using distributed space systems (DSS) are witnessing an emerging paradigm shift from traditional large single satellites to DSS acting in a collaborative manner. Several types of missions would be hardly achievable if not for a distributed spacecraft approach. An example of this is the long baseline space interferometry for synthetic aperture radar imaging of the TanDEM-X and TerraSAR-X mission [7]. Here, the two spacecraft, flying in formation allow an antenna separation of 500 m to 4000 m, unreachable using any currently existing single spacecraft.

The increasing performance requirements had led engineers and scientist to apply Precise Orbit Determination (POD) approaches to comply with more rigorous mission requirements. An example is given in [8]. Here, an 8-channel dual-frequency GPS receiver in combination with precise dynamical and measurement models is used for the geolocation of the observations of the European Space Agency Swarm Mission, launched in 2013 to study the dynamics of the Earth's magnetic field. Another example is the Sentinel-3 mission [9], where the measurements of the sea surface heights highly depend on the accurate knowledge of the spacecraft orbit, and the targeted uncertainty in radial direction is less than 2 cm. This is done in this case using a GPS receiver, a Doppler Orbitography and a Radiopositioning Integrated by Satellite Instrument and a complementary laser retroreflector for satellite laser ranging (see Figure 1.2).

In the small spacecraft realm, efforts like the PRISMA demonstration mission [11], with a full autonomous formation flying of two spacecraft, one of 150 kg and another of 40 kg, with an absolute and relative orbital accuracy of 2 mm and 0.1 mm respectively, show the growing interest of using small spacecraft for applications that require precise formation flying (see Figure 1.3).

1

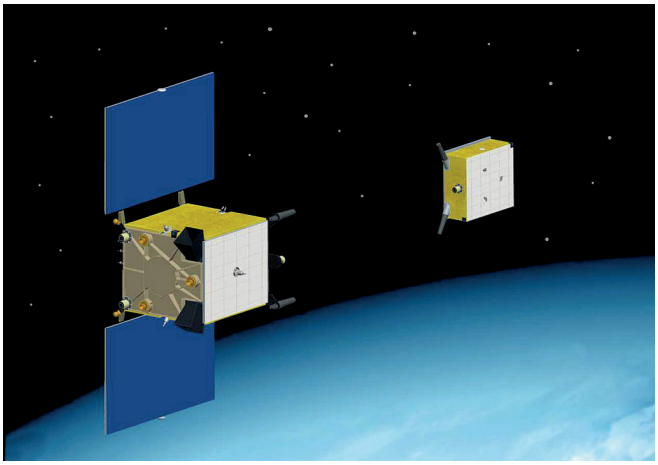

Figure 1.3: The PRISMA formation with the MAIN (left) and TARGET (right) satellites [12].

In order to enable DSS technologies, challenging research problems need to be solved. Among them, a critical field for mission success is spacecraft relative position and attitude estimation and control. For example the Darwin mission [13] features a distributed radiotelescope with the objective to detect Earth-like planets, where the required position stability is 5 nm over distances of 500 m between the spacecraft.

On the other hand, in the last years there has been a tendency towards declining financing budgets, provoking missions to be cancelled or to be partially or totally replaced by more cost-efficient missions. The latter is the case for the Darwin mission itself, that is not expected to go beyond its initial study [14]. However, some of its characteristics are now being planned for OLFAR, a space-based interferometer system, based on a swarm of 25-100 nanosatellites in a lunar orbit to map celestial radio sources in the frequency range of 0.1 - 10 MHz [15, 16]. There is a trend of replacing conventional satellites, of the size of a van, for swarms of smaller satellites working in collaboration. To illustrate this trend, Figure 1.4 shows different imaging satellites, giving a clear idea of the size differences. A satellite as the WorldView 3 NOAA satellite [17] has multispectral imaging capabilities that cannot be matched by a single PlanetLabs Imaging Nanosatellite. Nevertheless, PlanetLabs claims that its constellation has daily imaging capabilities of any part of the Earth. These capabilities were reported to allow a fast response to disasters such as the Nepal earthquake of 2015 ([2]), something impossible to accomplish with a single, large satellite.

### Types of Distributed Space Systems

Distributed space systems (DSS) may be classified in different ways, depending on different parameters. For example, Shaw et al. proposed that satellite systems may be interpreted as information transfer systems, where each satellite and ground station is a node in a network [19]. From here, it is possible to identify two formal

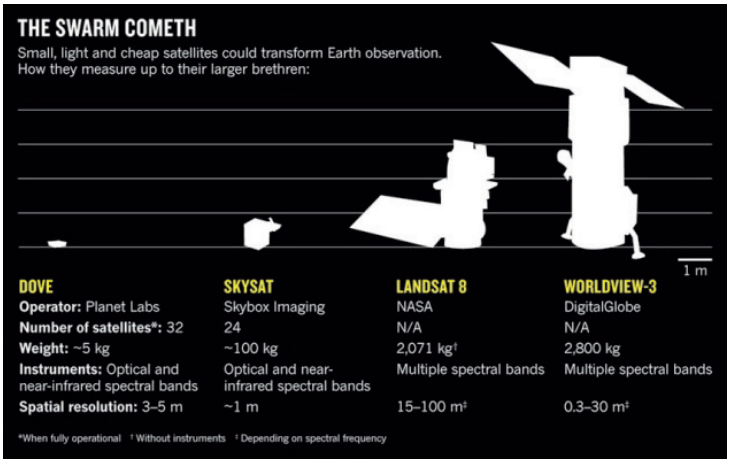


Figure 1.4: Comparison of imaging satellites: small satellites used in swarms vs large, conventional satellites. The concept of the spacecraft constellation by Planet Labs shows the utility of small spacecraft in formation, like the Dove satellite shown here [18].

types of DSS: constellations and clusters [20].

According to [20], constellations relate to scenarios with multiple and sparsely distributed satellites, which typically do not require precise formation control, but may require propulsive station-keeping. They usually communicate independently to ground (Ground Links) with rare use of cross-communication between satellites (Crosslinks). The Planet Labs multiple CubeSats system is a recent example of a constellation. Their goal is "to provide medium-to-high resolution imaging of the entire planet, on a daily, recurring basis" [21]. They are using inexpensive 2.5 unit (2.5 U) CubeSats (a length of approximately 20 cm height and 2.5 liters of volume), launched from e.g. the International Space Station for this purpose. Figure 1.5 shows the launch of Planet Labs satellites from the ISS.

Figure 1.5: Separation of two CubeSat from the ISS to build up the PlanetLabs constellation ([22]).

1

Clusters, in contrast, refer to scenarios where the satellites are close together in a similar orbit to achieve a common mission target. If the cluster requires that the satellites maintain precise positions and orientation with respect to each other, the system is referred to as a formation (Formation Flying). The PRISMA mission, previously introduced in this chapter, is an example of this concept. This mission conducted a spaceborne autonomous formation flying experiment (SAFE), that aims to demonstrate a fully autonomous, robust and precise formation flying of two spacecraft. Here, the guidance, navigation and control (GNC) system is designed to provide an accuracy of better than 25 m at distances between 100 to 2000 m, in order to represent the requirements of future formation flying missions [11]. If satellites do not require the precise maintenance of position or orientation with respect to each other, the system is classified as a "Free Flying" cluster .

Another classification of DSS, based on the distance between the satellites and the requirements of the control of their distances, is proposed in [23]. From the point of view of distance, the systems may be distinguished as local systems, with separations between spacecraft of a few meters, regional separation of a few 10 meters to several hundred of kilometers, to global systems with separation of more than a thousand kilometers. From here, DSS may be classified as

- **Rendezvous and docking DSS**: Typically involves two objects moving in the vicinity of each others. Example: ESA's Automatic Transfer Vehicle (ATV), that docks with the International Space Station (ISS) (Figure 1.7).
- **Formation Flying (FF) DSS**: FF is typically associated with a small number of spacecraft, flying in coordination, at regional intersatellite separations. Example: the Gravity Recovery and Climate Experiment (GRACE), launched in 2002. Its formation consists of two spacecraft with a separation of 250 km. Its objective is to obtain a better understanding of the gravity field of Earth: any irregularities in the Earth's gravity field cause small changes in the separation of the two spacecraft, that have an intersatellite link with an accuracy of 1 $\mu$m.
- **Constellation DSS**: Constellations refer to sets of satellites that achieve global coverage of Earth. Control accuracies of constellations are often low, and typically done at the ground control center. The US Global Position System (GPS), the corresponding Russian system GLONASS and the European system Galileo are all examples of constellations.
- **Swarm**: Swarms of satellites consist of several ten to several thousand of spacecraft deployed, with little control accuracy, that rely on the amount of satellites to acomplish a mission.

This classification is illustrated in Figure 1.6.

### Applications of Distributed Space Systems

DSS may also be classified according to their intended mission. In 2015, [26] classified thirty-nine small satellite DSS missions with respect to the applications they were designed for (see Figure 1.9 ).

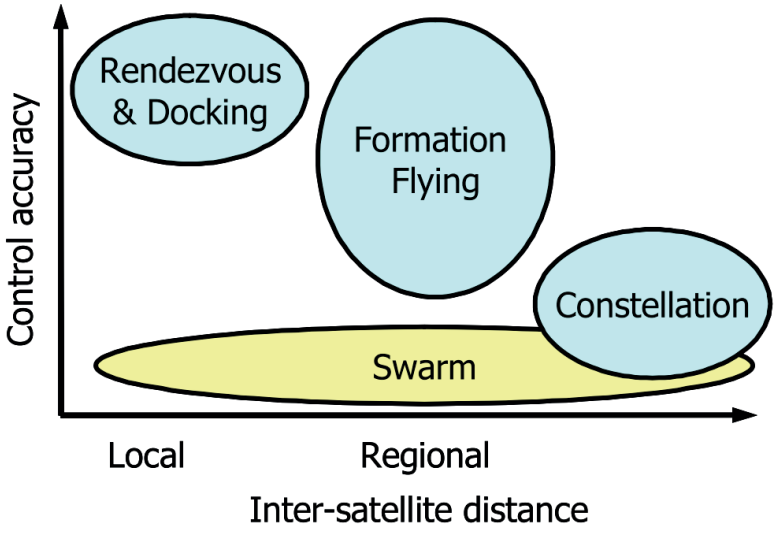


Figure 1.6: Distributed systems in space can be categorized with respect to their inter-satellite separation and their requirements on control accuracy (source [23]).

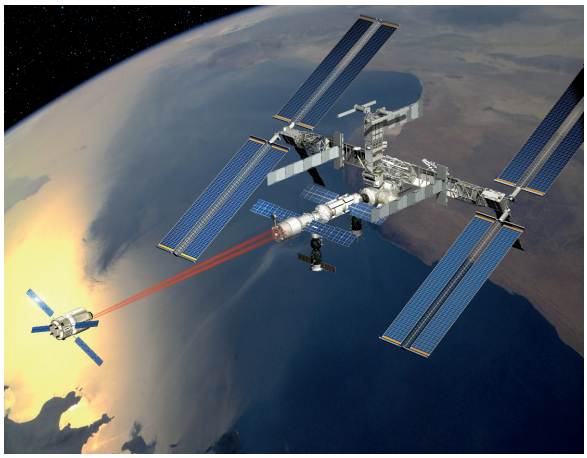

Figure 1.7: Artist's impression showing ATV docking with ISS, and example of a rendezvous and docking DSS (source [24]).

1

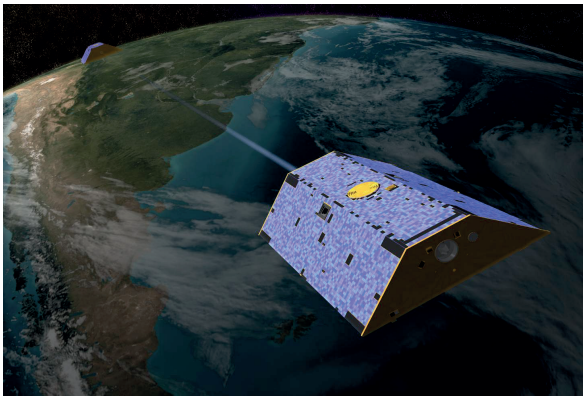

Figure 1.8: Illustration of the twin Gravity Recovery and Climate Experiment (GRACE) satellites in orbit, and example of a formation flying mission (source [25]).

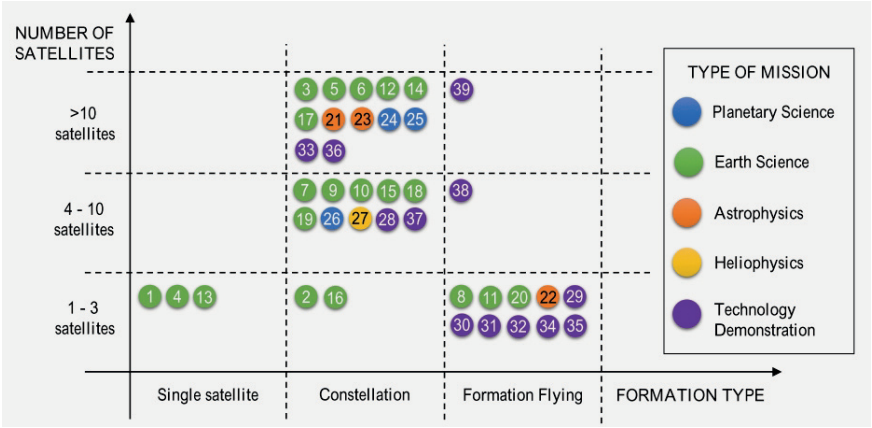


Figure 1.9: Categorization of thirty-nine multi-satellite missions based on their mission type, formation type and number of satellites (source [26]).

These categories are:

- **Earth Science Missions**: Any mission with the goal to contribute to scientific understanding of the Earth system dynamics. The authors cite, among many examples, the "Dynamic Ionosphere CubeSat Experiment" (DICE) (see Figure 1.10), a multi-university mission led by the Utah State University, where two 1.5U identical CubeSats are used to measure different parameters of the ionosphere [27].
- **Planetary Science Missions**: These missions are executed with the purpose to understand the planets and small bodies in our solar system. One example of a DSS Planetary Science mission is the "CubeSat Constellation at Mars" mission concept, led by the NASA Jet Propulsion Laboratory (JPL), with a constellation of sixty CubeSats around Mars, to study the electrical activity of this planet [28].
- **Astrophysics Missions**: Missions with the objective to understand the universe. The advancement of technology has enabled the possibility of obtaining valuable information from small satellites flying in formation. One example is the "OLFAR Mission" [29], led by Delft University of Technology, where a swarm of 50-100 identical nanosatellites would be deployed in the Moon orbit to observe the universe at frequencies below 30 MHz (see Fig. 1.11).
- **Heliophysics Missions**: These missions aim to study the very nature of the Sun and its effects on its surrounding space [30]. For example, a constellation of 6U Cubesat has been proposed to study the helioseismology and magnetic field of polar regions [31].
- **Technology Demonstration Missions**: These missions aim to "demonstrate the application of state-of-the-art technology in space" [26]. An example is the mission concept "High-speed, Multispectral, Adaptive Resolution Stereographic CubeSat Imaging Constellation" (HiMARC), led by Stanford University, that aims to launch four 3U synthetic aperture optical telescopes to provide stereographic imaging of Earth and other targets [32].

### GNC Capabilities and Requirements of Distributed Space Systems

The Guidance, Navigation and Control (GNC) subsystem of a spacecraft is defined as the system that includes the functionality for both orbit and attitude determination and control. For certain types of DSS, the GNC subsystem plays a crucial role as position and attitute requirements are driving the mission design.

The advancement on GNC technology is reflected by the use of GPS receivers, improvements on the efficiency of radio tracking, miniaturization of microelectromecanical devices (MEMS), and the general advancement in electronics performance (reflected in the Moore's Law mentioned before). Combining this with the improvement of the model of the dynamics of spacecraft, enable the possibility of using, for certain applications, small satellites in formation instead of a large spacecraft to accomplish a mission. At the same time, new kind of missions that were not possible

1

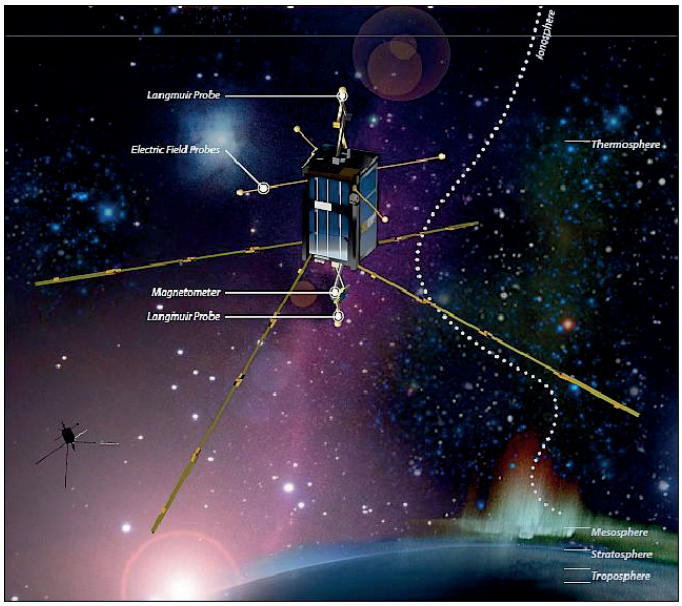


Figure 1.10: Artist's rendition of the DICE spacecraft in orbit (source [33]).

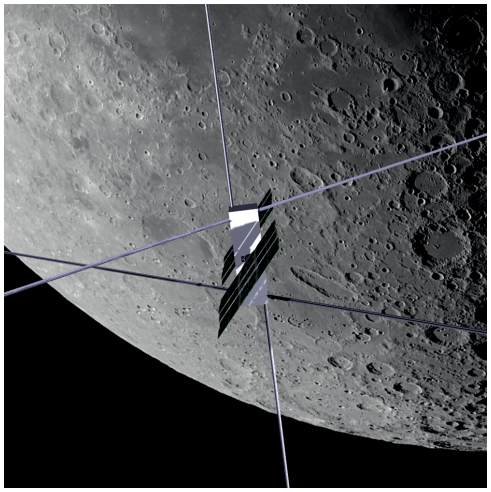

Figure 1.11: Impressions of one of the CubeSats of OLFAR Mission (source [34]).

| System | Classification | Performance | TRL Status |
|---|---|---|---|
| Reaction Wheels | Actuator | 0.001-0.3 N m peak torque, 0.015-8 N m s storage | 9 |
| Magnetorquers | Actuator | 0.1 Nm peak torque, 1.5 Nms storage | 9 |
| Star Trackers | Sensor | 25 arssec pointing knowledge | 9 |
| Sun Sensors | Sensor | 0.1° accuracy | 9 |
| Earth Sensors | Sensor | 0.25° accuracy | 9 |
| Gyroscopes | Sensor | 1° $h^{-1}$ bias stability, 0.1° $h^{-1/2}$ random walk | 9 |
| GPS Receivers | Sensor | 1.5 m position accuracy | 9 |
| Integrated Units | System | 0.002° pointing capability | 6 |

Table 1.1: GNC Subsystems capabilities [35]

with previous technology are now feasible with several satellites in formation. For example, the previously mentioned astrophysics mission OLFAR, where, because of the low frequency used to observe the universe (below 30 MHz) the aperture size of the instrument must be in the order of 100 km. For this reason, this aperture is proposed to be implemented by using formation flying of small satellites [29].

Regarding GNC technology, the NASA report "Small Spacecraft Technology State of the Art" from 2015 [35] summarizes the state of the art of GNC subsystems for small satellites (see Table 1.1). Here, the technology it classified by its "technology readiness level" (TRL). According to NASA's definition of TRL, a TRL of 1 or 2 indicates a situation of relatively high risk. 6 to 8 represent low-risk categories [36].

The NASA report explains that "the current trend in small spacecraft is the miniaturization of the existing technology. While 3-axis stabilized, GPS-equipped 100 kg class spacecraft have been flown over a decade, it has only been in the past few years that such technologies have become available for 10 kg class spacecraft".

New kind of missions are designed to take advantage of the current miniaturization trend. Due to this fact, several missions have been executed or proposed. To name a few examples of applications, [37] reports the capabilities that are enabled by the use of precision formation flying of two or more satellites, like interferometry, study of black holes or technology demonstrations. A few illustrative examples of this growing trend and the associated GNC requirements of such missions are summarized in Table 1.2.

### 1.1.1. Relative Spacecraft Dynamics

While the above section has focused on applications, architectures, and technology capabilities for DSS, the advancement in these areas rely in a crucial way on the underlying absolute and relative dynamics of spacecraft. For example, sensors of a GNC subsystem will sense absolute or relative position, velocity or angular rates, used for spacecraft dynamics estimation; and the actuators of a GNC subsystem will enable the spacecraft control.

1

| Mission | Short Description | GNC requirements |
|---|---|---|
| MASSIN | Mission concept: long telescopes using formation flying and diffractive optics. | Inter-space distance of 1000 km. Alignment precision and stability to keep the image on detectors of ≈100 mm in size. Retrospective knowledge of drift changing the direction of inter-spacecraft vector needs to be commensurate with the resolution [37] |
| TPF-I/Darwin | Two missions studies: one from NASA, another from ESA for infrared nulling interferometry purposes | Pointing maintenance to 10-50 milli-arcsec. Relative orbital accuracy 5 nm [13]. |
| MAXIM | Proposal: Study of black holes via X-ray imaging. | Distances on the order of 10-20 km. Precision requirements still under study [38]. |
| PRISMA | Technology demonstration mission for satellite formation flying and in-orbit servicing (operation from 2010 to 2014) | Distances of 100 to 2000 m. Absolute orbital accuracy 2 mm. Relative orbital accuracy 0.1 mm [11]. |

Table 1.2: Navigation requirements of selected Formation Flying missions. Elaborated from the information at [37].

Here dynamics is understood as the relationship between kinematics, forces, and torques affecting motion [39]. Kinematics is the branch of mechanics that studies aspects of motion apart from considerations of masses, forces and torques [40].

In this work, absolute dynamics modeling is understood as the description of a single spacecraft motion in terms of its orbit and attitude. The measurement and estimation of the dynamics is done either with the spacecraft own sensors to know its state for orbit and attitude with respect to the celestial body, like sun sensors (for its orientation with respect to the sun), magnetometers (for its orientation with respect to the magnetic field of Earth), GPS devices (to know its absolute position with respect to a frame that co-rotates with Earth) or measurements done from a celestial body such as the Earth, like radar tracking [41]. Typically, the absolute dynamics of a single spacecraft are described in an inertial reference frame.

On the other hand relative dynamics modeling is the description of the motion of any object with respect to the other. An example is when a spacecraft determines its attitude with respect to another spacecraft using a camera, or its relative position using GPS-like devices [42]. Typically, relative dynamics rely on non-inertial frames, due to the fact that the spacecraft used as a reference is usually assumed to be in motion.

When the relative dynamics of two spacecraft is described, typically a leader or chief spacecraft is defined as the one which hosts the reference frame for the description of the relative dynamics, while the follower or deputy is defined as the spacecraft which states are described with respect to the leader.

The first analytical solution for the relative spacecraft orbit dynamics representation was established in 1960 by Clohessy and Wiltshire (CW) [43]. This approach assumes that the orbit of a chief spacecraft is circular, the Earth gravity field is represented by its point mass, the distance between spacecraft is very small compared to the orbital radius, and neglects any other perturbations. This leads to a series of linear time-invariant equations that describes the relative position of both spacecraft. As [44] describes, the solution of the CW equations was concerned with rendezvous, hence the long-term solution of the equations was not a major concern. Extensions of this work were done to include elliptic Keplerian orbits (for example in [45]), without including any external perturbations. Latter results include representation of orbital disturbances (see for example [46] and [47]). However, in all these works, only the orbital dynamics were considered.

To the best knowledge of the author, the problem of spacecraft attitude relative dynamics modeling has been closely related to the joint relative orbit-attitude dynamics modeling problem. The advancements in this area are described in the next section.

### 1.1.2. Joint Representation of Orbit and Attitude Dynamics

In an ideal hypothetical situation, where a spacecraft would be considered as a point mass with its motion based on external forces (ignoring e.g. propulsion) its orbit dynamics would fundamentally not depend on the spacecraft's attitude.

Nevertheless, perturbations such as the atmospheric drag introduce a coupling

1

effect between orbit and attitude dynamics since the spacecraft's area with respect to the direction of the atmospheric particles, called effective area, causes drag acceleration and this effective spacecraft area depends on the spacecraft attitude. On the other part, any nonsymmetrical object of finite dimensions in orbit is subject to gravitational torque, caused by the variation of the Earth's gravitational force over the field. This means that any model that does not consider the coupling effect of orbit and attitude dynamics introduced by perturbations may be suboptimal.

However, despite the advancement in spacecraft relative dynamics estimation methods, classically the assumption that relative spacecraft orbital and attitude dynamics are not coupled has been deemed accurate enough for most estimation and control purposes, due to the fact that the coupling effect is too small to affect the required accuracy of most missions.

Nevertheless, recent works are taking into account the joint representation of attitude and orbital dynamics for improved guidance, navigation and control performance, in order to use dynamics models that better represent the physical world. For example, in the case of the joint representation of relative dynamics of spacecraft for control purposes, in [48, 49] the gravity-induced mutual coupling between orbital and attitude dynamics is taken into account when solving a spacecraft relative dynamics tracking problem using nonlinear control techniques. In [50] the coupling effect generated by the gravity gradient and the solar pressure is considered in the engineering model of the spacecraft formation control system for a space interferometry mission. Similarly, in [51] it is described how the gravity gradient, solar pressure and atmospheric drag are a source of coupling between attitude and orbital dynamics. Later, this dynamics model is applied for control purposes in [52]. Furthermore, the coupling effect generated by actuation is considered in [53–57]. The modeling of coupled dynamics for deep space missions is reported in [58, 59]. Practical use of the coupling between attitude and orbital dynamics is proposed by [60], where the differential drag between spacecraft is employed to control their relative distance.

A joint orbit and attitude representation for estimation purposes, was formulated by Chodas, as early as 1982 [1, 61]. He formulated an engineering model for an Extended Kalman Filter (EKF) where the joint orbit and attitude dynamics are coupled by perturbation forces and torques including the gravity gradient, aerodynamic torques and atmospheric drag for a very large spacecraft (7000 $m^2$ surface area) in a very low orbit (250 km altitude). This work is however limited to the analysis of a single spacecraft.

A research of similar characteristics may be found in the study done to track debris present in Geosynchronous Orbit (GEO) [62], with tracking done from ground. Due to their orbit, the dominant perturbation affecting both orbit and attitude dynamics is the solar radiation pressure.

In 1999, Psiaki [63] estimates both the orbit and the attitude of a single satellite by using only magnetometers and sun sensors. In this work the coupling between both states is given by the fact that the measurement depends on both orbit and attitude, not on the dynamics model.

In other papers addressing joint estimation of relative orbit and attitude dynam-

ics, like [64–68], a vision-based navigation system (VISNAV) provides the measurements of the spacecraft dynamics. In this scenario, the information provided by the VISNAV system allows a joint estimation of both position and attitude relative dynamics. The objective of the cited works where VISNAV is applied is not to determine how the coupling affects the estimation for the measurement of relative dynamics, but instead, how the estimation performance is affected by the use of different estimation algorithms, with an Extended Kalman Filter (EKF) in [64, 68], a square-root sigma-point Kalman filtering in [65], and an Unscented Kalman Filtering in [66, 67]. The work by [69] employs a similar joint estimation, where the coupling is a product of the measurement method. However, in this case, elevation, and azimuth between the target and the chaser, are measured by a laser rangefinder, a charge-coupled device (CCD), a rate gyroscope and one star sensor, installed on the chaser to measure its rate and attitude parameters.

In [70–73] the coupling between relative orbit and attitude dynamics for estimation purposes prompts from the assumption that the spacecraft orbit and attitude dynamics dynamics are modeled from arbitrary points on the spacecraft, not the center of mass or pressure of the spacecraft. Therefore, it is known as ”kinematic coupling”.

However, unlike the cited control application examples, the dynamic coupling between orbital and attitude dynamics has not been taken into account for estimation purposes. This simplification is typically justified by assuming that the magnitude of this coupling effect is negligible.

Nevertheless, to the best knowledge of the author, no work has been published yet where the coupling between the attitude and orbital dynamics caused by external perturbations is adopted in spacecraft relative dynamics models to improve their estimation accuracy, in a similar fashion as it has been done for a single spacecraft in the cited work of Chodas [1, 61], or in the same way that has been done for control purposes, in the aforementioned articles [48–60] .

Explicitly adopting the coupling between relative orbit and attitude may result in better a priori estimation of spacecraft dynamics during the mission analysis and preparation stage. Despite the fact that typically there is no need for that because the effect is small, there are applications that may benefit from a more accurate model, for example, control using differential drag, as done in [74]. Coupling may be added to a posteriori orbit and attitude determination processes, in order to improve its performance whenever there are no restrictions on computational power, and also to use this cross relation to estimate, for example, the atmospheric density producing a dynamic coupling between relative orbit and attitude.

Finally, taking into account such coupling may help improving the onboard filtering process of spacecraft relative dynamics, which is the main focus of this thesis, and the reason why real-time filtering techniques as the Kalman Filter are used in Chapter 6. Even when the approach presented in this thesis is CPU-intensive, the ongoing improvement on computational capability may enable its extended use even for small spacecraft in the near future, in order to improve the performance of the estimation process.

1

### 1.1.3. Magnitude of the Atmospheric Drag

In order to have a first notion of the magnitude of the atmospheric drag, the perturbation effect used in this thesis as the source of coupling, lets start with the widely accepted equation for atmospheric drag force [41]

$$\boldsymbol{a}_a = -\frac{1}{2}\frac{C_D\rho(\boldsymbol{r})}{m} A_{ef} v_s^2 \hat{\boldsymbol{v}}_s, \tag{1.1}$$

where $\rho(\boldsymbol{r})$ is the atmospheric density, $m$ is the mass of the spacecraft, $\boldsymbol{v}_s$ the velocity of the spacecraft surface with respect to the atmosphere and $\hat{\boldsymbol{v}}_s = \boldsymbol{v}_s/|\boldsymbol{v}_s|$ a unit vector, $C_D$ the drag coefficient of the spacecraft, and $A_{ef}$ the effective area of the spacecraft, with the dynamics described using the inertial frame.

The torque effect produced by the atmospheric drag when the spacecraft is described as a set of areas is given by

$$\boldsymbol{\tau}_a = -\frac{1}{2}\rho(\boldsymbol{r})\sum_{i=1}^{s} C_{D,i}A_i(\hat{\boldsymbol{n}}_i\boldsymbol{v}_s)(\boldsymbol{d}_i \times \boldsymbol{v}_s), \tag{1.2}$$

with $s$ is equal to the amount of planar surfaces composing the spacecraft,$A_i$ the magnitude of area $i$ and $\hat{\boldsymbol{n}}_i$ a unit vector perpendicular to the area $i$ and $\boldsymbol{d}_i$ the distance vector between the center of pressure of area $i$ and the center of mass of the spacecraft.

Both equations show a dependency of atmospheric density with respect to both altitude and the effective area of the spacecraft. The effective area for the torque equation (1.2) is expressed as $A_i(\hat{\boldsymbol{n}}_i\boldsymbol{v}_s)$. For more details with respect to the derivation of the equations, please refer to Chapter 3.

Given that the effective area of the spacecraft varies with respect to attitude, the atmospheric drag torque of a single spacecraft varies accordingly. For a 3-unit CubeSat (a satellite with a volume of 10x10x10 $cm^3$), the smallest spacecraft used, the largest of the planar areas is three times larger than the smallest planar area. For two spacecraft in formation, this may lead to considerable differences in drift.

In order to use Eq. 1.1 to have a first idea of the magnitude of drag in spacecraft dynamics, the change in their magnitude with respect to altitude is illustrated here. First, taking as a reference a satellite in a circular orbit, the orbital velocity of the spacecraft is given by ([41])

$$\boldsymbol{v}_{circ} = \sqrt{\frac{\mu}{a}} \tag{1.3}$$

with $\mu$ the gravitational coefficient of the Earth and $a$ the semi-major axis, that in this case, is equal to the altitude. From this equation Figure 1.12 is obtained. Here, the orbital velocity below 2000 km is shown, because it is in this zone that the work of this thesis is concerned.

Now, with respect to atmospheric density, [75, Ch.4] provides a table with the magnitude of $\rho(\boldsymbol{r})$ with respect to altitude as a result of the use of the Harris-Preister model. Based on this table, the variation of atmospheric density is illustrated in Figure 1.13, for both the case of minimum and maximum atmospheric density. The

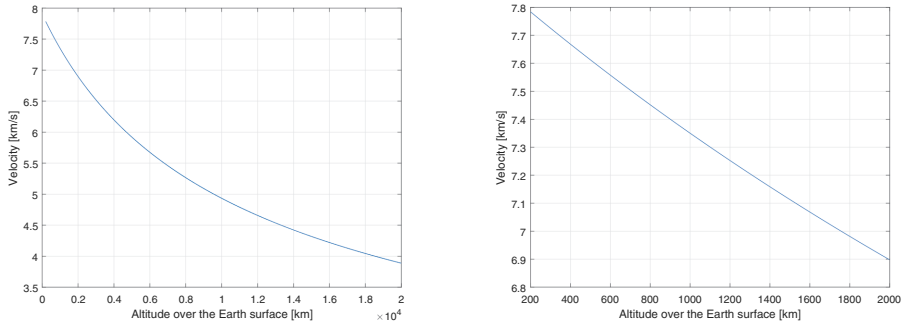


Figure 1.12: Orbital velocity with respect to altitude for a circular orbit from 200 to 20000 km (left) and from 200 to 2000 km (right).

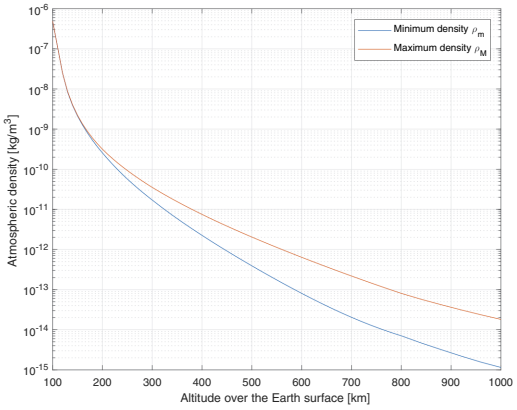


Figure 1.13: Atmospheric density with respect to altitude according to the Harris-Preister model. Based on table in [75, Ch.4].

variation of the atmospheric density at the same altitude between the minimum and the maximum is a function of the solar activity level.

Finally, to illustrate the magnitude of the atmospheric drag, take Figure 1.14, where the Harris-Preister model is used to model the atmospheric density, in order to calculate the fraction of orbital energy lost per revolution (for an explanation on the Harris-Preister model, the reader is referred to [41]). The term Force/area is used here to parametrize how many Newtows per square meter are affecting the spacecraft. From Equation 1.1, this relation leads to

$$\frac{m\boldsymbol{a}_a}{A_{ef}} = -\frac{1}{2}C_D\rho(\boldsymbol{r})\ v_s^2\hat{\boldsymbol{v}}_s, \tag{1.4}$$

meaning that, when this parametrization is used, the force/area relation depends both on velocity (Figure 1.12) and the atmospheric density (Figure 1.13),

1

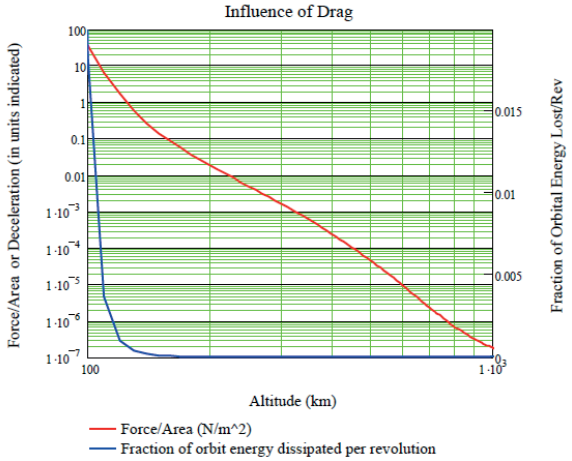


Figure 1.14: Influence of Drag for a 1000 kg satellite, 100 square meter drag area, and $C_D$ = 2.2. Harris-Preister model atmosphere [76].

both physical parameters that depend on the altitude.

As shown in Figure 1.14, a bit less than 1% of the orbital energy is lost per revolution when the altitude is 300 km, with a relation Force/Area of more than $10^{-3}$ N/m$^2$ in this specific case. The influence of this effect, from the point of view of relative dynamics, is the subject of this thesis.

In this work, it is assumed that the atmospheric density is known. Nevertheless, for completeness, it is important to notice that the modeling of the atmospheric density is a very active field, with several advancements in the last years, due to the availability of precise data from satellites in orbit. Figure 1.15 shows some of these models. For more information, refer to [76].

## 1.2. Overall Objectives

This PhD research has the objective to establish and characterize an integrated approach to the estimation of orbit and attitude for satellite formations. Here, the impact of a sophisticated spacecraft relative dynamics model taking into account the coupling between orbit and attitude dynamics on observability, theoretically and applied, is treated. As source of the dynamic coupling we consider the atmospheric drag, the largest non-gravitational effect affecting spacecraft trajectories in Low-Earth Orbit.

### Coupling influence in observability

The classical research method used to asses the observability of spacecraft navigation problems is the direct use of one or several estimators. This approach is clearly valuable and leads often to strong conclusions regarding the effect of different measurement technology, estimation methods or engineering dynamics models in the observability of the system. Nevertheless, the use of estimators to evaluate

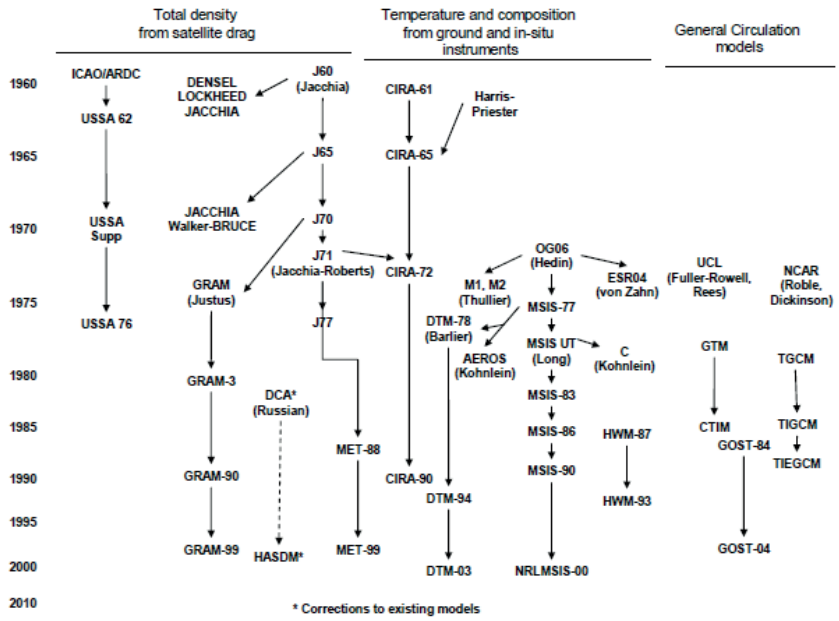


Figure 1.15: Development of models of atmospheric density of LEO [76].

observability is constrained by the limitations of the estimation method of choice.

On the other hand, systems theory provides mathematical methods to evaluate observability, like the use of the Observability Gramian for Linear Time-Variant (LTV) systems [77] or the use of the Lie Algebra method for nonlinear systems [78]. These methods lead to general conclusions about observability, that do not depend on the constraints of the estimation method, in contrast to the direct use of a filter for analysis purposes.

Despite the fact that these methods are of common use in systems theory, there are only few examples of their use in the evaluation of the observability of spacecraft relative dynamics (for example [63, 79–83]).

The use of systems theory observability methods for the evaluation of relative spacecraft dynamics has another advantage: observability determination techniques use the same linearized models of systems as controllability determination techniques. This means that all developments on coupling in the observability area may directly lead to respective advances in the controllability area and vice versa.

### Influence in estimation performance

In the last years, it has been stated that accounting for the coupling between orbit and attitude dynamics in the representation of spacecraft relative dynamics leads to models that improve the accuracy of the algorithms for control [48–52] and estimation [1, 61].

In order to validate this statement, a representation where the atmospheric

1

drag constitutes the coupling effect between orbit and attitude relative dynamics is evaluated and analyzed in order to determine how this joint representation can be exploited for estimation purposes.

Complementing the observability analysis, an estimator can be employed to demonstrate the impact of coupling between orbit and attitude on the state of the satellite formation.

## 1.3. Research Questions

The objective of this research is to determine how the coupling of orbit and attitude affects the estimation of the relative dynamics of spacecraft. To determine this, two research questions are formulated.

1. How does the coupling between attitude and orbit dynamics affect the observability of the relative dynamics of spacecraft?
2. How can the coupling between attitude and orbit dynamics be used to improve the estimation for relative dynamics of spacecraft?

The first question is general and refers to the concept of observability from system analysis. With this approach, it is possible to characterize the impact of coupling on the dynamics without the limitation of the estimation technology. Nevertheless, it is fundamental to show how estimation results are affected by such coupling. This is the realm of the second question. Both questions are addressed using the atmospheric drag as the source of coupling between orbit and attitude dynamics, taking into account both the force and the torque produced by atmospheric drag in LEO. The use of the nonlinear orbit and attitude equations in this work enables its use also for the evaluation of other formation flying scenarios, such as the collocation of geostationary satellites and their coupling due to the solar radiation pressure, its use in orbits with high inclinations, or the use of more than two satellites, to name a few.

## 1.4. Research Methodology

In order to answer the two research questions, a specific set of methodologies is employed.

First, a reference scenario for this research work is defined. This comprises two spacecraft in a circular and equatorial orbit around the Earth which dynamics are described by state-space equations. The orbit and attitude dynamics of the first spacecraft, named ”chief” are described using its absolute state: Cartesian coordinates are used for the position and velocity, and the attitude quaternion for its orientation.

The dynamics of the second spacecraft, named ”deputy”, are described as a function of its relative states with the respect to the chief: its relative position and attitude using the first spacecraft as the reference. Cartesian coordinates are used for the orbit dynamics description, to be able to use the direct physical force description of the perturbation, in this case, atmospheric drag. This choice enables

the use of this general model with any other perturbing forces ($J_2$, solar pressure, for example, may be added without any extra difficulty) to any possible orbit scenario (e.g. highly eccentric orbits and large intersatellite distances). In contrast, adding the effect of perturbations such as $J_2$ to the orbital elements description requires special procedures, and is normally constrained to special scenarios, as for example it is done by [84], where the $J_2$ model is linearized and valid only for orbits with small eccentricity.

This allows that the method proposed in this thesis may be used for any formation flying mission scenario without considerable changes. The relative rotation quaternion of the second spacecraft with respect to the first spacecraft is employed to describe its relative attitude dynamics.

It is noted that since we focus on observability with respect to dynamics, we use a very simple model for measurements. The measurements model is based on the assumption that all states measurements are done from the chief spacecraft, both its absolute dynamics with respect to the center of the Earth and the deputy relative dynamics with respect to the chief, using a space state description. This scenario is useful, for example, in the cases of uncooperative deputy spacecraft rendezvous and docking, with purposes of debris removal. Another example is formations where one spacecraft has better capabilities for navigation, or fractionated spacecraft, where the navigation is done by one module. In these scenarios some, very simple spacecraft, may not have a navigation module, but instead, the dynamics estimation of the complete constellation may be supported by more capable spacecraft. At the same time, this model is scalable to any number of deputy spacecraft.

The source of dynamics coupling used in this work is the atmospheric drag force and torque, due to its importance as the strongest non-gravitational force affecting spacecraft in very low Earth orbit. In order to better isolate the effect of this particular perturbation from other perturbations, an equatorial orbit was selected such that the best possible separation from the $J_2$ effect is achieved, justifying the assumption of not taking such effect into account. This leads to a clear separation of the effect of the atmospheric drag coupling, and therefore supports a better description of its effect on improving the spacecraft dynamics estimation.

In order to answer the first research question in general, independent from the estimation method, the concept of Observability Gramian (OG) is used. The OG is a method that allows the determination of the observability level of a linear time-variant (LTV) system described by space-state equations.

The advantage of the OG method over other observability determination methods, is that the application of alternative methods like the Lie-Algebra method for nonlinear systems (see for example [78] for a description of this method), typically only allows to conclude whether a system is observable or not. Thus two observable scenarios may not be compared with each other by evaluating their observability using the Lie-Algebra method. The application of the OG method to a system leads to a ”observability level” result, allowing the comparison of the observability level of two or more observable scenarios.

In order to use this method with the nonlinear dynamics of the scenario defined in this work, the gradient of the two-spacecraft system equations is analytically

determined. The partial derivatives of the absolute dynamics without perturbations are known [1]. However, the partial derivatives of the perturbed dynamics required to obtain the gradient of the two spacecraft set dynamics are derived in this thesis.

Due to the fact that the partial derivatives of the complete system had to be calculated to obtain the system gradient, all the space-state equations describing the spacecraft dynamics had to be described as a function of the spacecraft states, including all rotation matrices. This let to the series of analytical partial derivatives results presented in Chapter 4. This result is called here the symbolic gradient. These derivations are verified by propagating both the analytical result and the result of computing numerically the partial derivatives.

In order to calculate the gradient of the system equations, first, the spacecraft set dynamics are propagated using their nonlinear equations. The symbolic gradient is used in combination with the results of the spacecraft states from this propagation in order to calculate the gradient numerical value in every calculation step. In this way, the nonlinear system dynamics are simulated as if they were part of a LTV system. The result of the gradient in every step is used to calculate the value of the OG.

The OG result is used to determine the observability level of different scenarios, evaluating its variability as a function of the change of the effective areas of the spacecraft and the orbit altitude used of the formation. Due to the fact that the masses of the spacecraft are not changed in any propagation, the change of the effective areas may be seen as the change of the ”area-to-mass” ratio of the spacecraft in formation flight.

To answer the second research question, it has to be shown that considering the coupling between orbit and attitude on the dynamics model leads to an improved estimation on the application level. To accomplish this, the Extended Kalman Filter (EKF) is selected. The EKF is a widespread method used for spacecraft dynamics estimation, and makes use of the linearization of the dynamics model needed to propagate the OG results. To show that an EKF using coupling on the dynamics model is better than not using it, the filter is applied with two models: a model where the perturbations are simulated using white-Gaussian noise, and adjusting their magnitude to the best possible performance, and another using the coupled orbit-attitude model. For the former estimator, the best possible performance is defined as the best result in the estimation error variance of the orbit relative position after the complete propagation of dynamics is done.

## 1.5. Thesis Structure

This thesis is divided in two parts. The chapters 1-3 set up the necessary background in order to be able to answer the research questions. The chapters 5 and 6 correspond to the solution of the research questions of this research work. In Fig. 1.16, the structure of the thesis is shown. Here, the innovations developed for the thesis are highlighted in yellow.

In Chapter 2, the theoretical background necessary to obtain the results of the investigation is explained. Here, we introduce the use of attitude quaternions and the reference frames to be used for the description of the spacecraft dynamics.

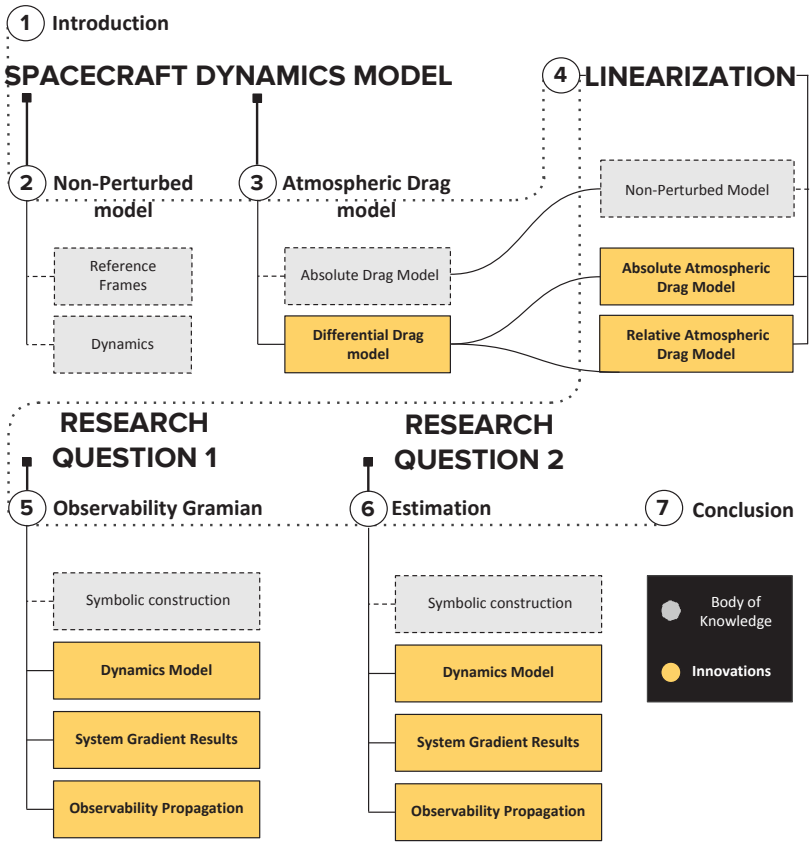


Figure 1.16: Thesis structure. Two parts are highlighted: the first one refers to the body of knowledge needed to answer the two research questions, and the second addresses the innovations from this thesis (in yellow).

1

Then, the dynamics of a single spacecraft (Chief) orbiting the Earth are described. Finally, the dynamics of a ”Deputy” spacecraft relative to the ”Chief” spacecraft are introduced. This leads to a complete description of the orbit and attitude dynamics of the two-spacecraft system.

In Chapter 3, the atmospheric drag perturbations, consisting of the atmospheric drag force and torque are introduced. These perturbations are described as the source of coupling between orbit and attitude dynamics. In order to consider the differential propagation into the dynamics models, the expressions for the atmospheric drag force and torque of the deputy spacecraft with respect to the chief spacecraft are derived in the orbital and body frames, respectively.

Both Chapters 2 and 3 constitute the complete model of the spacecraft dynamics used in the subsequent chapters.

In Chapter 4 the linearization of the models described in Chapter 2 and 3 is done. The linearization expressions are fundamental for the use in the observability analysis and estimation processes in the next chapters. These symbolic results lead to a symbolic Observability Gramian.

The second part of the thesis comprises two chapters with the results and innovations of this research.

Chapter 5 introduces the Observability Gramian (OG) as a method for the observability analysis. Here, the results of the use of the OG for the observability analysis of two spacecraft are presented. Special focus is given to the cases where observability is only possible using the coupling.

Chapter 6 uses the Extended Kalman Filter as a modeling tool to determine directly the results of the coupling. Here, it is shown that after the filters converge, the filter using the dynamics model that includes coupling shows a better performance in terms of the orbit dynamics error.

Chapter 7 summarizes the results of the thesis. It summarizes the research, highlights the motivations and presents, on a more abstract level, its conclusions. Next, it is explained how this work may be extended in the future: for example, the use of the linearization expressions for controllability analysis in the same fashion as the observability analysis is done in Chapter 5, and the use of more complex models to evaluate coupled dynamics estimation based on the results of Chapter 6.

# 2

# Spacecraft Relative Orbit and Attitude Dynamics

*This chapter introduces the theoretical background necessary for the development of this thesis. In here, the model of the absolute and relative dynamics of spacecraft in formation flying is described. Both absolute and relative orbital dynamics are described using Cartesian coordinates, in order to facilitate the addition of perturbations to the model, while attitude dynamics are described using the quaternion parametrization.*

## 2.1. Introduction

In order to develop new results within this research, the fundamental dynamic models in use are explained in this chapter. The models used to describe the dynamics of two satellites in orbit, a chief and a deputy spacecraft, are introduced.

The chapter starts with the description of the reference frames needed for this work. From here, the attitude and orbit dynamics of a single spacecraft in orbit using quaternions and Cartesian coordinates, respectively, are introduced. Next, the attitude and orbit dynamics of two spacecraft in orbit are described. The dynamics of a second spacecraft, or deputy, are described from the point of view of a Chief spacecraft. Here, it is assumed that the absolute dynamics of the Chief are known.

This leads to a complete state, constituted by the absolute dynamics of the Chief and the relative dynamics of the Deputy with respect to the Chief, that constitute the scenario analyzed in this thesis. Perturbations are part of the complete state, but are described in the next chapter.

Due to the fact that the coupling of orbit and attitude dynamics for the formation flying spacecraft introduced in the next chapter relates physical states described on different reference frames, all transformations needed on the ensuing chapters are introduced at the end of this chapter. All transformations are described using the spacecraft states introduced in this chapter. This is done because both the observability analysis in chapter 5 and the Extended Kalman Filter of chapter 6 require the linearization of all dynamics as a function of the states.

## 2.2. Representation of Dynamics

In order to describe the dynamics of two spacecraft in formation, there is a wide body of knowledge that includes different approaches. The work of Sullivan et al. [85], makes a description and categorization of the existing relative motion dynamics models. Here, closed-form analytical models are classified by the state representation used to parametrize it. At a broad level, models may be categorized in two broad approaches. First, models that use the translational representation of the relative state of a deputy spacecraft with respect to a chief in rectilinear or curvilinear coordinates. A second approach is the one that parametrizes the relative dynamics using the orbital element-based states. Here, the relative state is made up of linear or nonlinear combinations of the chief and deputy orbital elements. Within these two categories, the relative dynamics are further characterized by the reference orbit regime of applicability, for example nearly-circular orbits or orbits of arbitrary eccentricity. Another distinction is done when the description uses of nonlinear models or linearization assumptions.

In Figure 2.1 the classification of [85] is illustrated. Here, a subset of the surveyed models is chosen to represent the state of the art of the closed-form solutions of different state-space representations, briefly described here for reference.

Orbital dynamics models consider Keplerian refer to the models where the following assumptions are done [86]:

- There are no external or internal forces except gravity.

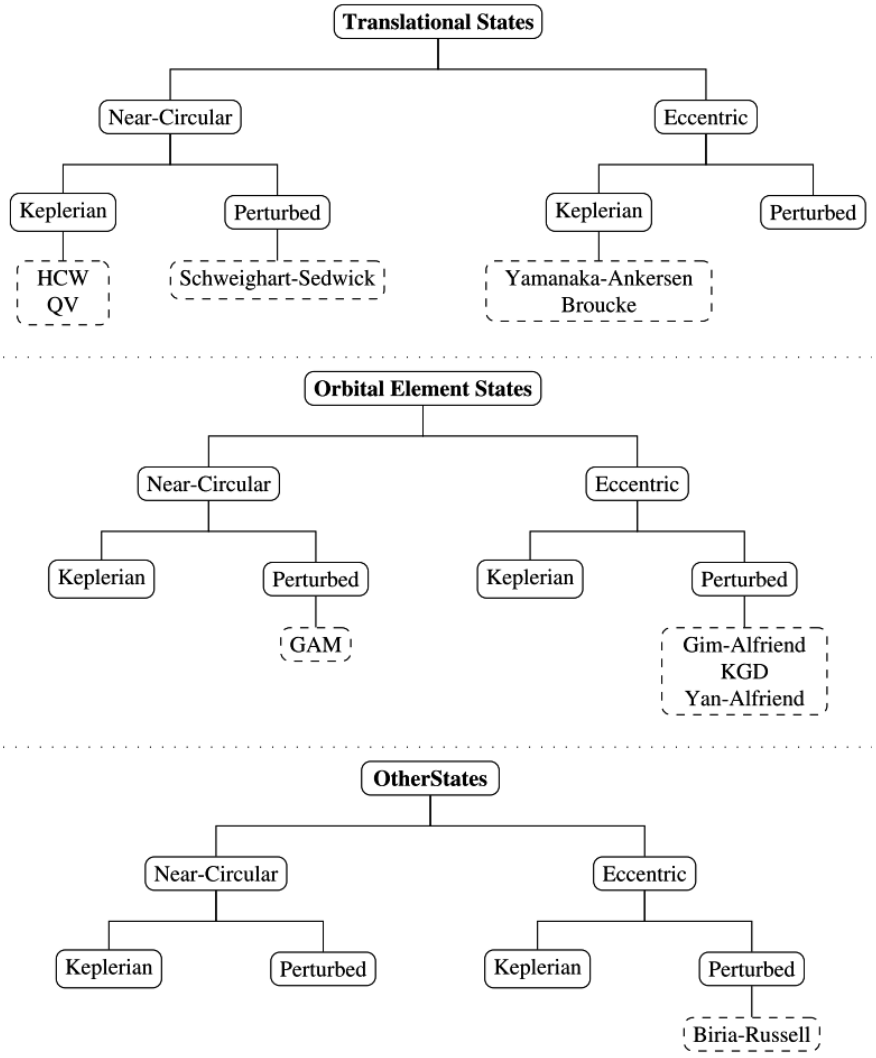


Figure 2.1: Categorization of closed-form relative dynamics models from [85]

- The gravitating bodies are spherical.
- There are no tidal forces.
- The primary's mass is much larger than the orbiting body's mass.
- The gravitational force is Newtonian.

In the category of Keplerian, near circular models, the Clohessy and Wiltshire model [43] used the Keplerian assumptions to derive a linearized form of the equations of relative motion, for spacecraft in close formation. Here, the linearization is done by retaining only the first-order terms in the Taylor expansion of the nonlinear differential gravity Keplerian orbit models. The resulting equations are know as the Hill-Clohessy-Wiltshire equations (HCW).

From the HCW equations, works like [87] derive extensions of the model that incorporate effects like the Earth oblateness $J_2$ perturbation [85].

In the case of translational states, with Keplerian orbits, but assuming that the orbits have arbitrary eccentricities, the Yamanaka and Ankersen model [88] uses a fundamental integral solution written in terms of Kepler's equation to construct the state transition matrix (STM) of the closed-form solution. This result is considered the state-of-the-art solution for linear propagation of relative position and velocity in eccentric orbit, and it is planned to be used in the proposed Proba-3 from ESA [85].

In the case of representations that use orbital element states, the "GAM model" [89] revisits the description of the relative motion between satellites flying in near-circular low-Earth-orbits by describing the motion through relative orbital elements, taking into account both the Earth's oblateness and the differential drag perturbation.

The works of [90], [91] and [92] consist of analytical solutions that include the effects of the reference orbit eccentricity and differential perturbations used to arrive at a description using differential orbital elements.

A different method from both broad categories, shown in Figure 2.1 is the relative motion model including $J_2$ and $J_3$ via Vinti's intermediary [93].

In this thesis, the model used for the parametrization of the spacecraft orbit dynamics consist of a non-Keplerian rectilinear coordinates model. The selection of this spacecraft parametrization of dynamics is mainly based on three factors: the first factor is the convenience of the model description to incorporate external perturbations. External perturbations from, e.g. atmospheric drag, are the source of coupling between orbit and attitude dynamics analyzed in this dissertation. Therefore, they need to be incorporated directly to the dynamics equations. Orbital elements are not used here, because, even when there are models using orbital elements incorporating perturbations like the one presented in [84], nevertheless they rely on an approximation of the perturbing effect, not their direct physical expression.

The second factor is preference for classic parametrization over newly explored approaches. This is justified because a widespread knowledge of the parametrization. At the same time, the successful use of a classic approach to answer the re-

search questions in this thesis is considered a fundamental step before proceeding with other dynamics parametrization. For example, a parametrization not selected for this work is the use of dual numbers to describe orbit and attitude dynamics of spacecraft, as done in [94] for control purposes. Nevertheless, dual numbers to parametrize spacecraft absolute and relative pose is considered a promising field and can be a future research field based on this dissertation.



The third factor is that the approach used for this thesis does not require any simplification to be used for any kind of complex scenario, since it is not linked to e.g. circular orbits.

In this research, the attitude of spacecraft is described using the quaternion representation, due to its extended use in the satellite attitude dynamics community. At the same time, because it allows to describe the attitude rate of change using the rotation rate, this approach allows the addition of any source of torque using its direct physical description, a requirement imposed in this research.

The absolute orbit dynamics of the chief is described using Cartesian coordinates, related to an Earth-centered inertial frame. For the case of the relative dynamics, a spacecraft-centered frame is used to describe the relative dynamics of the deputy spacecraft with respect to its chief.

A fundamental assumption in this research is that all reference frames used are known by the chief spacecraft.

### 2.2.1. Reference Frames

In order to describe spacecraft dynamics, the definition of the reference frames to be used is fundamental. Their selection obeys many criteria. For example, the selection of the frame may depend on the measuring scenario: the relative position of a ”Deputy” spacecraft is described using a frame fixed to a ”Chief” spacecraft. The attitude relative dynamics are described with respect to the body frame of the spacecraft from which measurements are done, due to the fact that the attitude sensors are fixed to its body. Other frames may be related to celestial bodies (the Earth, the sun), or to the position of stars (when using a Star Tracker). For example, in [48] an inertial frame is used to describe spacecraft orbit relative dynamics, and body frames are used to describe the attitude relative dynamics. Nevertheless, for this work, a frame fixed to and co-moving with the Chief spacecraft, as the one used in [86] is used to describe the relative orbit dynamics.

In order to describe the complete orbit and attitude dynamics of two spacecraft flying in formation, different frames are used. Due to the fact that this thesis is related to cross-relations between orbit and attitude states described in different frames, several transformations are necessary to describe all existing relations between the system states.

If a single inertial frame is used to describe all dynamics of the two satellites, all attitude dynamics would have to be translated to this frame description, leading to an unconventional, not particularly suited, attitude description. For example, given the fact that attitude sensors are usually attached to the spacecraft body, the use of a body frame to describe the dynamics description would be, in any case, unavoidable for estimation purposes. The use of a body frame for the description

of orbit dynamics would lead to similar kind of difficulties.

Finally, due to the fact that, for this work, it is necessary to analytically determine the linearization of all dynamics with respect to the spacecraft states (Eq. 2.30), all rotations are described as a function of such states.

2

In the sequel, the frames that are used in this work are described. All the rotations necessary in order to properly describe the complete coupled dynamics are described in Section 2.6 since the rotation depends on the state definitions done later in this Chapter.

#### Inertial Frame

Let $\mathcal{I}$ denote a inertial geocentric Cartesian, right-handed coordinate frame. The $x$-axis is directed to the vernal equinox direction, the $z$-axis is parallel to the axis of rotation of the Earth and the $y$-axis completes a right-hand orthogonal axis frame [95, p. 365]. In this work, $\mathcal{I}$ is denoted the Inertial Frame. In the following $\mathcal{I}$ will be the only considered inertial frame without loss of generality.

#### Euler-Hill Frame

Let $\mathcal{E}$ denote a local-vertical, local-horizontal (LVLH) rotating, right-handed, coordinate frame fixed to the chief spacecraft (S/C 1) . It is called the Euler-Hill frame (see Fig. 2.2). In $\mathcal{E}$, the $x$-axis points from the S/C 1 center of mass radially outwards, the $z$-axis points in the direction of the S/C 1 orbital angular momentum, and the $y$-axis completes the frame [86, Ch.4].

#### Body Frames

Consider two spacecraft, S/C 1 (chief) and S/C 2 (deputy), orbiting the Earth. Let $\mathcal{B}_1$ and $\mathcal{B}_2$ denote the spacecraft-centered Cartesian right-handed coordinate frames with origins at the spacecraft centers of mass of S/C 1 and S/C 2 respectively. For the body frames, the z-axis points in the direction of the highest moment of inertia, and the x and y-axes are parallel to the area vectors of the faces of the spacecraft (see Fig. 2.3 ).

## 2.3. Single Spacecraft Dynamics

In this section the orbit and attitude kinematics and dynamics of a single spacecraft are defined. Kinematics are defined as aspects of motion that can be analyzed without the consideration of forces or torques [96]. If forces or torques are involved the description is in the realm of dynamics.

### 2.3.1. Single Spacecraft Attitude

The description of the orientation of an object is a mathematical problem that has been studied since Euler, and has subsequently been developed by scholars like Jacobi, Hamilton, Cayley, Klein, Rodrigues and Gibbs [40].

The proper selection of the method to describe the attitude of the system and the appropriate reference frame to use depends greatly on the application to be used.

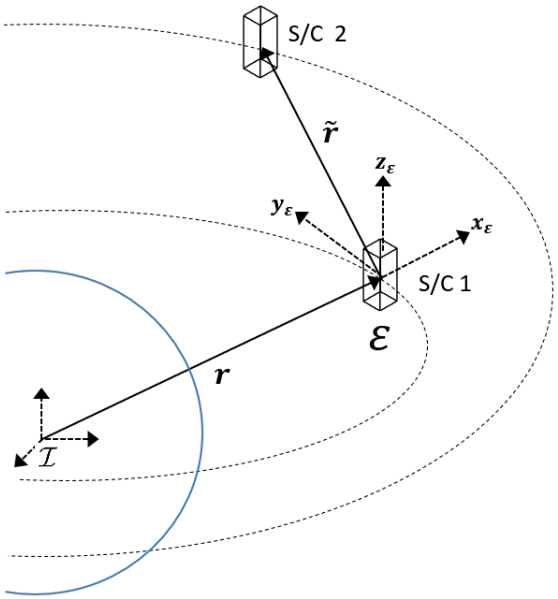


Figure 2.2: Definition of the Orbital Frame ($\mathcal{E}$)

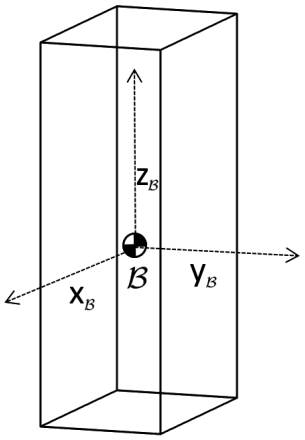


Figure 2.3: Definition of the Body Frame ($\mathcal{B}$)

In this work, it will always be assumed that spacecraft are rigid body systems. Nevertheless, all results from this thesis may be applied to flexible body system with little changes. In [40] a list of consideration about rigid body attitude coordinates is listed:



1. A minimum of three coordinates is required to describe the relative angular displacement between two reference frames.
2. Any minimal set of three attitude coordinates will contain at least one geometrical orientation where the coordinates are singular, namely at least two coordinates are undefined or not unique.
3. At or near such a geometric singularity, the corresponding kinematic differential equations are also singular.
4. The geometric singularities and associated numerical difficulties can be avoided altogether through a regularization. Redundant sets of four or more coordinates exist which are universally determined and contain no geometric singularities.

In order to avoid those singularities, the parametrization of attitude using quaternions has been selected in this work to describe the attitude of spacecraft.

### Attitude Kinematics

Consider two reference frames $\mathcal{N}$ and $\mathcal{B}$ defined using an orthonormal right-handed set of unit vectors $\hat{\boldsymbol{n}} \equiv [\hat{\boldsymbol{n}}_1, \hat{\boldsymbol{n}}_2, \hat{\boldsymbol{n}}_3]^T$ and $\hat{\boldsymbol{b}} \equiv [\hat{\boldsymbol{b}}_1, \hat{\boldsymbol{b}}_2, \hat{\boldsymbol{b}}_3]^T$. Let the three angles $\alpha_{1i}$ be the angles between the first coordinate $\hat{\boldsymbol{b}}_1$ and the axes of $\hat{\boldsymbol{n}}$. The cosines of these angles are called the direction cosines of $\hat{\boldsymbol{b}}_1$ relative to the $\mathcal{B}$ frame [40]. The unit vector $\hat{\boldsymbol{b}}_1$ can be projected onto $\hat{\boldsymbol{n}}$ as

$$\hat{\boldsymbol{b}}_1 = \cos(\alpha_{11})\hat{\boldsymbol{n}}_1 + \cos(\alpha_{12})\hat{\boldsymbol{n}}_2 + \cos(\alpha_{13})\hat{\boldsymbol{n}}_3 \tag{2.1}$$

These angles are illustrated in Figure 2.4 Expanding this result for the three unit vectors of $\boldsymbol{a}$, it is possible to describe the relation between the two vectors as

$$\hat{\boldsymbol{b}} = \begin{bmatrix} cos(\alpha_{11}) & cos(\alpha_{12}) & cos(\alpha_{13}) \\ cos(\alpha_{21}) & cos(\alpha_{22}) & cos(\alpha_{23}) \\ cos(\alpha_{31}) & cos(\alpha_{32}) & cos(\alpha_{33}) \end{bmatrix} \boldsymbol{n} = \boldsymbol{D}\hat{\boldsymbol{n}} \tag{2.2}$$

,

where the matrix $\boldsymbol{D}$ is called the direction cosine matrix (DCM).

The DCM is a parametrization of the attitude of a body with respect to a reference frame $\mathcal{N}$. There are other parametrizations that may be more convenient depending on the application. These applications are summarized in Table 2.1.

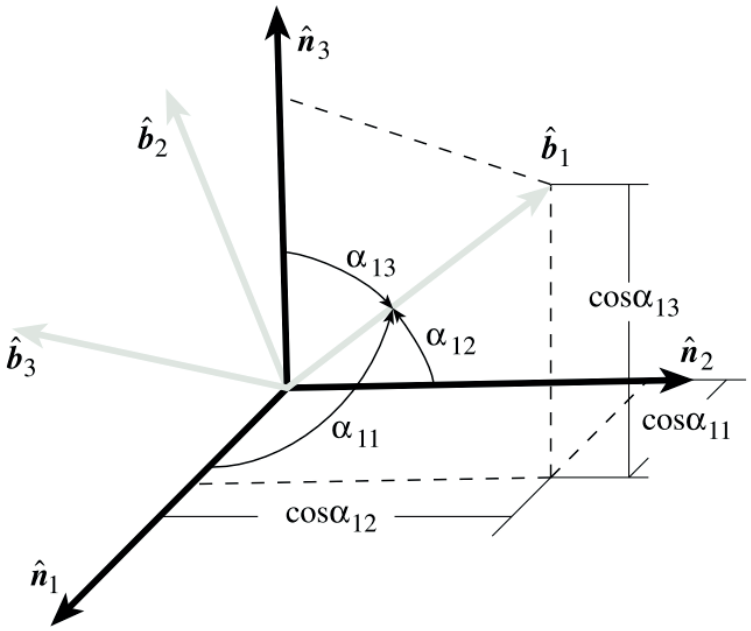


Figure 2.4: Direction cosines. Source [40]

| Parametrization | Advantages | Disadvantages | Common applications |
|---|---|---|---|
| Direction Cosine Matrix (DCM) | No Singularities. No Trigonometric Functions. Convenient product rule for successive rotations | Six redundant parameters | In analysis, to transform vectors from one reference frame to another |
| Euler Axis/Angle | Clear physical interpretation | One redundant parameter. Axis undefined when the sin of the angle used is equal to zero. . Trigonometric functions | Commanding slew maneuvers |
| Euler symmetric parameters (quaternion) | No Singularities. No trigonometric functions. Convenient product rule for successive rotations | One redundant parameter. No obvious physical interpretation. | Onboard inertial navigation |
| Gibbs Vector | No redundant parameters. No trigonometric functions. Convenient product rule for successive rotations | Infinite for 180-degree rotations | Analytic studies |
| Euler Angles | No redundant parameters. Physical interpretation is clear in some cases | Trigonometric functions. Singularity at some angles. No convenient product rule for successive rotations | Analytic Studies. Input/output onboard attitude control of 3-axis stabilized spacecraft |

Table 2.1: Alternative Representations of Three-Axis Attitude [39]

### Attitude Description using Quaternions

In this work, the selected parametrization for the description of attitude is the quaternion, often also known as the "Euler-Rodrigues" parameters [96]. Quaternions have multiple advantages in comparison to other attitude parametrizations. For example, on the Euler angle parametrization the propagation of attitude is not smooth. This smoothness is however fundamental for the proper performance of estimation methods like the Kalman Filter.

Another well-known attitude parametrization is the aforementioned rotation matrix between two frames, where usually one inertial frame is being used as a reference. The disadvantage of this method is that it leads to a description of attitude using nine non-independent elements, and it obeys six constraints imposed by the orthogonality of the attitude matrix.

The least amount of elements that may be used to describe attitude without singularities is four. Starting from the fact that any rotation may be described using a single rotation axis and an angle describing the rotation about this axis, the quaternion is defined by 4-elements, with a vector part $\boldsymbol{e}$ and scalar part $q$ given as [96, 97]

$$\boldsymbol{q} = \begin{bmatrix} \boldsymbol{e} \\ q \end{bmatrix} \tag{2.3}$$

where

$$\boldsymbol{e} = \hat{\boldsymbol{e}} \sin(\vartheta), q = \cos(\vartheta) \tag{2.4}$$

with $\hat{\boldsymbol{e}}$ being a unit vector defining an axis of rotation (or Euler axis) and $\vartheta$ being the angle of rotation around this axis. This parametrization has only one constraint.

Let $\Xi(\boldsymbol{q})$ denote

$$\Xi(\boldsymbol{q}) = \begin{bmatrix} \boldsymbol{e}^{\times} + q\mathbf{1}_3 \\ -\boldsymbol{e}^T \end{bmatrix} \text{ with } \boldsymbol{e}^{\times} = \begin{bmatrix} 0 & -e_3 & e_2 \\ e_3 & 0 & -e_1 \\ -e_2 & e_1 & 0 \end{bmatrix}. \tag{2.5}$$

From here, we can define the kinematics of a spacecraft using quaternions as [39]

$$\dot{\boldsymbol{q}} = \frac{1}{2}\Xi(\boldsymbol{q})\boldsymbol{\omega}. \tag{2.6}$$

The quaternions used for rotation purposes are quaternions with a unit norm, by the definition given in equation 2.4 [96]. By using a unit vector as the axis of rotation, there is only one way to describe a single rotation using this method. For estimation purposes, the quaternions parametrization has the problem that its elements are not-linear independent. Several versions of the Extended Kalman Filter (EKF), as the additive EKF, or the Multiplicative EKF, among others, have been developed to overcome this problem (see [97] for a survey in nonlinear attitude estimation methods).

### Attitude Dynamics

The fundamental equation of attitude dynamics describes the variation of the angular momentum vector $d\boldsymbol{L}/dt$ to an applied torque $\boldsymbol{\tau}$ [39, Chap.16] in the spacecraft body frame ($\mathcal{B}$)

$$\frac{d\boldsymbol{L}}{dt} = -\boldsymbol{\omega}^{\times}\boldsymbol{L} + \boldsymbol{\tau} \tag{2.7}$$

and the torque defined as

$$\boldsymbol{\tau} \equiv \sum_{i=1}^{n} \boldsymbol{d}_i^{\times}\boldsymbol{F}_i, \tag{2.8}$$

with $\boldsymbol{\omega}$ being the instantaneous angular velocity vector of the body, and $\boldsymbol{F}_i$ the applied force vector located in a point $\boldsymbol{d}_i$ from the point of view of the center of mass of the body. $\boldsymbol{I}$ is a symmetric 3x3 moment of inertia tensor, with

$$\boldsymbol{L} = \boldsymbol{I}\boldsymbol{\omega}. \tag{2.9}$$

In this work, $\boldsymbol{I}$ is assumed a constant matrix.

Using (2.9) in (2.8) it is possible to arrive at an expression for attitude dynamics used in this work

$$\boldsymbol{I}\frac{d\boldsymbol{\omega}}{dt} = -\boldsymbol{\omega}^{\times}\boldsymbol{I}\boldsymbol{\omega} + \boldsymbol{\tau}. \tag{2.10}$$

A spacecraft in an orbit about the Earth is subject to various torques. There are torques originated from the spacecraft and its environment, leading to gravity-related torques, torques due to atmospheric solar radiation or electromagnetic field. Here, we assume that one of the angular torques affecting spacecraft is due to the fact that the gravitational field is not uniform over the spacecraft's body. This leads to a gravitational torque about the mass center [98]. If the following assumptions are made

- only the Earth body is considered,
- the Earth a spherically symmetrical mass distribution,
- the spacecraft is small compared to its distance from the mass center of the Earth,
- the spacecraft consist of a single body,

the gravitational torque in the inertial frame is given by

$$\boldsymbol{\tau}_g = 3\frac{\mu}{r^5}\boldsymbol{r}^{\times}\boldsymbol{I}\boldsymbol{r} \tag{2.11}$$

with $\mu = 398600.4405 \pm 0.001$ km$^3$s$^{-2}$ the gravitational coefficient of Earth, $\boldsymbol{r}$ is the position of the spacecraft with respect to the center of the Earth. When this torque is expressed in $\mathcal{B}$, then it is given by

$$\boldsymbol{\tau}_g = 3\frac{\mu}{r^5}(D(\boldsymbol{q})\boldsymbol{r})^{\times}(\boldsymbol{I}D(\boldsymbol{q})\boldsymbol{r}). \tag{2.12}$$

Another torque affecting spacecraft at very low attitudes is the atmospheric drag torque. The effect of atmospheric drag is the focus of this thesis and thus it is described in more detail in the next chapter.



### 2.3.2. Spacecraft Orbit Dynamics

If the mass of a satellite is considered negligible compared to Earth's mass, and under the assumption that the Earth is spherically symmetric, the acceleration $\ddot{\boldsymbol{r}}$ of a satellite is given by the Newton's law of gravity [41]

$$\ddot{\boldsymbol{r}} = -\frac{GM_E}{r^3}\boldsymbol{r} \tag{2.13}$$

where $GM_E$ is known as the gravitational coefficient of the Earth and given by

$$\mu = GM_E = 398600.4405 \pm 0.001 \text{ km}^3\text{s}^{-2} \tag{2.14}$$

Due to its rotation the Earth is not a perfect sphere. Its form is approximately the one of an oblate spheroid with an equatorial diameter that is about 20 km larger than the polar diameter [41]. If the Earth form is approximated to an oblate sphere, the effect caused by the oblateness perturbation is called $J_2$ effect [40]. This effect is considered negligible in this research due to the fact that only equatorial orbits are used. Another force affecting spacecraft at very low attitudes is the atmospheric drag perturbation. The effect of atmospheric drag is the focus of this thesis and thus it is described in more detail in the next chapter.

## 2.4. Relative Spacecraft Dynamics

Here the relative orbit and attitude dynamics of a follower (deputy) spacecraft are described with respect to a leader (chief) satellite.

### 2.4.1. Relative Spacecraft Attitude

Let $\boldsymbol{\omega}$ denote the angular velocity vector of the frame $\mathcal{B}$ with respect to $\mathcal{I}$ projected along $\mathcal{B}$. Let $\boldsymbol{q}$, with vector part $\boldsymbol{e}$ and scalar part $q$, denote the quaternion of the rotation from $\mathcal{I}$ to $\mathcal{B}$. Let $\mathbf{1}_3$ be the identity matrix in $\mathbb{R}^3$.

Finally, define $\tilde{\boldsymbol{q}} = (\tilde{\boldsymbol{e}}, \tilde{q})$ and $\tilde{\boldsymbol{\omega}}$ as the relative quaternion and relative angular velocity vector, respectively, of S/C 2 with respect to S/C 1, defined as

$$\tilde{\boldsymbol{q}} = (\boldsymbol{q}_{\mathcal{B}_1})^{-1} * \boldsymbol{q}_{\mathcal{B}_2} \tag{2.15}$$

$$\tilde{\boldsymbol{\omega}} = \boldsymbol{\omega}_2|_{\mathcal{B}2} - \boldsymbol{\omega}|_{\mathcal{B}2} \tag{2.16}$$

with $\boldsymbol{q}_{\mathcal{B}_2}$ the quaternion of rotation from $\mathcal{I}$ to $\mathcal{B}_2$ and $\boldsymbol{\omega}_2|_{\mathcal{B}2}$ the rotation rate of $\mathcal{B}_2$ with respect to $\mathcal{I}$ projected in $\mathcal{B}_2$. Here, $\boldsymbol{q}^{-1}$ and $*$ denote the quaternion inverse and

composition operations, respectively [39, App. D]. According to [48] the attitude dynamics of the follower spacecraft relative to the leader spacecraft is given by

$$\dot{\tilde{\boldsymbol{\omega}}} = \boldsymbol{I}_2^{-1}\{\boldsymbol{I}_2\,[\boldsymbol{D}(\tilde{\boldsymbol{q}})\,\boldsymbol{\omega}+\tilde{\boldsymbol{\omega}}]\times[\boldsymbol{D}(\tilde{\boldsymbol{q}})\,\boldsymbol{\omega}+\tilde{\boldsymbol{\omega}}] - \boldsymbol{I}_2\,[\boldsymbol{D}(\tilde{\boldsymbol{q}})\,\boldsymbol{\omega}+\tilde{\boldsymbol{\omega}}]\times\tilde{\boldsymbol{\omega}} - \boldsymbol{I}_2\boldsymbol{D}(\tilde{\boldsymbol{q}})\boldsymbol{I}_1^{-1}\,[(\boldsymbol{I}_1\,\boldsymbol{\omega})\times\boldsymbol{\omega}+\boldsymbol{\tau}_1]+\boldsymbol{\tau}_2\}, \tag{2.17}$$

with $\boldsymbol{I}_2$ is the inertia tensor of the deputy spacecraft around its center of mass in the frame $\mathcal{B}_2$, and $\boldsymbol{D}(\tilde{\boldsymbol{q}})$ denotes the matrix of the rotation from $\mathcal{B}_1$ to $\mathcal{B}_2$, i.e.:

$$\boldsymbol{D}(\tilde{\boldsymbol{q}}) = (\tilde{q}^2 - \tilde{\boldsymbol{e}}^T\tilde{\boldsymbol{e}})\mathbf{1}_3 + 2\tilde{\boldsymbol{e}}\tilde{\boldsymbol{e}}^T - 2\,q\tilde{\boldsymbol{e}}^{\times}. \tag{2.18}$$

### 2.4.2. Relative Spacecraft Orbit

Let $\boldsymbol{r}$ and $\boldsymbol{r}_2$ be the position vector of the center of mass of a chief and a deputy spacecraft, respectively, measured from the center of the Earth, and let $\tilde{\boldsymbol{r}}$ and $\tilde{\boldsymbol{v}}$ denote the relative position and velocity vectors of S/C 2 with respect to S/C 1 , i.e,

$$\tilde{\boldsymbol{r}} = \boldsymbol{r}_2 - \boldsymbol{r} \tag{2.19}$$

$$\tilde{\boldsymbol{v}} = \frac{d\tilde{\boldsymbol{r}}}{dt}. \tag{2.20}$$

Let $(\tilde{r}_x, \tilde{r}_y, \tilde{r}_z, \tilde{v}_x, \tilde{v}_y, \tilde{v}_z)$ denote the components of $\tilde{\boldsymbol{r}}$ and $\tilde{\boldsymbol{v}}$ respectively.

Taking Eq. 2.13 to describe the position of each spacecraft, we have that [86]

$$\dot{\tilde{\boldsymbol{v}}} = -\frac{\mu\tilde{\boldsymbol{r}}}{\tilde{r}^3} + \frac{\mu\boldsymbol{r}}{r^3} \tag{2.21}$$

In order to express the relative acceleration in $\mathcal{E}$, it must be considered that [86, Ch.4]

$$\ddot{\tilde{\boldsymbol{r}}} = \frac{d^2\tilde{\boldsymbol{r}}}{dt^2} + 2\boldsymbol{\Omega}^{\times}\frac{d\tilde{\boldsymbol{r}}}{dt} + \frac{d\boldsymbol{\Omega}^{\times}}{dt}\,\tilde{\boldsymbol{r}} + \boldsymbol{\Omega}^{\times}(\boldsymbol{\Omega}^{\times}\tilde{\boldsymbol{r}}) \tag{2.22}$$

where $\boldsymbol{\Omega}$ denotes the angular velocity vector of frame $\mathcal{E}$ relative to frame $\mathcal{I}$.

Due to the definition of the orbital frame, we have that

$$\boldsymbol{\Omega}|_{\mathcal{E}} = \boldsymbol{\Omega} = \begin{bmatrix} 0 \\ 0 \\ \Omega \end{bmatrix}. \tag{2.23}$$

Expressing $\Omega$ as a function of the spacecraft states, we have that

$$\Omega = \frac{|\boldsymbol{r}^{\times}\boldsymbol{v}|}{|\boldsymbol{r}|^2}, \tag{2.24}$$

$$\dot{\Omega} = \frac{(\boldsymbol{r}^{\times}\boldsymbol{v})^T(\boldsymbol{r}^{\times}\dot{\boldsymbol{v}})}{|r|^2|\boldsymbol{r}^{\times}\boldsymbol{v}||} - 2 * |\boldsymbol{r}^{\times}\boldsymbol{v}|\frac{\boldsymbol{r}^T\boldsymbol{v}}{|\boldsymbol{r}|^4}, \tag{2.25}$$

and the position vector of the Chief in $\mathcal{E}$ is

$$\boldsymbol{r} = \begin{bmatrix} r \\ 0 \\ 0 \end{bmatrix}. \tag{2.26}$$

If (2.23), (2.26) and (2.22) are substituted in (2.21), it yields to the following equations of relative orbital motion in $\mathcal{E}$

$$\dot{\tilde{\boldsymbol{r}}} = \tilde{\boldsymbol{v}} \tag{2.27}$$

$$\dot{\tilde{\boldsymbol{v}}} = \begin{bmatrix} \frac{\mu}{r^2} - \frac{\mu(r+\tilde{r}_x)}{\alpha^3} + 2\Omega\tilde{v}_y + \dot{\Omega}\tilde{r}_y + \Omega^2\tilde{r}_x + \Delta a_{p_x} \\ -\frac{\mu\tilde{r}_y}{\alpha^3} - 2\Omega\tilde{v}_x - \dot{\Omega}\tilde{r}_x + \Omega^2\tilde{r}_y + \Delta a_{p_y} \\ -\frac{\mu\tilde{r}_z}{\alpha^3} + \Delta a_{p_z} \end{bmatrix}. \tag{2.28}$$

with

$$\alpha = \sqrt{(r+\tilde{r}_x)^2 + \tilde{r}_y^2 + \tilde{r}_z^2} \tag{2.29}$$

and differential external forces given by $\Delta\boldsymbol{a_p} = [\Delta a_{p_x}, \Delta a_{p_y}, \Delta a_{p_z}]^T$.

## 2.5. Formation Flying Dynamics

Consider two spacecraft, S/C 1 (chief) and S/C 2 (deputy), orbiting the Earth.

Under the assumption of rigid bodies, the orbital and attitude dynamics of the two satellites is governed by the following system of equations [39, Ch. 16], [86, Ch. 4]

$$\dot{\boldsymbol{x}} = \begin{bmatrix} \dot{\boldsymbol{r}} \\ \dot{\boldsymbol{v}} \\ \dot{\boldsymbol{q}} \\ \boldsymbol{I}_1\dot{\boldsymbol{\omega}} \\ \dot{\tilde{\boldsymbol{r}}} \\ \dot{\tilde{\boldsymbol{v}}} \\ \dot{\tilde{\boldsymbol{q}}} \\ \dot{\tilde{\boldsymbol{\omega}}} \end{bmatrix} = \begin{bmatrix} \boldsymbol{v} \\ -\frac{\mu}{r^3}\boldsymbol{r} + \boldsymbol{a}_p \\ \frac{1}{2}\Xi(\boldsymbol{q})\boldsymbol{\omega} \\ -\boldsymbol{\omega}^{\times}\boldsymbol{I}_1\boldsymbol{\omega} + \boldsymbol{\tau}_1 \\ \tilde{\boldsymbol{v}} \\ \boldsymbol{p}(\boldsymbol{x}) + \Delta\boldsymbol{a_p} \\ \frac{1}{2}\Xi(\tilde{\boldsymbol{q}})\,\tilde{\boldsymbol{\omega}} \\ \mathrm{g}(\boldsymbol{\omega}_1, \tilde{\boldsymbol{\omega}}, \tilde{\boldsymbol{q}}) \end{bmatrix} \tag{2.30}$$

where

$$\boldsymbol{p}(x) = \begin{bmatrix} \frac{\mu}{r^2} - \frac{\mu(r+\tilde{r}_x)}{\alpha^3} + 2\Omega\tilde{v}_y + \dot{\Omega}\tilde{r}_y + \Omega^2\tilde{r}_x \\ -\frac{\mu\tilde{r}_y}{\alpha^3} - 2\Omega\tilde{v}_x - \dot{\Omega}\tilde{r}_x + \Omega^2\tilde{r}_y \\ -\frac{\mu\tilde{r}_z}{\alpha^3} \end{bmatrix}, \tag{2.31}$$

with differential external forces are given by $\Delta\boldsymbol{a_p} = [\Delta a_{p_x}, \Delta a_{p_y}, \Delta a_{p_z}]^T$ and

$$\begin{aligned} \mathrm{g}(\boldsymbol{x}) = \boldsymbol{I}_2^{-1}\{&\boldsymbol{I}_2\,[\boldsymbol{D}(\tilde{\boldsymbol{q}})\,\boldsymbol{\omega} + \tilde{\boldsymbol{\omega}}] \times [\boldsymbol{D}(\tilde{\boldsymbol{q}})\,\boldsymbol{\omega} + \tilde{\boldsymbol{\omega}}] - \boldsymbol{I}_2\,[\boldsymbol{D}(\tilde{\boldsymbol{q}})\,\boldsymbol{\omega} + \tilde{\boldsymbol{\omega}}] \times \tilde{\boldsymbol{\omega}} \\ &-\boldsymbol{I}_2\boldsymbol{D}(\tilde{\boldsymbol{q}})\boldsymbol{I}_1^{-1}\,[(\boldsymbol{I}_1\,\boldsymbol{\omega}) \times \boldsymbol{\omega} + \boldsymbol{\tau}_1] + \boldsymbol{\tau}_2\Big\}. \end{aligned} \tag{2.32}$$

Table 2.2: Description of rotations

| From | To | Notation / (Inverse rotation notation) | Components of the state dependency |
|---|---|---|---|
| $\mathcal{I}$ | $\mathcal{E}$ | $\boldsymbol{D}\|_{\mathcal{I}}^{\mathcal{E}}$ /($\boldsymbol{D}\|_{\mathcal{E}}^{\mathcal{I}}$) | $\boldsymbol{r},\boldsymbol{v}$ |
| $\mathcal{I}$ | $\mathcal{B}_1$ | $\boldsymbol{D}^T(\boldsymbol{q})$/($\boldsymbol{D}(\boldsymbol{q})$) | $\boldsymbol{q}$ |
| $\mathcal{B}_1$ | $\mathcal{B}_2$ | $\boldsymbol{D}(\tilde{\boldsymbol{q}})$/($\boldsymbol{D}^T(\tilde{\boldsymbol{q}})$) | $\tilde{\boldsymbol{q}}$ |
| $\mathcal{I}$ | $\mathcal{B}_2$ | $\boldsymbol{D}(\tilde{\boldsymbol{q}})\boldsymbol{D}^T(\boldsymbol{q})$/($\boldsymbol{D}(\boldsymbol{q})\boldsymbol{D}^T(\tilde{\boldsymbol{q}})$) | $\boldsymbol{q},\tilde{\boldsymbol{q}}$ |

Here, $\Omega$ denotes the absolute value of the angular velocity between the frames $\mathcal{I}$ and the $\mathcal{E}$, and $\boldsymbol{a}_p$ and $\boldsymbol{\tau}_1$ represent the external force and torque vectors perturbing the dynamics of S/C 1, while $\Delta\boldsymbol{a_p}$ represents the differential acceleration affecting the relative orbital dynamics and $\boldsymbol{\tau}_2$ the total torque acting on the deputy spacecraft.

This model can therefore incorporate any external forces (e.g. $J_2$ , solar pressure, control forces), or torques (e.g. gravitational torques, control torques) influencing the spacecraft dynamics. For this reason, this equation is valid for any orbiting two-spacecraft system, no matter its altitude, relative distance, inclination, or how elliptical their orbits are. In this work, the external forces ($\boldsymbol{a}_p, \Delta a_p, \boldsymbol{\tau}_1$ and $\boldsymbol{\tau}_2$) are associated to atmospheric drag only. They are the source of coupling between orbit ant attitude dynamics, due to the fact that the atmospheric drag effect depends of the orientation of the spacecraft. The full description of this effect is the subject of Chapter 3.

## 2.6. Transformations of Reference Frames

Several rotations between frames are needed in this work in order to derive the expressions for the spacecraft state and its perturbations. Most of these frames are accelerating frames. Due to this fact, the kinematics of rotating frames also have to be taken into account in the description of the states of this work. These rotations are listed on Table 2.2.

These rotations are illustrated in Figure 2.5.

### 2.6.1. Rotation from the Inertial to the Euler-Hill Frame

In order to rotate a vector from the Earth-centered inertial frame $\mathcal{I}$ to the Euler-Hill frame centered in the chief spacecraft ($\mathcal{E}$), the absolute position $\boldsymbol{r}$ vector and the velocity vector $\boldsymbol{v}$ are used. These frames are used to describe the dynamics of the Chief spacecraft and the relative dynamics of the Deputy spacecraft with respect to the Chief, respectively.

Euler rotations are used to derive the corresponding rotation matrices, but these derivations are done such that all matrices are functions only of the state components of the dynamics derived defined for this work, given by equation 2.30. Classically, these rotation matrices use trigonometric functions as part of their expression. These trigonometric functions are expressed as a function of the state components,

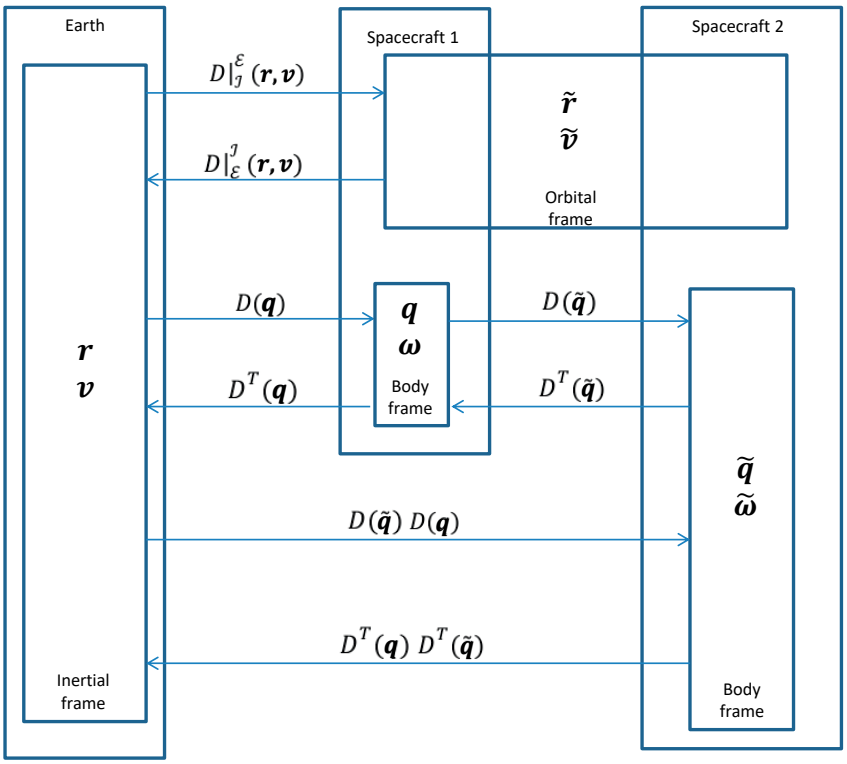


Figure 2.5: Rotations necessary to describe the relative dynamics of two spacecraft using Cartesian coordinates and the quaternion description of attitude.

enabling the possibility of linearization of the equations of the dynamics with respect to the states in a straightforward way. This linearization is necessary for the observability analysis done in Chapter 5 and the use of the Extended Kalman Filter of Chapter 6.

2

Using a "1-2-1" Euler rotation [39], with the first rotation is given by a rotation of the $x$ axis by an angle $\varphi$, lets replace the trigonometric functions by

$$\cos\varphi = \frac{r_3}{\sqrt{{r_2}^2 + {r_3}^2}}, \sin\varphi = -\frac{r_2}{\sqrt{{r_2}^2 + {r_3}^2}}. \tag{2.33}$$

For this reason, the first rotation is given by

$$\boldsymbol{D}(\varphi) = \frac{1}{\sqrt{{r_2}^2 + {r_3}^2}} \begin{bmatrix} \sqrt{{r_2}^2 + {r_3}^2} & 0 & 0 \\ 0 & r_3 & -r_2 \\ 0 & r_2 & r_3 \end{bmatrix}. \tag{2.34}$$

The second rotation is given by an angle $\theta$ as

$$\cos\theta = \frac{r_1}{\sqrt{{r_1}^2 + {r_2}^2 + {r_3}^2}} = \frac{r_1}{r} \tag{2.35}$$

$$\sin\theta = -\frac{\sqrt{{r_2}^2 + {r_3}^2}}{\sqrt{{r_1}^2 + {r_2}^2 + {r_3}^2}} = -\frac{\sqrt{{r_2}^2 + {r_3}^2}}{r}. \tag{2.36}$$

So

$$\boldsymbol{D}(\theta) = \frac{1}{r} \begin{bmatrix} r_1 & 0 & \sqrt{{r_2}^2 + {r_3}^2} \\ 0 & r & \\ -\sqrt{r_2^2 + r_3^2} & 0 & r_1 \end{bmatrix}. \tag{2.37}$$

Expressing the third rotation requires the velocity vector expression after the first two rotations. Lets define this velocity vector as

$$\boldsymbol{v}' = \boldsymbol{D}(\theta)\boldsymbol{D}(\varphi)\boldsymbol{v} \tag{2.38}$$

meaning that

$$\boldsymbol{v}' = \frac{1}{r}\frac{1}{\sqrt{{r_2}^2 + {r_3}^2}} \begin{bmatrix} r_1 & 0 & \sqrt{{r_2}^2 + {r_3}^2} \\ 0 & r & \\ -\sqrt{{r_2}^2 + {r_3}^2} & 0 & r_1 \end{bmatrix} \begin{bmatrix} \sqrt{{r_2}^2 + {r_3}^2} & 0 & 0 \\ 0 & r_3 & r_2 \\ 0 & -r_2 & r_3 \end{bmatrix} \boldsymbol{v}. \tag{2.39}$$

The angle required for the third rotation $\psi$ is given as a function of $\boldsymbol{v}'$ as

$$\cos\psi = \frac{\boldsymbol{v}'_y}{\sqrt{{\boldsymbol{v}'_y}^2 + {\boldsymbol{v}'_z}^2}}, \sin\varphi = \frac{\boldsymbol{v}'_z}{\sqrt{{\boldsymbol{v}'_y}^2 + {\boldsymbol{v}'_z}^2}}. \tag{2.40}$$

This leads to

$$\boldsymbol{D}(\psi) = \frac{1}{\sqrt{\boldsymbol{v'}_y{}^2 + \boldsymbol{v'}_z{}^2}} \begin{bmatrix} \sqrt{\boldsymbol{v'}_y{}^2 + \boldsymbol{v'}_z{}^2} & 0 & 0 \\ 0 & \boldsymbol{v'}_y & \boldsymbol{v'}_z \\ 0 & -\boldsymbol{v'}_z & \boldsymbol{v'}_y \end{bmatrix}. \tag{2.41}$$

The full transformation to rotate a vector from $\mathcal{I}$ to $\mathcal{E}$ as a function of the spacecraft system states is therefore

$$\begin{aligned} \boldsymbol{D}|_{\mathcal{E}}^{\mathcal{I}} \;=\; & \boldsymbol{D}(\psi)\boldsymbol{D}(\theta)\boldsymbol{D}(\varphi) = \\ & \frac{1}{r}\frac{1}{\sqrt{r_2{}^2 + r_3{}^2}}\frac{1}{\sqrt{\boldsymbol{v}'_y{}^2 + \boldsymbol{v}'_z{}^2}} \begin{bmatrix} \sqrt{\boldsymbol{v'}_y{}^2 + \boldsymbol{v'}_z{}^2} & 0 & 0 \\ 0 & \boldsymbol{v'}_y & \boldsymbol{v'}_z \\ 0 & -\boldsymbol{v'}_z & \boldsymbol{v'}_y \end{bmatrix} \\ & \begin{bmatrix} r_1 & 0 & \sqrt{r_2{}^2 + r_3{}^2} \\ 0 & r & \\ -\sqrt{r_2{}^2 + r_3{}^2} & 0 & r_1 \end{bmatrix} \begin{bmatrix} \sqrt{r_2{}^2 + r_3{}^2} & 0 & 0 \\ 0 & r_3 & r_2 \\ 0 & -r_2 & r_3 \end{bmatrix}. \end{aligned} \tag{2.42}$$

### Rotation Rate from the Inertial to the Euler-Hill Frame

It is known that the rotation of $\mathcal{E}$ with respect to $\mathcal{I}$ described in $\mathcal{E}$ $\Omega|_{\mathcal{E}}^{\mathcal{I}\to\mathcal{E}}$ is normal to its $\mathcal{E}$ frame. For this reason it may be described as

$$\Omega|_{\mathcal{E}}^{\mathcal{I}\to\mathcal{E}} = \begin{bmatrix} 0 \\ 0 \\ \dot{\theta} \end{bmatrix} \tag{2.43}$$

where $\dot{\theta}$ is the true anomaly of the spacecraft. It is necessary to express this value in the Cartesian coordinate frame that its being used to represent the absolute dynamics of the spacecraft. Since

$$\Omega|_{\mathcal{E}}^{\mathcal{I}\to\mathcal{E}} = \frac{\boldsymbol{r}^{\times}\boldsymbol{v}}{r^2} \tag{2.44}$$

the true anomaly is obtained as

$$\dot{\theta} = \left|\frac{\boldsymbol{r}^{\times}\boldsymbol{v}}{\boldsymbol{r}^2}\right|. \tag{2.45}$$

## 2.6.2. Rate of Change of Vectors in Rotating Frames

In this work, frames like the Euler-Hill frame and the body frames are accelerating frames. In order to express the rate of change of a vector firstly defined in an inertial frame in a rotating frame, the rotation rate between these frames has to be taken into account.

Let $\boldsymbol{a}|_{\mathcal{I}}$ be any vector on an inertial frame $\mathcal{I}$. Now, lets assume that there is a non-inertial rotating frame $N$ and denote this vector projected in this frame as $\boldsymbol{a}|_N$. Then, there exist a rotation matrix $\boldsymbol{A}$ relating the vector in both frames such that

$$\boldsymbol{a}|_N = \boldsymbol{A}\,\boldsymbol{a}|_{\mathcal{I}}\,. \tag{2.46}$$

For convenience, from now on, we denote $\boldsymbol{a}|_N$ as $\boldsymbol{a}$. The derivative of $\boldsymbol{a}$ in this expression is due to the time variation of both $\boldsymbol{a}|_{\mathcal{I}}$ and $\boldsymbol{A}$, where the variation of $\boldsymbol{A}$ results from the change of orientation of the two reference systems. For this reason, we have that [39, Ch. 16]

$$\frac{d\boldsymbol{a}}{dt} = \frac{d\boldsymbol{A}}{dt}\,\boldsymbol{a}|_{\mathcal{I}} + \boldsymbol{A}\frac{d\,\boldsymbol{a}|_{\mathcal{I}}}{dt}. \tag{2.47}$$

Given the fact that

$$\frac{d\boldsymbol{A}}{dt} = \Omega^{\times}\boldsymbol{A}, \tag{2.48}$$

with $\boldsymbol{\Omega} = [\Omega_u, \Omega_v, \Omega_w]^T$ the rotation rate of $N$ with respect to $\mathcal{I}$ and $\Omega^{\times}$ the skew-symmetric matrix

$$\Omega^{\times} = \begin{bmatrix} 0 & \Omega_w & -\Omega_v \\ -\Omega_w & 0 & \Omega_u \\ \Omega_v & -\Omega_u & \Omega \end{bmatrix}. \tag{2.49}$$

Given that $\boldsymbol{a} = \boldsymbol{A}\,\boldsymbol{a}|_{\mathcal{I}}$ then

$$\frac{d\boldsymbol{a}}{dt} = \dot{\boldsymbol{a}} = \Omega^{\times}\boldsymbol{a} + \mathring{\boldsymbol{a}}, \tag{2.50}$$

with $\mathring{\boldsymbol{a}}$ the derivative of $\boldsymbol{a}|_{\mathcal{I}}$ projected in the non-inertial frame $\boldsymbol{a}|_{\mathcal{I}}$, that is

$$\mathring{\boldsymbol{a}} = \boldsymbol{A}\frac{d\,\boldsymbol{a}|_{\mathcal{I}}}{dt}. \tag{2.51}$$

The apparent acceleration due to the rotation of a frame with respect to another, shown in equation 2.50 is known as the Coriolis effect. It has to be taking into account whenever a vector expressed in an accelerated frame is transformed into another frame, for example between any inertial to any body frame, or from an inertial frame to an Euler-Hill frame.

# 3

# Atmospheric Perturbations of Relative Dynamics

*This chapter describes how the atmospheric drag force and torque constitute a source of coupling between attitude and position for both the absolute and the relative dynamics of spacecraft. The expressions of the atmospheric perturbations of a deputy spacecraft as a function of its relative dynamics with respect to a chief spacecraft are derived. This allows to handle complex mission scenarios, such as formations with spacecraft that differ in their rotational states, or rendez-vous with uncontrolled objects with purposes of debris removal. Finally, the difference is shown between this advanced model for timely varying cross-section areas of the spacecraft and a model where the effective area of the spacecraft does not vary with time.*

## 3.1. Introduction

The atmospheric drag perturbs both the orbit and the attitude of the spacecraft. Its effect depends on the cross-sectional area of the spacecraft and is modeled as a force in orbit dynamics and as a torque in attitude dynamics. Typically, due to its low magnitude, many applications use the average of the effective areas of spacecraft to approximate its effect. This method may not be suitable for precision applications. In this chapter, spacecraft are modeled as a composition of flat rectangular areas in order to calculate the effect of the atmospheric perturbation. This model takes into account the coupling between orbit and attitude because the variation of the effective area of the spacecraft depends on attitude, and because the atmospheric density depends on the distance of the spacecraft to the center of the Earth, thus the orbit. Both the absolute and differential drag effect on the dynamics are derived in analytical form here. Finally, how this coupling may vary the atmospheric drag perturbation depending on the variable spacecraft attitude is illustrated at the end of the Chapter.



## 3.2. Atmospheric Drag as a Source of Coupling

The strongest non-gravitational perturbation of orbital dynamics for altitudes below approximately 750 km is atmospheric drag. This is true for missions at an altitude of around 300 km for both absolute [99] and relative orbital dynamics [100]. An overview of the magnitude of the atmospheric drag in LEO compared to other effects is provided in Figure 3.1 for absolute dynamics and Figure 3.2 for relative dynamics. In this section, the effect of the atmospheric drag on satellite formations on low orbits, considered the largest non-gravitational force acting on spacecraft relative dynamics, is described.

The acceleration produced by atmospheric drag on a single spacecraft is classically modeled as

$$\boldsymbol{a}_a = -\frac{1}{2}\frac{C_D \rho(\boldsymbol{r})}{m} A_{ef} v_s^2 \hat{\boldsymbol{v}}_s, \tag{3.1}$$

where $\rho(\boldsymbol{r})$ is the atmospheric density, $m$ is the mass of the spacecraft, $\boldsymbol{v}_s$ the velocity of the spacecraft surface with respect to the atmosphere and $\hat{\boldsymbol{v}}_s = \boldsymbol{v}_s/|\boldsymbol{v}_s|$ a unit vector, $C_D$ the drag coefficient of the spacecraft, and $A_{ef}$ the effective area of the spacecraft, with the dynamics described using the inertial frame. This expression assumes that the variation of the effective area is small enough to be considered constant, and that the drag coefficient is constant across the complete external surface of the spacecraft.

The velocity of the spacecraft surface with respect to the atmosphere is given by

$$\boldsymbol{v}_s = \boldsymbol{v} - \boldsymbol{v}_{at}, \tag{3.2}$$

where $\boldsymbol{v}_{at}$ represents the velocity of the atmosphere. If it is assumed that the atmosphere corotates with Earth with an angular velocity given by $\boldsymbol{\omega_E}$ then

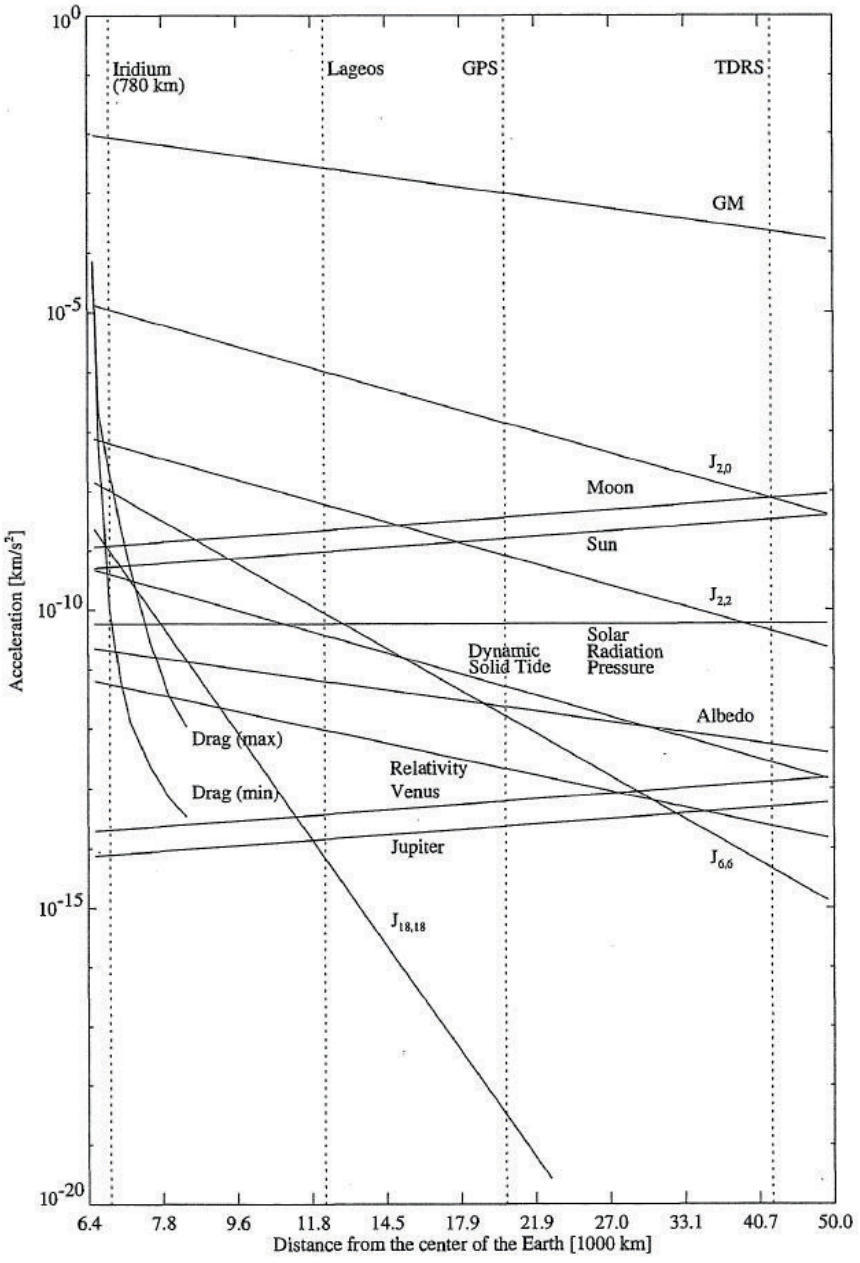


Figure 3.1: Order of magnitude of various perturbing accelerations of a satellite orbit [41].

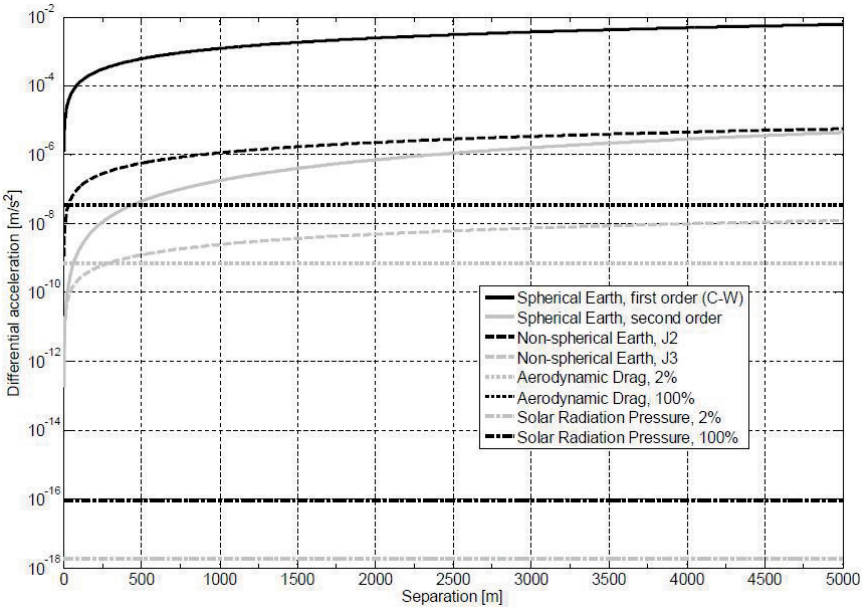


Figure 3.2: Order of magnitude of various differential perturbations for close near-circular formation as a function of spacecraft separation [100].

$$\boldsymbol{v}_{at} = \boldsymbol{\omega_E}^{\times}\boldsymbol{r}. \tag{3.3}$$

Take a spacecraft with a specific geometric form, for example, the one shown in Fig. 3.3. If lift and normal forces are neglected, the torque produced by the atmospheric perturbation on the $i$-th area of a spacecraft is given by

$$\boldsymbol{\tau}_{a,i} = -\frac{1}{2}C_{D,i}\rho(\boldsymbol{r})A_i v_s^2(\boldsymbol{d}_i^{\times}\hat{\boldsymbol{v}}_s), \tag{3.4}$$

with $\boldsymbol{d}_i$ the distance between the center of pressure of the area $i$ and the center of mass of the spacecraft .

In order to characterize how the effect of the atmospheric perturbation depends on the geometry of the spacecraft, its effective area is calculated. In general, the effective area of a spacecraft $A_{ef}$ is given by the surface integral (3.5)

$$A_{ef} = \int_S (\boldsymbol{n}_{dA}^T\hat{\boldsymbol{v}}_s)dA, \tag{3.5}$$

with $\boldsymbol{n}_{dA}$ the vector normal to the differential area $dA$. In many applications, the surface of the spacecraft may be accurately represented by a finite set of flat areas, as shown in Figure 3.3. If a spacecraft is sufficiently modeled as a number of planes, only the component that is perpendicular to the area will have an perturbing effect. Its magnitude, per area, is equal to the projection of the velocity vector of

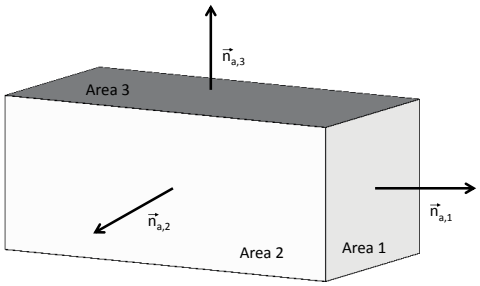


Figure 3.3: Representation of a spacecraft as a composition of areas

the surface in the norm of the $i$-th area of the spacecraft, $\boldsymbol{n}_i{}^T\boldsymbol{v}_{s,i}$. This means that the total effective area is given by

$$A_{ef} = \sum_{i=1}^{s} A_i(\hat{\boldsymbol{n}}_i^T\hat{\boldsymbol{v}}_s), \tag{3.6}$$

where $s$ is equal to the amount of planar surfaces composing the spacecraft,$A_i$ the magnitude of area $i$ amd $\hat{\boldsymbol{n}}_i$ a unit vector perpendicular to the area $i$.

When a spacecraft is modeled as a number of planar surfaces, it is possible to insert 3.6 in 3.1, and take into account that every planar surface may have a different value of drag coefficient ($C_D$) to determine the acceleration produced by the atmospheric drag force.

This leads to the expression of the total atmospheric drag acceleration when the spacecraft is modeled as a set of areas

$$\boldsymbol{a}_a = -\frac{1}{2}\rho(\boldsymbol{r})\left(\sum_{i=1}^{s} C_{D,i}A_i(\hat{\boldsymbol{n}}_i^T\hat{\boldsymbol{v}}_s)\right)v_s^2\hat{\boldsymbol{v}}_s. \tag{3.7}$$

In an similar fashion, the torque effect produced by the atmospheric drag when the spacecraft is described as a set of areas is given by

$$\boldsymbol{\tau}_a = -\frac{1}{2}\rho(\boldsymbol{r})\sum_{i=1}^{s} C_{D,i}A_i(\hat{\boldsymbol{n}}_i\boldsymbol{v}_s)(\boldsymbol{d}_i \times \boldsymbol{v}_s), \tag{3.8}$$

with $\boldsymbol{d}_i$ the distance between the center of pressure of area $i$ and the center of mass of the spacecraft.

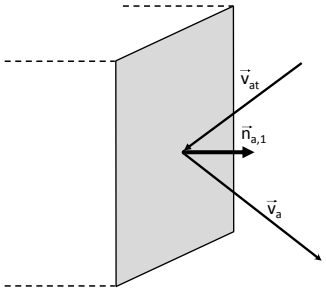


Figure 3.4: Representation of interaction of atmosphere particles with surface of a spacecraft. Specular reflection is assumed.

From (3.7) and (3.8) it can be seen that, apart for a case where a satellite is a perfect sphere, the equations present a dependency between orbit and attitude dynamics. In the case of the dynamic coupling due to the atmospheric drag force affecting the orbit dynamics, the effective area of the spacecraft is a direct function of the attitude via the vector $\hat{\boldsymbol{n}}_i$. In the case of the atmospheric drag torque, the magnitude of the torque affecting the satellite depends on the altitude of the spacecraft via the atmospheric density $\rho(\boldsymbol{r})$, hence, it is a direct dependency on its orbit. In this work, the dependency between atmospheric drag force and attitude is the source of coupling studied in Chapters 6 and 7.

## 3.3. Single Spacecraft Atmospheric Drag Perturbation

In the previous chapter the complete space-state system under analysis was presented. The previous section explained how to model the determination of the effective area of a spacecraft. Now, in this section, the expressions are derived for the acceleration due to atmospheric drag projected on the inertial frame, and for the torque perturbation on the body frame, showing the cross relation between orbit and attitude dynamics. With this, the dynamics model necessary for this work is complete.

The rotation matrices used here between reference frames were described and derived in section 2.6. For notation purposes, expressing a vector $\boldsymbol{\alpha}$ like $\boldsymbol{\alpha}|_{\mathcal{B}}$, $\boldsymbol{\alpha}|_{\mathcal{I}}$ and $\boldsymbol{\alpha}|_{\mathcal{E}}$, represents its projection in the reference frames $\mathcal{B}$,$\mathcal{I}$ and $\mathcal{E}$ respectively.

Using (3.7), the normal vector to every $i$ area of the spacecraft $\boldsymbol{n}_i$ is well known in the spacecraft body frame $\mathcal{B}$. For this reason, from now on, it will be assumed that $\boldsymbol{n}_i|_{\mathcal{B}} = \boldsymbol{n}_i$. In order to determine the expression of $\boldsymbol{n}_i$ in the inertial frame $\mathcal{I}$, the fact that $\boldsymbol{q}$ is the rotation quaternion from the inertial to the body frame of the spacecraft is used. From this, we obtain

$$\boldsymbol{n}_i|_{\mathcal{I}} = \boldsymbol{D}^T(\boldsymbol{q})\, \boldsymbol{n}_i|_{\mathcal{B}} = \boldsymbol{D}^T(\boldsymbol{q})\boldsymbol{n}_i. \tag{3.9}$$

From here, if (3.9) and (3.3) are replaced in (3.7) the complete expression of the atmospheric acceleration perturbation affecting the spacecraft is given by

$$\boldsymbol{a}_a = -\frac{1}{2}\frac{C_D\rho(\boldsymbol{r})}{m}\sum_{i=1}^{s} A_i \left\{\left(\boldsymbol{D}^T(\boldsymbol{q})\boldsymbol{n}_i\right)^T (\boldsymbol{v}-\boldsymbol{\omega_E}^{\times}\boldsymbol{r})\right\}(\boldsymbol{v}-\boldsymbol{\omega_E}^{\times}\boldsymbol{r}). \quad (3.10)$$

In the case of the atmospheric drag torque affecting the spacecraft, it needs to be expressed in $\mathcal{B}$. We have that the velocity of the spacecraft surface is known in $\mathcal{I}$ as $\boldsymbol{v}_s = \boldsymbol{v} - \boldsymbol{v}_{at} = \boldsymbol{v} - \boldsymbol{\omega_E}^{\times}\boldsymbol{r}$. In order to obtain its value in $\mathcal{B}$ it is necessary to make a rotation such that

$$\boldsymbol{v}_s|_{\mathcal{B}} = \boldsymbol{D}(\boldsymbol{q})\boldsymbol{v}_s = \boldsymbol{D}(\boldsymbol{q})(\boldsymbol{v}-\boldsymbol{\omega_E}^{\times}\boldsymbol{r}). \quad (3.11)$$

Replacing Eq. 3.11 in 3.8 we arrive to the expression of the atmospheric drag torque affecting the spacecraft in $\mathcal{B}$

$$\boldsymbol{\tau}_a = -\frac{1}{2}C_D\rho(\boldsymbol{r})\sum_{i=1}^{s} A_i \left(\boldsymbol{n}_i^T\boldsymbol{D}(\boldsymbol{q})(\boldsymbol{v}-\boldsymbol{\omega_E}^{\times}\boldsymbol{r})\right)\boldsymbol{d}_i^{\times}\left[\boldsymbol{D}(\boldsymbol{q})(\boldsymbol{v}-\boldsymbol{\omega_E}^{\times}\boldsymbol{r})\right]. \quad (3.12)$$

## 3.4. Differential Atmospheric Drag Perturbations

In order to describe the effect of the differential atmospheric drag perturbations effects in the frames where the dynamics states of Eq. 2.30 are defined, it is necessary to describe them using the frames $\mathcal{E}$ for orbit dynamics and $\mathcal{B}$ for attitude dynamics.

### 3.4.1. Forces

We take the vector of the acceleration caused by the atmospheric drag acceleration ( 3.1), in order to derive the expression for the differential drag $\Delta\boldsymbol{a_p}$ affecting the relative dynamics as a function of the states. For the deputy spacecraft, we have

$$\boldsymbol{r}_2|_{\mathcal{E}} = \boldsymbol{r}|_{\mathcal{E}} + \tilde{\boldsymbol{r}} \quad (3.13)$$

$$\boldsymbol{v}_{s,2}\big|_{\mathcal{E}} = \boldsymbol{v}|_{\mathcal{E}} + \tilde{\boldsymbol{v}} - \boldsymbol{v}_a|_{\mathcal{E}}, \quad (3.14)$$

where $\boldsymbol{r}_2$ is the position of spacecraft 2 with respect to the center of Earth and $\boldsymbol{v}_{s,2}$ is its velocity with respect to the atmosphere. Here $\tilde{\boldsymbol{r}}$ is in the frame $\mathcal{E}$, but the notation is dropped because the state is defined in this frame already. To determine the relative position vector of the second spacecraft, the definition of this frame leads to $\boldsymbol{r}|_{\mathcal{E}} = [r,0,0]^T$, so

$$\boldsymbol{r}_2|_{\mathcal{E}} = \begin{bmatrix} r+\tilde{r}_x \\ \tilde{r}_y \\ \tilde{r}_z \end{bmatrix}. \quad (3.15)$$

Taking the orbital rate of the reference orbit as $\Omega$ leads to

$$\boldsymbol{v}|_{\mathcal{E}} = \begin{bmatrix} \dot{r} \\ r\Omega \\ 0 \end{bmatrix} = \begin{bmatrix} \frac{\boldsymbol{r}^T\boldsymbol{v}}{r} \\ r\left|\frac{\boldsymbol{r}^{\times}\boldsymbol{v}}{\boldsymbol{r}^2}\right| \\ 0 \end{bmatrix}. \tag{3.16}$$

To determine the expression for the velocity of the atmosphere projected in $\mathcal{E}$, the rotation between $\mathcal{I}$ and $\mathcal{E}$ is used

$$\boldsymbol{v}_a|_{\mathcal{E}} = \boldsymbol{D}|_{\mathcal{I}}^{\mathcal{E}}\,\boldsymbol{v}_a = \boldsymbol{D}|_{\mathcal{I}}^{\mathcal{E}}\,(\boldsymbol{\omega_E}^{\times}\,\boldsymbol{r}_2|_{\mathcal{E}}) = \boldsymbol{D}|_{\mathcal{I}}^{\mathcal{E}}\left(\boldsymbol{\omega_E}^{\times}\begin{bmatrix} r+\tilde{r}_x \\ \tilde{r}_y \\ \tilde{r}_z \end{bmatrix}\right), \tag{3.17}$$

where $\boldsymbol{D}|_{\mathcal{I}}^{\mathcal{E}}$ is the rotation matrix from $\mathcal{I}$ to $\mathcal{E}$. This rotation can be obtained using the guidelines described in [101].

From here, it is possible to obtain

$$\boldsymbol{v}_2|_{\mathcal{E}} = \begin{bmatrix} \frac{\boldsymbol{r}^T\boldsymbol{v}}{r} \\ r\left|\frac{\boldsymbol{r}^{\times}\boldsymbol{v}}{\boldsymbol{r}^2}\right| \\ 0 \end{bmatrix} + \tilde{\boldsymbol{v}} - \boldsymbol{D}|_{\mathcal{E}}^{\mathcal{I}}\left(\boldsymbol{\omega_E}^{\times}\begin{bmatrix} r+\tilde{r}_x \\ \tilde{r}_y \\ \tilde{r}_z \end{bmatrix}\right). \tag{3.18}$$

Finally, an expression for the vector normal to any area $i$ of spacecraft 2, $\boldsymbol{n}_{2,i}|_{\mathcal{E}}$, is required. This vector is known in the body frame of the deputy spacecraft $\mathcal{B}_2$. The projection of this vector in $\mathcal{E}$ is given by

$$\boldsymbol{n}_{2,i}|_{\mathcal{E}} = \boldsymbol{D}|_{\mathcal{I}}^{\mathcal{E}}\,\boldsymbol{D}^T(\boldsymbol{q})\boldsymbol{D}^T(\tilde{\boldsymbol{q}})\boldsymbol{n}_{2,i}, \tag{3.19}$$

where $\boldsymbol{n}_{2,i}$ is the normal vector to the area $i$ of S/C 2 in $\mathcal{B}_2$.

Substituing (3.15), (3.18) and (3.19) in (3.7) we have all the elements necessary to express the atmospheric drag acceleration of the second spacecraft relative to the first spacecraft using the states of the system (2.30). The differential drag is then expressed as

$$\Delta\boldsymbol{a_p} = \Delta\boldsymbol{a_p}|_{\mathcal{E}} = \boldsymbol{a}_{a,2}|_{\mathcal{E}} - \boldsymbol{D}|_{\mathcal{I}}^{\mathcal{E}}\,\boldsymbol{a}_{a,1}|_{\mathcal{I}}\,, \tag{3.20}$$

where the frame notation is dropped from $\Delta\boldsymbol{a_p}$ for simplification purposes and with $\boldsymbol{a}_{a,1}|_{\mathcal{I}} = \boldsymbol{a}_{a,1}$ derived in the previous section.

### 3.4.2. Torques

The expression of the atmospheric drag torque affecting the deputy spacecraft projected in $\mathcal{B}_2$ as a function of the states of the system is determined in this section.

Taking the expression of the atmospheric drag torque (3.8) to determine the absolute value of $\boldsymbol{r}_2$, the result from (3.15) may be used. Also, both the normal vectors to the areas $\hat{\boldsymbol{n}}_i$ and the distance vector between the center of pressure and the center of mass per area $\boldsymbol{d}_{2,i}$ projected in $\mathcal{B}_2$ are assumed to be known. Given

this condition, in order to compute the torque affecting spacecraft 2, it is only left to determine the velocity of the deputy spacecraft with respect to the atmosphere projected on $\mathcal{B}_2$. Since

$$\boldsymbol{v}_{s,2}\big|_{\mathcal{B}2} = \boldsymbol{D}(\tilde{\boldsymbol{q}})\boldsymbol{D}(\boldsymbol{q})\left(\boldsymbol{v} + \tilde{\boldsymbol{v}}|_{\mathcal{J}} - \boldsymbol{v}_a|_{\mathcal{J}}\right), \tag{3.21}$$

with

$$\tilde{\boldsymbol{v}}|_{\mathcal{J}} = \boldsymbol{D}|_{\mathcal{E}}^{\mathcal{J}}\,\tilde{\boldsymbol{v}} + \left(\Omega|_{\mathcal{J}}^{\mathcal{J}\to\mathcal{E}}\right)^{\times}\boldsymbol{r} = \boldsymbol{D}|_{\mathcal{E}}^{\mathcal{J}}\,\tilde{\boldsymbol{v}} + \frac{(\boldsymbol{r}^{\times}\boldsymbol{v})^{\times}}{r^2}\tilde{\boldsymbol{r}} \tag{3.22}$$

$$\boldsymbol{v}_{a,2}\big|_{\mathcal{J}} = \boldsymbol{\omega}_E^{\times}\boldsymbol{r}_2 = \boldsymbol{\omega}_E^{\times}\left(\boldsymbol{r} + \boldsymbol{D}|_{\mathcal{E}}^{\mathcal{J}}\,\tilde{\boldsymbol{r}}\right), \tag{3.23}$$

the final expression for the deputy spacecraft velocity with respect to the atmosphere is

$$\boldsymbol{v}_2|_{\mathcal{B}2} = \boldsymbol{D}(\tilde{\boldsymbol{q}})\boldsymbol{D}(\boldsymbol{q})\left(\boldsymbol{v} + \boldsymbol{D}|_{\mathcal{E}}^{\mathcal{J}}\,\tilde{\boldsymbol{v}} + \frac{(\boldsymbol{r}^{\times}\boldsymbol{v})^{\times}}{r^2}\tilde{\boldsymbol{r}} - \boldsymbol{\omega}_E^{\times}\left(\boldsymbol{r} + \boldsymbol{D}|_{\mathcal{E}}^{\mathcal{J}}\,\tilde{\boldsymbol{r}}\right)\right). \tag{3.24}$$

By substituting (3.15) and (3.24) in (3.7) it is possible to arrive at the expression of the atmospheric drag torque affecting the deputy spacecraft as a function of the states expressed in frame $\mathcal{B}_2$.

## 3.5. Magnitude of the Atmospheric Drag

In order to show how the atmospheric drag model that takes into account the coupling between orbit and attitude dynamics of spacecraft influences the satellite dynamics, the propagation of these effects over one orbit using the models derived in this section is shown.

Consider a two-spacecraft system orbiting the Earth with dynamics described in (2.30). These two spacecraft follow a circular equatorial orbit with an initial altitude of 300 km in an along-track configuration with a relative distance of 1000 km.

These spacecraft are both 3 unit (3U) CubeSats, with 1 unit, or 1U, representing a $10x10x10$ cm$^3$ volume, in a configuration leading to $30x10x10$ cm$^3$ satellites.

The conditions of the dynamics and the spacecraft characteristics used in the propagation are given in Table 3.1. Two different initial conditions are used in the simulations for the rotation state: one with no initial rotation for any of the spacecraft, and one with an initial rotation for both of them. These initial conditions are used to assess the impact of the rotation when coupling is taken into account.

It is assumed that both spacecraft are in a circular orbit. It is also assumed that the atmospheric density is known, given by its value at solar radiation maximum, $3.96x10^{-11}$ kg/m$^3$. Propagation is performed using a Variable-step ode45 (Dormand-Prince) integrator with a maximum step size of 0.01 s. In Figure 3.5 the propagation of the magnitude of different accelerations due to atmospheric drag is shown. It can be seen how the effect differs when the spacecraft has an initial rotation condition and when it doesn't. For comparison purposes, the magnitude of

Table 3.1: Configuration of the dynamics of the system under study.

| **Initial Conditions.** | | |
|---|---|---|
| Spacecraft | **S/C 1** | **S/C 2** |
| Position [km] | $[300 + R_E, 0, 0]$ | $(300 + R_E)[\cos\theta_2, \sin\theta_2, 0]$ |
| Velocity [km/s] | $[0, 7.7142, 0]$ | $7.7142[-\sin\theta_2, \cos\theta_2, 0]$ |
| Attitude quaternion | $[0, 0, 0, 1]$ | $[0, 0, 0, 1]$ |
| Rotation rate for the rotating case [rad/s] | $[0, \pi/18, 0]$ | $[0, 0, \pi/18]$ |
| True anomaly $\theta$ [rad] | 0 | $R_A/(R_E + R_A)$ |
| Along-track separation ($R_A$) [km] | 1000 | |
| **Spacecraft mechanical characteristics.** | | |
| Mass (m) [kg] | 3.6 | 3.6 |
| Inertia matrix ($\boldsymbol{I}$) [kg.m$^2$] | diag$[0.055, 0.055, 0.017]$ | diag$[0.055, 0.055, 0.017]$ |
| Drag coefficient ($C_D$) | 2.3 | 2.3 |
| Spacecraft volume [cm$^3$] | 10x10x30 | 10x10x30 |

the effect of the atmospheric drag force if the spacecraft has a non-varying effective area of 0.03 m$^2$ (the largest of the sides of the spacecraft rectangular shape) and 0.01 m$^2$ (the smallest of the sides of the spacecraft rectangular shape) is shown. For reference, the propagation of the dynamics of the attitude states of the spacecraft for this propagation is shown in Figure 3.6.

It may be seen from Figure 3.5 that the average acceleration of a single spacecraft is approximately 2.3 x $10^{-5}$ N/kg. The variation about that average is approximately $\pm 0.3 \times 10^{-5}$ N/kg caused by coupling. This means that in this case, the coupling effect on absolute acceleration are about 15% for the non-rotating case.

Now, the propagation of the magnitude of the differential atmospheric drag under the same conditions is shown in Fig. 3.7. This effect is the fundamental in this research work, given the fact that if both spacecraft have a very similar atmospheric drag perturbation, the average of its effect may be enough to model drag for most applications. Nevertheless, if the differential drag effect increases, it is shown that for precision applications, its consideration may have an impact for estimation purposes.

It is clear, again, how the difference in initial conditions affect the magnitude of the differential drag. The effect of rotation creates a differential drag magnitude larger than the case where no initial rotation is used. The average effect with no initial rotation is $5.18\times10^{-7}$ N/kg, but in the initial rotation case its average is $3.87\times10^{-6}$ N/kg. This means that the magnitude of the differential atmospheric drag effect is only 13% in the case of no initial rotation compared to the initial rotation case. For reference purposes, in 3.8 the propagation of the relative attitude states is shown.

Nevertheless, for both cases, there is a differential drag. In the case with no initial rotation, it may be clearly seen in 3.8 that a small rotation due to the perturbation itself is present, creating a differential drag effect.

Both figures demonstrate how the atmospheric drag acceleration is affected by the attitude of the spacecraft, even with small spacecraft as a three-unit CubeSat. In Chapters 5 and 6, the effect of this perturbation in terms of its observability and estimation is analyzed.

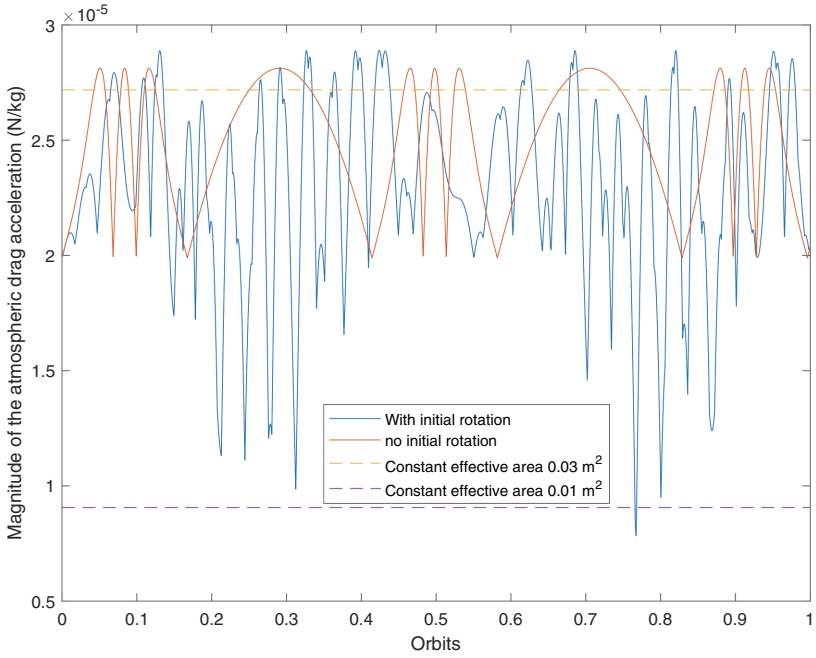


Figure 3.5: Propagation of the atmospheric drag acceleration over one orbit for the conditions given by Table 3.1.

3

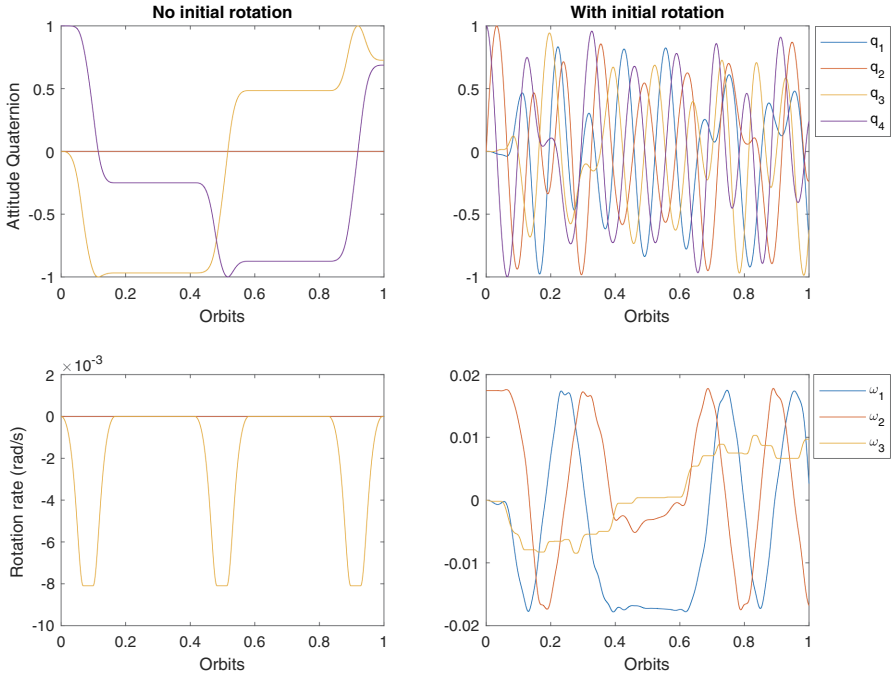


Figure 3.6: Propagation of attitude states over one orbit for the conditions given by Table 3.1.

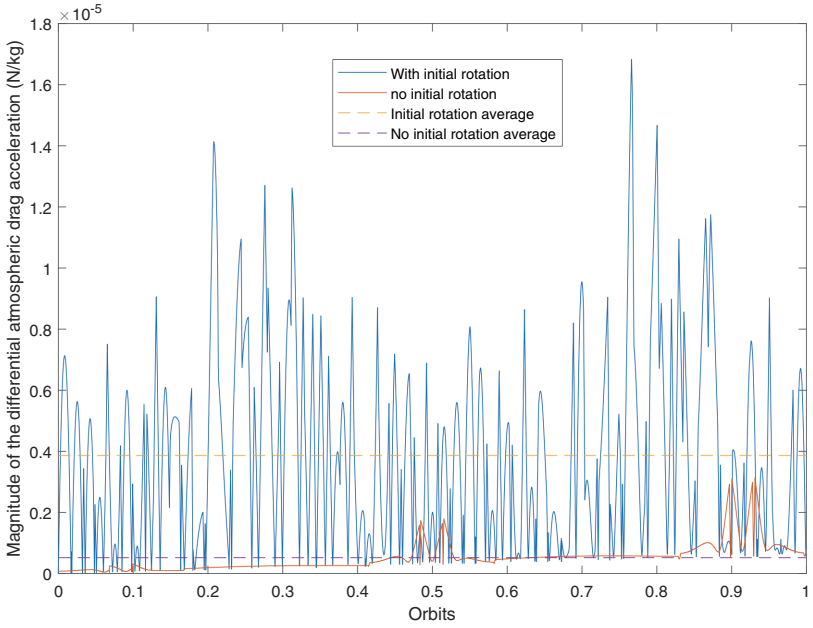


Figure 3.7: Propagation of the differential atmospheric drag acceleration over one orbit for the conditions given by Table 3.1.

3

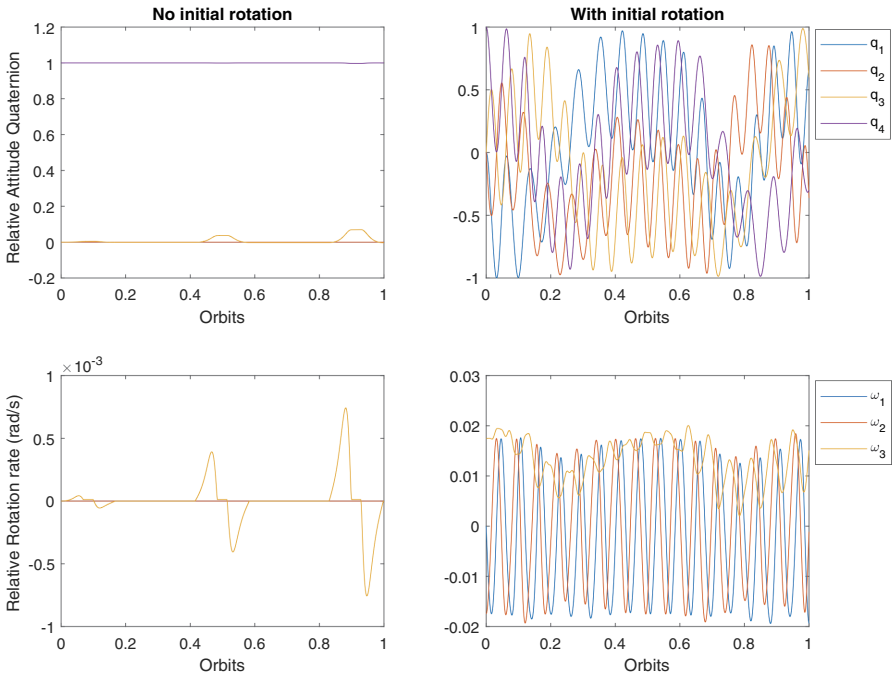


Figure 3.8: Propagation of the differential atmospheric drag acceleration over one orbit for the conditions given by Table 3.1.

# 4

# Linearized State Model

*In this chapter, the derivation of the linearization of the absolute and relative spacecraft dynamics perturbed by atmospheric drag is presented. The results given here are necessary to prepare for the observability analysis and the estimation implementation of the next chapters. The obtained partial derivatives are a valuable source of information. Their propagation provides a first measure of the coupling between orbit and attitude absolute and relative dynamics.*

## 4.1. Introduction

The description of the absolute and relative dynamics of two spacecraft flying in formation, taking into account the coupling due to atmospheric drag, as introduced at Chapters 2 and 3 is fundamentally nonlinear.

Due to the complexity of the description of relative dynamics presented in the previous chapters, it is hardly possible to use nonlinear methods to accomplish the goal of this thesis work. Typically, any direct use of nonlinear dynamics for estimation and control requires a case-to-case analysis that is out of the scope of this research. Nevertheless, the linearization of the system under analysis enables to use the methods proposed in this work: the Observability Gramian (OG) for the observability analysis (Chapter 5), and the Kalman Filter (KF) for estimation purposes (Chapter 6).



The OG method requires that the system under analysis to be a linear time-variant system. For this reason, the linearization of the nonlinear system under study is mandatory for the application of the OG. On the other part, nonlinear systems states may be estimated by using an extension of the KF, called the Extended Kalman Filter (EKF). The EKF uses the linearization of a nonlinear system in order to define the equations of the filter.

Nonlinear dynamic systems are linearized around nominal values of their state and control signal vectors. The linearized equations describing the dynamics of a system are considered sufficient if the difference between the nominal and the actual solution can be described by a set of linear differential equations, called linear perturbation equations [102], described in this Chapter in detail.

In the following section, the results of the derivation that lead to the analytic expressions of the linearization of the spacecraft dynamics system, described in Chapter 2 (2.30), are presented.

For a more comprehensive analysis, linearization with respect to both $J_2$ and the gravitational torque effect are included in this chapter. Although they are not the main focus of this thesis, its documentation is fundamental in order to expand this work to non-equatorial orbits in the future.

## 4.2. Linear Perturbation Equations

When a system is linearized, the approximation is considered good if the difference between the full non-linear equations and the linearized equations can be described by a system of linear differential equations, called linear perturbation equations [102]. The approximation may be done by a Taylor series expansion of the nonlinear system.

Taking the following space-state model of a nonlinear system [102, 103]

$$\dot{\boldsymbol{x}}(t) = \boldsymbol{f}(\boldsymbol{x}(t), \boldsymbol{u}(t), t) + \boldsymbol{G}(t)\boldsymbol{w}(t), \tag{4.1}$$

and its associated measurement model

$$\boldsymbol{z}(t) = \boldsymbol{h}(\boldsymbol{x}(t), \boldsymbol{u}(t)) + \boldsymbol{v}(t), \tag{4.2}$$

with $\boldsymbol{x} \in \mathbb{R}^n$ the system state, $\boldsymbol{u}(t) \in \mathbb{R}^l$ a deterministic quantity representing the input of the system, $\boldsymbol{z} \in \mathbb{R}^m$ the output of the measurement system, $\boldsymbol{G}(t)$ a matrix in $\mathbb{R}^{nxn}$, and finally $\boldsymbol{w}(t) \in \mathbb{R}^n$ and $\boldsymbol{v}(t) \in \mathbb{R}^m$ representing the state and output perturbations, assumed to be zero-mean Gaussian noise processes. This means that the errors are not correlated so that

$$E\left\{\boldsymbol{v}_k(t)\boldsymbol{v}_j^T(t)\right\} = \begin{cases} 0 & k \neq j \\ R_k(t) & k = j \end{cases} \tag{4.3}$$

$$E\left\{\boldsymbol{w}_k(t)\boldsymbol{w}_j^T(t)\right\} = \begin{cases} 0 & k \neq j \\ Q_k(t) & k = j \end{cases} \tag{4.4}$$

where $E\{a\}$ represents the expected value of variable $a$. For this reason $\boldsymbol{Q}(t)$ and $\boldsymbol{R}(t)$ constitute diagonal matrices. These equations represent the system to be linearized.



Take the nonlinear system of equation (4.1) and (4.2). If this system is expanded around a nominal state $\boldsymbol{x}^*$ and control vector $\boldsymbol{u}^*$, let

$$\delta\boldsymbol{x}(t) = \boldsymbol{x}(t) - \boldsymbol{x}^*(t), \delta\boldsymbol{u}(t) = \boldsymbol{u}(t) - \boldsymbol{u}^*(t). \tag{4.5}$$

Then, using the Taylor expansion, it may be represented as [102]

$$\begin{aligned} \boldsymbol{f}(\boldsymbol{x}(t),\boldsymbol{u}(t),t) \quad = \quad & \boldsymbol{f}(\boldsymbol{x}^*(t),\boldsymbol{u}^*(t),t) + \boldsymbol{F}_x[\boldsymbol{x}(t),\boldsymbol{u}(t),t]\delta\boldsymbol{x} + \boldsymbol{F}_u[\boldsymbol{x}(t),\boldsymbol{u}(t),t]\delta\boldsymbol{u}(t) \\ & +\mathcal{O}, \end{aligned} \tag{4.6}$$

where $\boldsymbol{F}_x \in \mathbb{R}^{n\times n}$,$\boldsymbol{F}_u \in \mathbb{R}^{n\times l}$ are the Jacobian matrices with $n$ being the number of states and $l$ being the number of control variables and $\mathcal{O}$ representing the higher order terms in the state. This means that

$$\boldsymbol{F}_x[\boldsymbol{x}(t),\boldsymbol{u}(t),t] = \frac{\partial}{\partial \boldsymbol{x}}\boldsymbol{f}[\boldsymbol{x}(t),\boldsymbol{u}(t),t] = \begin{bmatrix} \frac{\partial f_1}{\partial x_1^*} & \frac{\partial f_1}{\partial x_2^*} & \cdots & \frac{\partial f_1}{\partial x_{n-1}^*} & \frac{\partial f_1}{\partial x_n^*} \\ \frac{\partial f_2}{\partial x_1^*} & \frac{\partial f_2}{\partial x_2^*} & \cdots & \frac{\partial f_2}{\partial x_{n-1}^*} & \frac{\partial f_2}{\partial x_n^*} \\ \vdots & \vdots & \ddots & \vdots & \vdots \\ \frac{\partial f_n}{\partial x_1^*} & \frac{\partial f_n}{\partial x_2^*} & \cdots & \frac{\partial f_n}{\partial x_{n-1}^*} & \frac{\partial f_n}{\partial x_n^*} \end{bmatrix}, \tag{4.7}$$

$$\boldsymbol{F}_u[\boldsymbol{x}(t),\boldsymbol{u}(t),t] = \frac{\partial}{\partial \boldsymbol{u}}\boldsymbol{f}[\boldsymbol{x}(t),\boldsymbol{u}(t),t] = \begin{bmatrix} \frac{\partial f_1}{\partial u_1^*} & \frac{\partial f_1}{\partial u_2^*} & \cdots & \frac{\partial f_1}{\partial u_{n-1}^*} & \frac{\partial f_1}{\partial u_n^*} \\ \frac{\partial f_2}{\partial u_1^*} & \frac{\partial f_2}{\partial u_2^*} & \cdots & \frac{\partial f_2}{\partial u_{n-1}^*} & \frac{\partial f_2}{\partial u_n^*} \\ \vdots & \vdots & \ddots & \vdots & \vdots \\ \frac{\partial f_n}{\partial u_1^*} & \frac{\partial f_n}{\partial u_2^*} & \cdots & \frac{\partial f_n}{\partial u_{n-1}^*} & \frac{\partial f_n}{\partial u_n^*} \end{bmatrix}, \tag{4.8}$$

with $\boldsymbol{F}_x[\boldsymbol{x}(t),\boldsymbol{u}(t),t]$ is called the state transition matrix [41] and $\boldsymbol{F}_u[\boldsymbol{x}(t),\boldsymbol{u}(t),t]$ the partials of the dynamics with respect to the control variable. Here the notation

$$\frac{\partial f_i}{\partial u_j^*} = \left.\frac{\partial f_i}{\partial u_j}\right|_{u_j=u_j^*} \tag{4.9}$$

is used for simplicity purposes. Please recall that in this thesis, if there is a vector $\boldsymbol{a} = [a_1 a_2 a_3]^T$, then $\boldsymbol{a}^{\times}$ is given by the matrix

$$\boldsymbol{a}^{\times} = \begin{bmatrix} 0 & -a_3 & a_2 \\ a_3 & 0 & -a_1 \\ -a_2 & a_1 & 0 \end{bmatrix}. \tag{4.10}$$

### 4.2.1. Derivation of the Linearized System



Let this system be linearized around a nominal value of the state $\boldsymbol{x}^*(t)$ and the input $\boldsymbol{u}^*(t)$. Then

$$\frac{d}{dt}\delta\boldsymbol{x}(t) = \delta\dot{\boldsymbol{x}}(t) = \dot{\boldsymbol{x}}(t) - \dot{\boldsymbol{x}}^*(t) = f(\boldsymbol{x}(t),\boldsymbol{u}(t),t) - f(\boldsymbol{x}^*(t),\boldsymbol{u}^*(t),t) + \boldsymbol{G}(t)\boldsymbol{w}(t). \tag{4.11}$$

If (4.6) is substituted in (4.11) and the higher order terms are neglected, the following equation is obtained

$$\frac{d}{dt}\delta\boldsymbol{x}(t) = \boldsymbol{F}_x[\boldsymbol{x}^*(t),\boldsymbol{u}^*(t),t]\delta\boldsymbol{x} - \boldsymbol{F}_u[\boldsymbol{x}^*(t),\boldsymbol{u}^*(t),t]\delta\boldsymbol{u} + \boldsymbol{G}(t)\boldsymbol{w}(t). \tag{4.12}$$

For more details on the linearization theory, the reader is referred to [102].

## 4.3. Spacecraft Dynamics Linearization

For this work, only the State Transition Matrix $\boldsymbol{F}_x[\boldsymbol{x}(t),\boldsymbol{u}(t),t]$ will be derived. The linearization of the measurements model (4.2) is not necessary, due to the fact that it is assumed that the states can be measured directly, and $\boldsymbol{F}_u[\boldsymbol{x}^*(t),\boldsymbol{u}^*(t),t]$ is not required because all the analysis is done assuming that no control is being applied on the spacecraft. The reason for this is that the focus of this research is only the effect of the coupled orbit-attitude dynamics representation. If done otherwise, the model of the measurements and control may affect the observability analysis, and it would be difficult to differentiate the effects from the dynamic coupling from the effects of the measurement or the control method.

### 4.3.1. Linearization of the Absolute Dynamics

The partial derivatives of the unperturbed absolute dynamics are well known, and shown in Table 4.1 for completeness (See [61] for the details on their derivation). The atmospheric drag torque and force partial derivatives are derived for this work. In this work, all scenarios assume a constant, known value of the atmospheric density. Hence the partial derivatives with respect to the density are always null.

Table 4.1: Absolute Orbital and Attitude State Partial Derivatives. Source [61]

| | | | |
|---|---|---|---|
| $\frac{\partial \dot{\boldsymbol{r}}}{\partial \boldsymbol{r}}$ | 0 | $\frac{\partial \dot{\boldsymbol{q}}}{\partial \boldsymbol{r}}$ | 0 |
| $\frac{\partial \dot{\boldsymbol{r}}}{\partial \boldsymbol{v}}$ | $I_3$ | $\frac{\partial \dot{\boldsymbol{q}}}{\partial \boldsymbol{v}}$ | 0 |
| $\frac{\partial \dot{\boldsymbol{r}}}{\partial \boldsymbol{q}}$ | 0 | $\frac{\partial \dot{\boldsymbol{q}}}{\partial \boldsymbol{q}}$ | $\frac{1}{2}\Omega(\boldsymbol{\omega})$ |
| $\frac{\partial \dot{\boldsymbol{r}}}{\partial \boldsymbol{\omega}}$ | 0 | $\frac{\partial \dot{\boldsymbol{q}}}{\partial \boldsymbol{\omega}}$ | $\frac{1}{2}\Xi(\boldsymbol{q})$ |
| $\frac{\partial \dot{\boldsymbol{v}}}{\partial \boldsymbol{r}}$ | $\frac{3\mu}{r^5}\boldsymbol{r}\boldsymbol{r}^T - \frac{\mu}{r^3}I_3 + \frac{\partial \boldsymbol{a}_a}{\partial \boldsymbol{r}}$ | $\frac{\partial \dot{\boldsymbol{\omega}}}{\partial \boldsymbol{r}}$ | $J^{-1}\frac{\partial \boldsymbol{\tau}_g}{\partial \boldsymbol{q}}$ |
| $\frac{\partial \dot{\boldsymbol{v}}}{\partial \boldsymbol{v}}$ | $\frac{\partial \boldsymbol{a}_a}{\partial \boldsymbol{v}}$ | $\frac{\partial \dot{\boldsymbol{\omega}}}{\partial \boldsymbol{v}}$ | 0 |
| $\frac{\partial \dot{\boldsymbol{v}}}{\partial \boldsymbol{q}}$ | $\frac{\partial \boldsymbol{a}_a}{\partial \boldsymbol{q}}$ | $\frac{\partial \dot{\boldsymbol{\omega}}}{\partial \boldsymbol{q}}$ | $J^{-1}\frac{\partial \boldsymbol{\tau}_g}{\partial \boldsymbol{q}}$ |
| $\frac{\partial \dot{\boldsymbol{v}}}{\partial \boldsymbol{\omega}}$ | 0 | $\frac{\partial \dot{\boldsymbol{\omega}}}{\partial \boldsymbol{\omega}}$ | $-\boldsymbol{I}^{-1}\boldsymbol{\omega}^{\times}\boldsymbol{I} + \boldsymbol{I}^{-1}\left[(\boldsymbol{I}\boldsymbol{\omega})^{\times}\right]$ |

4

### Atmospheric Drag Force

The expression for the atmospheric drag force which influences the dynamics of the Chief spacecraft projected in $\mathcal{I}$ derived in the previous chapter (Equation 3.10) and repeated here for convenience, is given by

$$\boldsymbol{a}_a = -\frac{1}{2}\frac{C_D\rho(\boldsymbol{r})}{m}\sum_{i=1}^{s} A_i \left\{\left(\boldsymbol{D}^T(\boldsymbol{q})\boldsymbol{n}_i\right)^T (\boldsymbol{v} - \boldsymbol{\omega_E}^{\times}\boldsymbol{r})\right\}(\boldsymbol{v} - \boldsymbol{\omega_E}^{\times}\boldsymbol{r}). \quad (4.13)$$

The partial derivatives of $\boldsymbol{a}_a$ with respect to the absolute state components are presented in Table 4.2.

Table 4.2: Partial derivatives of the atmospheric drag

| | |
|---|---|
| $\frac{\partial \boldsymbol{a}_a}{\partial \boldsymbol{r}}$ | $\frac{\rho(\boldsymbol{r})}{2m}\sum_{i=1}^{k} C_i A_i$ $\left\{((\boldsymbol{v} - \boldsymbol{\omega}_E^{\times}\boldsymbol{r})^T\boldsymbol{D}(\boldsymbol{q})\boldsymbol{n}_i)(\boldsymbol{\omega}_E^{\times}) + (\boldsymbol{v} - \boldsymbol{\omega}_E^{\times}\boldsymbol{r})(\boldsymbol{D}(\boldsymbol{q})\boldsymbol{n}_i)^T(\boldsymbol{\omega}_E^{\times})\right\}$ $-\frac{1}{2m}\left(\sum_{i=1}^{k} C_i A_i \left\{\left(D(\boldsymbol{q})^T\boldsymbol{n}_i\right)^T (\boldsymbol{v} - \boldsymbol{\omega}_E^{\times}\boldsymbol{r})\right\}(\boldsymbol{v} - \boldsymbol{\omega}_E^{\times}\boldsymbol{r})\right)\frac{\partial \rho(\boldsymbol{r})}{\partial \boldsymbol{r}}$ |
| $\frac{\partial \boldsymbol{a}_a}{\partial \boldsymbol{v}}$ | $-\frac{\rho(\boldsymbol{r})}{2m}\sum_{i=1}^{k} C_i A_i \left(((\boldsymbol{v} - \boldsymbol{\omega}_E^{\times}\boldsymbol{r})^T\boldsymbol{D}(\boldsymbol{q})\boldsymbol{n}_i)I_3 + (\boldsymbol{v} - \boldsymbol{\omega}_E^{\times}\boldsymbol{r})(\boldsymbol{D}(\boldsymbol{q})\boldsymbol{n}_i)^T\right)$ |
| $\frac{\partial \boldsymbol{a}_a}{\partial \boldsymbol{q}}$ | $-\frac{\rho(r)}{2m}\sum_{i=1}^{k} H(\boldsymbol{n}_i^T\boldsymbol{D}(\boldsymbol{q})(\boldsymbol{v} - \boldsymbol{\omega}_E^{\times}\boldsymbol{r}))C_i A_i(\boldsymbol{v} - \boldsymbol{\omega}_E^{\times}\boldsymbol{r})\left((\boldsymbol{v} - \boldsymbol{\omega}_E^{\times}\boldsymbol{r})^T\sum_{j=1}^{3}\frac{\partial \boldsymbol{D}(\boldsymbol{q})_{[:,j]}}{\partial \boldsymbol{q}}\hat{n}_{[j]}\right)$ |
| $\frac{\partial \boldsymbol{a}_a}{\partial \boldsymbol{\omega}}$ | 0 |

where

$$\frac{\partial \boldsymbol{D}(\boldsymbol{q})_{[:,1]}}{\partial \boldsymbol{q}} = 2\begin{bmatrix} q_1 & -q_2 & -q_3 & +q_4 \\ q_2 & q_1 & -q_4 & -q_3 \\ q_3 & q_4 & q_1 & q_2 \end{bmatrix} \tag{4.14}$$

$$\frac{\partial \boldsymbol{D}(\boldsymbol{q})_{[:,2]}}{\partial \boldsymbol{q}} = 2\begin{bmatrix} q_2 & q_1 & q_4 & q_3 \\ -q_1 & q_2 & -q_3 & q_4 \\ -q_4 & q_3 & q_2 & -q_1 \end{bmatrix} \tag{4.15}$$

$$\frac{\partial \boldsymbol{D}(\boldsymbol{q})_{[:,3]}}{\partial \boldsymbol{q}} = 2\begin{bmatrix} q_3 & -q_4 & q_1 & -q_2 \\ q_4 & q_3 & q_2 & q_1 \\ -q_1 & -q_2 & q_3 & q_4 \end{bmatrix}. \tag{4.16}$$

4

### Atmospheric Drag Torque

The expression for the atmospheric drag torque influencing the dynamics of the Chief spacecraft projected in $\mathcal{B}$ and derived in the previous chapter is given by

$$\boldsymbol{\tau}_a = -\frac{1}{2}C_D\rho(\boldsymbol{r})\sum_{i=1}^{s} A_i \left(\boldsymbol{n}_i^T\boldsymbol{D}(\boldsymbol{q})(\boldsymbol{v}-\boldsymbol{\omega_E}^{\times}\boldsymbol{r})\right)\boldsymbol{d}_i^{\times}\left[\boldsymbol{D}(\boldsymbol{q})(\boldsymbol{v}-\boldsymbol{\omega_E}^{\times}\boldsymbol{r})\right]. \tag{4.17}$$

The partial derivatives of $\boldsymbol{\tau}_a$ with respect to the absolute states are presented in Table 4.3.

Table 4.3: Partial derivatives of the atmospheric drag torque

| | |
|---|---|
| $\frac{\partial \boldsymbol{\tau}_a}{\partial \boldsymbol{r}}$ | $\rho(\boldsymbol{r})\sum_{i=1}^{s} A_i C_i \left((\boldsymbol{n}_i{}^T\boldsymbol{D}(\boldsymbol{q})(\boldsymbol{v}-\boldsymbol{\omega}_E^{\times}\boldsymbol{r}))(\boldsymbol{d}_i^{\times}\boldsymbol{D}(\boldsymbol{q})\boldsymbol{\omega}_E^{\times})\right.$ $\left.+(\boldsymbol{d}_i^{\times}\boldsymbol{D}(\boldsymbol{q})(\boldsymbol{v}-\boldsymbol{\omega}_E^{\times}\boldsymbol{r}))(\boldsymbol{n}_i^T\boldsymbol{D}(\boldsymbol{q})\boldsymbol{\omega}_E^{\times})\right)+$ $\rho(\boldsymbol{r})\sum_{i=1}^{s}\left(A_i C_i \left(\boldsymbol{n}_i^T\boldsymbol{D}(\boldsymbol{q})(\boldsymbol{v}-\boldsymbol{\omega}_E^{\times}\boldsymbol{r})\right)\left(\boldsymbol{d}_i^{\times}\boldsymbol{D}(\boldsymbol{q})(\boldsymbol{v}-\boldsymbol{\omega}_E^{\times}\boldsymbol{r})\right)\right)\frac{\partial \rho(\boldsymbol{r})}{\partial \boldsymbol{r}}$ |
| $\frac{\partial \boldsymbol{\tau}_a}{\partial \boldsymbol{v}}$ | $\rho(\boldsymbol{r})\sum_{i=1}^{s} A_i C_i \left((\boldsymbol{n}_i^T\boldsymbol{D}(\boldsymbol{q})(\boldsymbol{v}-\boldsymbol{\omega}_E^{\times}\boldsymbol{r}))(\boldsymbol{d}_i^{\times}\boldsymbol{D}(\boldsymbol{q})) + (\boldsymbol{d_i}^{\times}\boldsymbol{D}(\boldsymbol{q})(\boldsymbol{v}-\boldsymbol{\omega}_E^{\times}\boldsymbol{r}))(\boldsymbol{n}_i^T\boldsymbol{D}(\boldsymbol{q}))\right)$ |
| $\frac{\partial \boldsymbol{\tau}_a}{\partial \boldsymbol{q}}$ | $\rho(\boldsymbol{r})\sum_{i=1}^{s} A_i C_i \left(\boldsymbol{n}_i^T\boldsymbol{D}(\boldsymbol{q})(\boldsymbol{v}-\boldsymbol{\omega}_E^{\times}\boldsymbol{r})\right.$ $\left.\sum_{j=1}^{3}(\boldsymbol{d}_i^{\times}(\boldsymbol{v}-\boldsymbol{\omega}_E^{\times}\boldsymbol{r}))_{[j]}\frac{\partial \boldsymbol{D}(\boldsymbol{q})_{[:,1]}}{\partial \boldsymbol{q}} + \boldsymbol{D}(\boldsymbol{q})(\boldsymbol{d}_i^{\times}(\boldsymbol{v}-\boldsymbol{\omega}_E^{\times}\boldsymbol{r}))\sum_{j=1}^{3}(\boldsymbol{v}-\boldsymbol{\omega}_E^{\times}\boldsymbol{r})_{[j]}\frac{\partial \boldsymbol{D}(\boldsymbol{q})_{[:,j]}}{\partial \boldsymbol{q}}\right)$ |
| $\frac{\partial \boldsymbol{\tau}_a}{\partial \boldsymbol{\omega}}$ | 0 |

### The $J_2$ Effect

The $J_2$ effect projected in $\mathcal{I}$, as described in [40], is given by

$$\boldsymbol{a}_{J2} = -\frac{3\mu \boldsymbol{r}_E^2}{2mr^4} J_2 \left( \left( 1 - 5\frac{r_z^2}{r^2} \right) \frac{\boldsymbol{r}}{r} + 2\frac{r_z}{r}\hat{\boldsymbol{z}} \right) \tag{4.18}$$

with $m$ the mass of the spacecraft, $\boldsymbol{r}_E$ being the Equatorial radius of Earth, $r$ the absolute value of the position $\boldsymbol{r}$, $r_z$ the z-axis component of the $\boldsymbol{r}$ state, $\hat{\boldsymbol{z}} = [0, 0, 1]^T$, $\mu$ the gravity coefficient of the Earth, and $J_2$ the first zonal harmonic for Earth.

Its partial derivatives are given here for completeness.

Table 4.4: $J_2$-effect partial derivatives

| | |
|---|---|
| $\frac{\partial \boldsymbol{a}_{J2}}{\partial \boldsymbol{r}}$ | $-\frac{3}{2}\mu J_2 \frac{\boldsymbol{r}_E^2}{r^4}\left(\left(1-5\frac{r_3^2}{r^2}\right)\left(\frac{1}{r}I_3 - \frac{\boldsymbol{r}\boldsymbol{r}^T}{r^3}\right) + \frac{\boldsymbol{r}}{r}\left(5\frac{r_3^2\boldsymbol{r}^T}{r^4} - 10\frac{r_3\hat{\boldsymbol{z}}^T}{r^2}\right) + 2\left(-\frac{r_3\hat{\boldsymbol{z}}\boldsymbol{r}^T}{r^3} + \frac{\hat{\boldsymbol{z}}\hat{\boldsymbol{z}}^T}{r}\right)\right) + 6\mu J_2 \boldsymbol{r}_E^2 \left(\left(1-5\frac{r_3^2}{r^2}\right)\frac{\boldsymbol{r}}{r} - 2\frac{r_3}{r}\hat{\boldsymbol{z}}\right)\left(\frac{\boldsymbol{r}^T}{r^6}\right)$ |
| $\frac{\partial \boldsymbol{a}_{J2}}{\partial \boldsymbol{v}}$ | 0 |
| $\frac{\partial \boldsymbol{a}_{J2}}{\partial \boldsymbol{q}}$ | 0 |
| $\frac{\partial \boldsymbol{a}_{J2}}{\partial \boldsymbol{\omega}}$ | 0 |

### Gravitational Torque Effect

Any nonsymmetrical object of finite dimensions in orbit is subject to a gravitational torque because of the variation in the Earth's gravitational object over the object [39]. If a spherical mass distribution of the Earth is assumed, this torque, projected in frame $\mathcal{B}$, is given [39] as

$$\boldsymbol{\tau}_g = 3\frac{\mu}{r^5}(\boldsymbol{r}|_{\mathcal{B}})^{\times}(\boldsymbol{I}\boldsymbol{r}|_{\mathcal{B}}). \tag{4.19}$$

Recall that in this work it has been assumed that $\boldsymbol{r} = \boldsymbol{r}|_{\mathcal{I}}$. This means that $\boldsymbol{r}|_{\mathcal{B}} = D(\boldsymbol{q})\boldsymbol{r}$ so

$$\boldsymbol{\tau}_g = 3\frac{\mu}{r^5}(D(\boldsymbol{q})\boldsymbol{r})^{\times}(\boldsymbol{I}D(\boldsymbol{q})\boldsymbol{r}). \tag{4.20}$$

Its partial derivatives are given here for completeness.

$$\frac{\partial \boldsymbol{\tau}_g}{\partial \boldsymbol{r}} = 3\mu\left\{\frac{1}{r^5}\left[((D(\boldsymbol{q})\boldsymbol{r})^{\times}(\boldsymbol{I}D(\boldsymbol{q}))) - ((\boldsymbol{I}D(\boldsymbol{q})\boldsymbol{r})^{\times}D(\boldsymbol{q}))\right] + (D(\boldsymbol{q})\boldsymbol{r})^{\times}(\boldsymbol{I}D(\boldsymbol{q})\boldsymbol{r})\left(\frac{-5\boldsymbol{r}^T}{r^7}\right)\right\} \tag{4.21}$$

$$\frac{\partial \boldsymbol{\tau}_g}{\partial \boldsymbol{v}} = 0 \tag{4.22}$$

$$\frac{\partial \boldsymbol{\tau}_g}{\partial \boldsymbol{q}} = 3\frac{\mu}{r^5}\left((D(\boldsymbol{q})\boldsymbol{r})^{\times}\left(\boldsymbol{I}\sum_{j=1}^{3}\beta_j(\boldsymbol{q})r_j\right) - (\boldsymbol{I}D(\boldsymbol{q})\boldsymbol{r})^{\times}\left(\sum_{j=1}^{3}\beta_j(\boldsymbol{q})r_j\right)\right) \tag{4.23}$$

$$\frac{\partial \boldsymbol{\tau}_g}{\partial \boldsymbol{\omega}} = 0 \tag{4.24}$$

where

$$\beta_1(\boldsymbol{q}) = 2\begin{bmatrix} q_1 & q_2 & -q_3 & -q_4 \\ -q_4 & q_3 & q_2 & -q_1 \\ q_3 & q_4 & q_1 & q_2 \end{bmatrix} \tag{4.25}$$

$$\beta_2(\boldsymbol{q}) = 2\begin{bmatrix} q_4 & q_3 & q_2 & q_1 \\ q_1 & -q_2 & q_3 & -q_4 \\ q_2 & -q_1 & q_4 & q_3 \end{bmatrix} \tag{4.26}$$

$$\beta_3(\boldsymbol{q}) = 2\begin{bmatrix} -q_3 & q_4 & -q_1 & q_2 \\ q_2 & q_1 & q_4 & q_3 \\ q_1 & -q_2 & -q_3 & q_4 \end{bmatrix}. \tag{4.27}$$

### 4.3.2. Linearization of the Relative Dynamics

The linearization of the relative dynamics is based on the relative dynamics model presented in Chapter 2. For the purposes of this work, specially for the derivation of these derivatives, the expressions for relative dynamics were derived in the previous chapter as a function of the states only. This means, for example, that the angular velocity of the orbital frame with respect to the inertial frame was given always in terms of those states, and no simplifications were assumed. Therefore, the results presented here will be of use for the analysis of observability and controllability of relative spacecraft dynamics in future research.

It is noted that due to the lengthy derivation and for clarity purposes, in this work the partial derivatives of the rotation matrices is not given. Nevertheless, they are considered in the propagation of dynamics done in the next chapters.

#### Unperturbed Relative Dynamics

The unperturbed relative dynamics refer to the relative dynamics obtained in Chapter 2, without considering perturbations. Perturbations, due to their complexity, are considered separately.

Table 4.5: Orbital relative dynamics state partial derivatives with respect to absolute states.

| | |
|---|---|
| $\frac{\partial \dot{\tilde{v}}_x}{\partial \boldsymbol{r}}$ | $-2\mu\left(\frac{\boldsymbol{r}^T}{r^4}\right)-\mu\left[\frac{1}{\left[(r+\tilde{r}_x)^2+\tilde{r}_y^2+\tilde{r}_z^2\right]^{3/2}}+3\left(\frac{(r+\tilde{r}_x)^2}{\left[(r+\tilde{r}_x)^2+\tilde{r}_y^2+\tilde{r}_z^2\right]^{5/2}}\right)\right]\frac{\boldsymbol{r}^T}{r}+2\frac{\partial}{\partial \boldsymbol{r}}(\Omega)\,\tilde{v}_y$ $+\frac{\partial}{\partial \boldsymbol{r}}(\dot{\Omega})\,\tilde{r}_y+2\Omega\frac{\partial}{\partial \boldsymbol{r}}(\Omega)\,\tilde{r}_x+\frac{\partial \Delta a_{p_x}}{\partial \boldsymbol{r}}$ |
| $\frac{\partial \dot{\tilde{v}}_y}{\partial \boldsymbol{r}}$ | $3\mu\tilde{r}_y\left(\frac{r+\tilde{r}_x}{\left[(r+\tilde{r}_x)^2+\tilde{r}_y^2+\tilde{r}_z^2\right]^{5/2}}\right)\frac{\boldsymbol{r}^T}{r}-2\frac{\partial}{\partial \boldsymbol{r}}(\Omega)\,\tilde{v}_x-\frac{\partial}{\partial \boldsymbol{r}}(\dot{\Omega})\,\tilde{r}_x+2\Omega\frac{\partial}{\partial \boldsymbol{r}}(\Omega)\,\tilde{r}_y+\frac{\partial \Delta a_{p_x}}{\partial \boldsymbol{r}}$ |
| $\frac{\partial \dot{\tilde{v}}_z}{\partial \boldsymbol{r}}$ | $3\mu\tilde{r}_z\left(\frac{r+\tilde{r}_x}{\left[(r+\tilde{r}_x)^2+\tilde{r}_y^2+\tilde{r}_z^2\right]^{5/2}}\right)\frac{\boldsymbol{r}^T}{r}+\frac{\partial \Delta a_{p_z}}{\partial \boldsymbol{r}}$ |
| $\frac{\partial \dot{\tilde{\boldsymbol{v}}}}{\partial \boldsymbol{v}}$ | $2\frac{\partial \Omega}{\partial \boldsymbol{v}}\begin{bmatrix}\tilde{v}_y\\ \tilde{v}_x\\ 0\end{bmatrix}+\frac{\partial \dot{\Omega}}{\partial \boldsymbol{v}}\begin{bmatrix}\tilde{r}_y\\ \tilde{r}_x\\ 0\end{bmatrix}+2\Omega\frac{\partial \Omega}{\partial \boldsymbol{v}}\begin{bmatrix}\tilde{r}_x\\ \tilde{r}_y\\ 0\end{bmatrix}+\frac{\partial \Delta \boldsymbol{a_p}}{\partial \boldsymbol{v}}$ |

Table 4.6: Orbital relative dynamics state partial derivatives

| | |
|---|---|
| $\frac{\partial \dot{\tilde{v}}_x}{\partial \tilde{r}_x}$ | $-\frac{\mu}{\left[(r+\tilde{r}_x)^2+\tilde{r}_y^2+\tilde{r}_z^2\right]^{3/2}}+3\frac{\mu(r+\tilde{r}_x)}{\left[(r+\tilde{r}_x)^2+\tilde{r}_y^2+\tilde{r}_z^2\right]^{5/2}}\tilde{r}_x+\Omega^2+\frac{\partial \Delta a_{p_x}}{\partial \tilde{r}_x}$ |
| $\frac{\partial \dot{\tilde{v}}_x}{\partial \tilde{r}_y}$ | $3\left(\frac{\mu(r+\tilde{r}_x)}{\left[(r+\tilde{r}_x)^2+\tilde{r}_y^2+\tilde{r}_z^2\right]^{3/2}}\right)\tilde{r}_y+\dot{\Omega}+\frac{\partial \Delta a_{p_x}}{\partial \tilde{r}_y}$ |
| $\frac{\partial \dot{\tilde{v}}_x}{\partial \tilde{r}_z}$ | $\frac{3\mu\tilde{r}_z}{((r+\tilde{r}_x)^2+\tilde{r}_y^2+\tilde{r}_z^2)^{5/2}}+\frac{\partial \Delta a_{p_x}}{\partial \tilde{r}_z}$ |
| $\frac{\partial \dot{\tilde{v}}_y}{\partial \tilde{r}_x}$ | $\frac{3\mu\tilde{r}_x\tilde{r}_y}{((r+\tilde{r}_x)^2+\tilde{r}_y^2+\tilde{r}_z^2)^{5/2}}-\dot{\Omega}+\frac{\partial \Delta a_{p_y}}{\partial \tilde{r}_x}$ |
| $\frac{\partial \dot{\tilde{v}}_y}{\partial \tilde{r}_y}$ | $-\mu\frac{1}{((r+\tilde{r}_x)^2+\tilde{r}_y^2+\tilde{r}_z^2)^{3/2}}+\frac{3\mu\tilde{r}_y^2}{((r+\tilde{r}_x)^2+\tilde{r}_y^2+\tilde{r}_z^2)^{5/2}}+\Omega^2+\frac{\partial \Delta a_{p_y}}{\partial \tilde{r}_y}$ |
| $\frac{\partial \dot{\tilde{v}}_y}{\partial \tilde{r}_z}$ | $\frac{3\mu\tilde{r}_y\tilde{r}_z}{((r+\tilde{r}_x)^2+\tilde{r}_y^2+\tilde{r}_z^2)^{5/2}}+\frac{\partial \Delta a_{p_y}}{\partial \tilde{r}_z}$ |
| $\frac{\partial \dot{\tilde{v}}_z}{\partial \tilde{r}_x}$ | $\frac{3\mu\tilde{r}_x\tilde{r}_z}{((r+\tilde{r}_x)^2+\tilde{r}_y^2+\tilde{r}_z^2)^{5/2}}+\frac{\partial \Delta a_{p_y}}{\partial \tilde{r}_x}$ |
| $\frac{\partial \dot{\tilde{v}}_z}{\partial \tilde{r}_y}$ | $\frac{3\mu\tilde{r}_y\tilde{r}_z}{((r+\tilde{r}_x)^2+\tilde{r}_y^2+\tilde{r}_z^2)^{5/2}}+\frac{\partial \Delta a_{p_z}}{\partial \tilde{r}_y}$ |
| $\frac{\partial \dot{\tilde{v}}_z}{\partial \tilde{r}_z}$ | $\frac{3\mu\tilde{r}_z^2}{((r+\tilde{r}_x)^2+\tilde{r}_y^2+\tilde{r}_z^2)^{5/2}}+\frac{\partial \Delta a_{p_y}}{\partial \tilde{r}_z}$ |
| $\frac{\partial \dot{\tilde{\boldsymbol{v}}}}{\partial \tilde{\boldsymbol{v}}}$ | $\begin{bmatrix}0 & 2\Omega & 0\\ -2\Omega & 0 & 0\\ 0 & 0 & 0\end{bmatrix}$ |

Table 4.7: Attitude relative dynamics state partial derivatives

| | |
|---|---|
| $\frac{\partial \boldsymbol{I}_2\tilde{\boldsymbol{\omega}}}{\partial \boldsymbol{r}}$ | $-(\boldsymbol{I}_2\boldsymbol{D}(\tilde{\boldsymbol{q}})\boldsymbol{I}_1^{-1})\frac{\partial \boldsymbol{\tau}_1}{\partial \boldsymbol{r}} + \frac{\partial \boldsymbol{\tau}_2}{\partial \boldsymbol{r}}$ |
| $\frac{\partial \boldsymbol{I}_2\tilde{\boldsymbol{\omega}}}{\partial \boldsymbol{v}}$ | $-(\boldsymbol{I}_2\boldsymbol{D}(\tilde{\boldsymbol{q}})\boldsymbol{I}_1^{-1})\frac{\partial \boldsymbol{\tau}_1}{\partial \boldsymbol{v}} + \frac{\partial \boldsymbol{\tau}_2}{\partial \boldsymbol{v}}$ |
| $\frac{\partial \boldsymbol{I}_2\tilde{\boldsymbol{\omega}}}{\partial \boldsymbol{q}}$ | $-(\boldsymbol{I}_2\boldsymbol{D}(\tilde{\boldsymbol{q}})\boldsymbol{I}_1^{-1})\frac{\partial \boldsymbol{\tau}_1}{\partial \boldsymbol{q}} + \frac{\partial \boldsymbol{\tau}_2}{\partial \boldsymbol{q}}$ |
| $\frac{\partial \boldsymbol{I}_2\tilde{\boldsymbol{\omega}}}{\partial \boldsymbol{\omega}}$ | $-(\tilde{\boldsymbol{\omega}} + \boldsymbol{D}(\tilde{\boldsymbol{q}})\boldsymbol{\omega})^{\times}(\boldsymbol{I}_2\boldsymbol{D}(\tilde{\boldsymbol{q}})) + (\boldsymbol{I}_2(\tilde{\boldsymbol{\omega}} + \boldsymbol{D}(\tilde{\boldsymbol{q}})\boldsymbol{\omega}))\boldsymbol{D}(\tilde{\boldsymbol{q}})^{\times} + \tilde{\boldsymbol{\omega}}^{\times}(\boldsymbol{I}_2\boldsymbol{D}(\tilde{\boldsymbol{q}}))$ $-(\boldsymbol{I}_2\boldsymbol{D}(\tilde{\boldsymbol{q}})\boldsymbol{I}_1^{-1})\left((\boldsymbol{I}_1\boldsymbol{\omega})^{\times} - \boldsymbol{\omega}^{\times}\boldsymbol{I}_1 + \frac{\partial \boldsymbol{\tau}_1}{\partial \boldsymbol{\omega}}\right) + \frac{\partial \boldsymbol{\tau}_2}{\partial \boldsymbol{\omega}}$ |
| $\frac{\partial \boldsymbol{I}_2\tilde{\boldsymbol{\omega}}}{\partial \tilde{\boldsymbol{r}}}$ | $\frac{\partial \boldsymbol{\tau}_2}{\partial \tilde{\boldsymbol{r}}}$ |
| $\frac{\partial \boldsymbol{I}_2\tilde{\boldsymbol{\omega}}}{\partial \tilde{\boldsymbol{v}}}$ | $\frac{\partial \boldsymbol{\tau}_2}{\partial \tilde{\boldsymbol{v}}}$ |
| $\frac{\partial \boldsymbol{I}_2\tilde{\boldsymbol{\omega}}}{\partial \tilde{\boldsymbol{q}}}$ | $\left[-\left[\boldsymbol{D}(\tilde{\boldsymbol{q}})\,\boldsymbol{\omega} + \tilde{\boldsymbol{\omega}}\right]^{\times} + (\tilde{\boldsymbol{\omega}}^{\times})\right]\left[\boldsymbol{I}_2\begin{bmatrix} \boldsymbol{\omega}^T\frac{\partial}{\partial \tilde{\boldsymbol{q}}}\boldsymbol{D}^T_{[1,:]}(\tilde{\boldsymbol{q}}) \\ \boldsymbol{\omega}^T\frac{\partial}{\partial \tilde{\boldsymbol{q}}}\boldsymbol{D}^T_{[2,:]}(\tilde{\boldsymbol{q}}) \\ \boldsymbol{\omega}^T\frac{\partial}{\partial \tilde{\boldsymbol{q}}}\boldsymbol{D}^T_{[3,:]}(\tilde{\boldsymbol{q}}) \end{bmatrix}\right] + (\boldsymbol{I}_2\left[\boldsymbol{D}(\tilde{\boldsymbol{q}})\,\boldsymbol{\omega} + \tilde{\boldsymbol{\omega}}\right])^{\times}$ $\begin{bmatrix} \boldsymbol{\omega}^T\frac{\partial}{\partial \tilde{\boldsymbol{q}}}\boldsymbol{D}^T_{[1,:]}(\tilde{\boldsymbol{q}}) \\ \boldsymbol{\omega}^T\frac{\partial}{\partial \tilde{\boldsymbol{q}}}\boldsymbol{D}^T_{[2,:]}(\tilde{\boldsymbol{q}}) \\ \boldsymbol{\omega}^T\frac{\partial}{\partial \tilde{\boldsymbol{q}}}\boldsymbol{D}^T_{[3,:]}(\tilde{\boldsymbol{q}}) \end{bmatrix} - \left(\boldsymbol{I}_2\begin{bmatrix} (\boldsymbol{I}_1^{-1}(-\boldsymbol{\omega}^{\times}(\boldsymbol{I}_1\boldsymbol{\omega}) + \boldsymbol{\tau}_1))^T\frac{\partial}{\partial \tilde{\boldsymbol{q}}}\boldsymbol{D}^T_{[1,:]}(\tilde{\boldsymbol{q}}) \\ (\boldsymbol{I}_1^{-1}(-\boldsymbol{\omega}^{\times}(\boldsymbol{I}_1\boldsymbol{\omega}) + \boldsymbol{\tau}_1))^T\frac{\partial}{\partial \tilde{\boldsymbol{q}}}\boldsymbol{D}^T_{[2,:]}(\tilde{\boldsymbol{q}}) \\ (\boldsymbol{I}_1^{-1}(-\boldsymbol{\omega}^{\times}(\boldsymbol{I}_1\boldsymbol{\omega}) + \boldsymbol{\tau}_1))^T\frac{\partial}{\partial \tilde{\boldsymbol{q}}}\boldsymbol{D}^T_{[3,:]}(\tilde{\boldsymbol{q}}) \end{bmatrix}\right) + \frac{\partial \boldsymbol{\tau}_2}{\partial \tilde{\boldsymbol{q}}}$ |
| $\frac{\partial \boldsymbol{I}_2\tilde{\boldsymbol{\omega}}}{\partial \tilde{\boldsymbol{\omega}}}$ | $-(\tilde{\boldsymbol{\omega}} + \boldsymbol{D}(\tilde{\boldsymbol{q}})\boldsymbol{\omega})^{\times}\boldsymbol{I}_2 + (\boldsymbol{I}_2(\tilde{\boldsymbol{\omega}} + \boldsymbol{D}(\tilde{\boldsymbol{q}})\boldsymbol{\omega}))^{\times} - (\boldsymbol{I}_2\boldsymbol{D}(\tilde{\boldsymbol{q}})\boldsymbol{\omega})^{\times} + \frac{\partial \boldsymbol{\tau}_2}{\partial \tilde{\boldsymbol{\omega}}}$ |

where

$$\boldsymbol{D}^T_{[1,:]}(\boldsymbol{q}) = 2\begin{bmatrix} q_1 & -q_2 & -q_3 & q_4 \\ q_2 & q_1 & q_4 & q_3 \\ q_3 & -q_4 & q_1 & -q_2 \end{bmatrix} \tag{4.28}$$

$$\boldsymbol{D}^T_{[1,:]}(\boldsymbol{q}) = 2\begin{bmatrix} q_2 & q_1 & -q_4 & -q_3 \\ -q_1 & q_2 & -q_3 & q_4 \\ q_4 & q_3 & q_2 & q_1 \end{bmatrix} \tag{4.29}$$

$$\boldsymbol{D}^T_{[1,:]}(\boldsymbol{q}) = 2\begin{bmatrix} q_3 & q_4 & q_1 & q_2 \\ -q_4 & q_3 & q_2 & -q_1 \\ -q_1 & -q_2 & q_3 & q_4 \end{bmatrix} \tag{4.30}$$

### Differential Atmospheric Drag Force

Taking the expression for the atmospheric drag force projected in the $\mathcal{J}$ frame derived (3.20), this leads to

$$
\begin{aligned}
\frac{\partial\, \boldsymbol{a}_{a,2}\big|_{\mathcal{I}}}{\partial \boldsymbol{r}} \;=\; & \frac{1}{2}\frac{C_{D,2}A_{d,i}}{m_2}\Big\{(\boldsymbol{D}(\boldsymbol{q}\oplus\tilde{\boldsymbol{q}})\boldsymbol{n}_{2,A})^T(\boldsymbol{v}+\boldsymbol{D}|_{\mathcal{I}}^{\mathcal{E}}\,\tilde{\boldsymbol{v}}|_{\mathcal{E}}+\Omega|_{\mathcal{E}}^{\mathcal{I}\to\mathcal{E}^{\times}}\boldsymbol{r}+\omega_{Et}^{\times}(\boldsymbol{r}+\boldsymbol{D}|_{\mathcal{I}}^{\mathcal{E}}\tilde{\boldsymbol{r}}))\Big)\\
&\Big(\boldsymbol{v}+\boldsymbol{D}|_{\mathcal{I}}^{\mathcal{E}}\,\tilde{\boldsymbol{v}}|_{\mathcal{E}}+\Omega|_{\mathcal{E}}^{\mathcal{I}\to\mathcal{E}^{\times}}\boldsymbol{r}+\omega_{Et}^{\times}(\boldsymbol{r}+\boldsymbol{D}|_{\mathcal{I}}^{\mathcal{E}}\tilde{\boldsymbol{r}})\Big)\\
&\rho(h_i)\exp\left(\frac{h_i-|\boldsymbol{r}+\boldsymbol{D}|_{\mathcal{I}}^{\mathcal{E}}\tilde{\boldsymbol{r}}}{H_m}\right)\left(\frac{\boldsymbol{r}^T}{|\boldsymbol{r}|H_m}+\frac{1}{H_m}\frac{\partial\,\boldsymbol{D}|_{\mathcal{I}}^{\mathcal{E}}\tilde{\boldsymbol{r}}}{\partial\boldsymbol{r}}\right)+\\
&\rho(\boldsymbol{r}+\boldsymbol{D}|_{\mathcal{I}}^{\mathcal{E}}\tilde{\boldsymbol{r}})\Big((\boldsymbol{D}(\boldsymbol{q}\oplus\tilde{\boldsymbol{q}})\boldsymbol{n}_{2,A})^T(\boldsymbol{v}+\boldsymbol{D}|_{\mathcal{I}}^{\mathcal{E}}\,\tilde{\boldsymbol{v}}|_{\mathcal{E}}+\Omega|_{\mathcal{E}}^{\mathcal{I}\to\mathcal{E}^{\times}}\boldsymbol{r}+\omega_{Et}^{\times}(\boldsymbol{r}+\boldsymbol{D}|_{\mathcal{I}}^{\mathcal{E}}\tilde{\boldsymbol{r}}))\Big)\\
&\left(\frac{\partial\,\boldsymbol{D}|_{\mathcal{I}}^{\mathcal{E}}\tilde{\boldsymbol{v}}}{\partial\boldsymbol{r}}+\Omega|_{\mathcal{E}}^{\mathcal{I}\to\mathcal{E}^{\times}}+\frac{\partial\,\Omega|_{\mathcal{E}}^{\mathcal{I}\to\mathcal{E}^{\times}}}{\partial\boldsymbol{r}}\boldsymbol{r}+\omega_{Et}^{\times}+\frac{\partial\omega_{Et}^{\times}\,\boldsymbol{D}|_{\mathcal{I}}^{\mathcal{E}}\tilde{\boldsymbol{r}}}{\partial\boldsymbol{r}}\right)+\\
&(\boldsymbol{v}+\boldsymbol{D}|_{\mathcal{I}}^{\mathcal{E}}\,\tilde{\boldsymbol{v}}|_{\mathcal{E}}+\Omega|_{\mathcal{E}}^{\mathcal{I}\to\mathcal{E}^{\times}}\boldsymbol{r}+\omega_{Et}^{\times}(\boldsymbol{r}+\boldsymbol{D}|_{\mathcal{I}}^{\mathcal{E}}\tilde{\boldsymbol{r}}))(\boldsymbol{D}(\boldsymbol{q}\oplus\tilde{\boldsymbol{q}})\boldsymbol{n}_{2,A})^T\\
&\left(\frac{\partial\,\boldsymbol{D}|_{\mathcal{I}}^{\mathcal{E}}\tilde{\boldsymbol{v}}}{\partial\boldsymbol{r}}+\Omega|_{\mathcal{E}}^{\mathcal{I}\to\mathcal{E}^{\times}}+\frac{\partial\,\Omega|_{\mathcal{E}}^{\mathcal{I}\to\mathcal{E}^{\times}}}{\partial\boldsymbol{r}}\boldsymbol{r}+\omega_{Et}^{\times}+\frac{\partial\omega_{Et}^{\times}\,\boldsymbol{D}|_{\mathcal{I}}^{\mathcal{E}}\tilde{\boldsymbol{r}}}{\partial\boldsymbol{r}}\right)\Big\}
\end{aligned}
\tag{4.31}
$$

$$
\begin{aligned}
\frac{\partial\, \boldsymbol{a}_{a,2}\big|_{\mathcal{I}}}{\partial \boldsymbol{v}} \;=\; & \frac{1}{2}\frac{C_{D,2}A_{d,i}}{m_2}\Big\{(\boldsymbol{D}(\boldsymbol{q}\oplus\tilde{\boldsymbol{q}})\boldsymbol{n}_{2,A})^T(\boldsymbol{v}+\boldsymbol{D}|_{\mathcal{I}}^{\mathcal{E}}\,\tilde{\boldsymbol{v}}|_{\mathcal{E}}+\Omega|_{\mathcal{E}}^{\mathcal{I}\to\mathcal{E}^{\times}}\boldsymbol{r}+\omega_{Et}^{\times}(\boldsymbol{r}+\boldsymbol{D}|_{\mathcal{I}}^{\mathcal{E}}\tilde{\boldsymbol{r}}))\\
&(\boldsymbol{v}+\boldsymbol{D}|_{\mathcal{I}}^{\mathcal{E}}\,\tilde{\boldsymbol{v}}|_{\mathcal{E}}+\Omega|_{\mathcal{E}}^{\mathcal{I}\to\mathcal{E}^{\times}}\boldsymbol{r}+\omega_{Et}^{\times}(\boldsymbol{r}+\boldsymbol{D}|_{\mathcal{I}}^{\mathcal{E}}\tilde{\boldsymbol{r}}))\\
&\left(\rho(h_i)\exp\left(\frac{h_i-|\boldsymbol{r}+\boldsymbol{D}|_{\mathcal{I}}^{\mathcal{E}}\tilde{\boldsymbol{r}}}{H_m}\right)\left(\frac{\partial\,\boldsymbol{D}|_{\mathcal{I}}^{\mathcal{E}}\tilde{\boldsymbol{r}}}{\partial\boldsymbol{v}}\right)\right)+\\
&\rho(\boldsymbol{r}+\boldsymbol{D}|_{\mathcal{I}}^{\mathcal{E}}\tilde{\boldsymbol{r}})\Big(\boldsymbol{v}+\boldsymbol{D}|_{\mathcal{I}}^{\mathcal{E}}\,\tilde{\boldsymbol{v}}|_{\mathcal{E}}+\Omega|_{\mathcal{E}}^{\mathcal{I}\to\mathcal{E}^{\times}}\boldsymbol{r}+\omega_{Et}^{\times}(\boldsymbol{r}+\boldsymbol{D}|_{\mathcal{I}}^{\mathcal{E}}\tilde{\boldsymbol{r}})\Big)\\
&\left((\boldsymbol{D}(\boldsymbol{q}\oplus\tilde{\boldsymbol{q}})\boldsymbol{n}_{2,A})^T\left(I_3+\frac{\partial\,\boldsymbol{D}|_{\mathcal{I}}^{\mathcal{E}}}{\partial\boldsymbol{v}}+\frac{\partial\,\Omega|_{\mathcal{E}}^{\mathcal{I}\to\mathcal{E}^{\times}}}{\partial\boldsymbol{v}}\boldsymbol{r}\right)\right)+\\
&(\boldsymbol{D}(\boldsymbol{q}\oplus\tilde{\boldsymbol{q}})\boldsymbol{n}_{2,A})^T\Big(\boldsymbol{v}+\boldsymbol{D}|_{\mathcal{I}}^{\mathcal{E}}\,\tilde{\boldsymbol{v}}|_{\mathcal{E}}+\Omega|_{\mathcal{E}}^{\mathcal{I}\to\mathcal{E}^{\times}}\boldsymbol{r}+\omega_{Et}^{\times}(\boldsymbol{r}+\boldsymbol{D}|_{\mathcal{I}}^{\mathcal{E}}\tilde{\boldsymbol{r}})\Big)\\
&\left(I_3+\frac{\partial\,\boldsymbol{D}|_{\mathcal{I}}^{\mathcal{E}}}{\partial\boldsymbol{v}}+\frac{\partial\,\Omega|_{\mathcal{E}}^{\mathcal{I}\to\mathcal{E}^{\times}}}{\partial\boldsymbol{v}}\boldsymbol{r}\right)\Big\}
\end{aligned}
\tag{4.32}
$$

$$\frac{\partial\, \boldsymbol{a}_{a,2}\big|_{\mathcal{I}}}{\partial \boldsymbol{q}} = \frac{1}{2}\frac{C_{D,2}A_{d,i}}{m_2}\rho(\boldsymbol{r}+\boldsymbol{D}|_{\mathcal{I}}^{\mathcal{E}}\tilde{\boldsymbol{r}}) \left\{\left(\boldsymbol{v}+\boldsymbol{D}|_{\mathcal{I}}^{\mathcal{E}}\tilde{\boldsymbol{v}}|_{\mathcal{E}}+\Omega|_{\mathcal{E}}^{\mathcal{I}\to\mathcal{E}^{\times}}\boldsymbol{r}+\omega_{Et}^{\times}(\boldsymbol{r}+\boldsymbol{D}|_{\mathcal{I}}^{\mathcal{E}}\tilde{\boldsymbol{r}})\right) \left[\left(\boldsymbol{v}+\boldsymbol{D}|_{\mathcal{I}}^{\mathcal{E}}\tilde{\boldsymbol{v}}|_{\mathcal{E}}+\Omega|_{\mathcal{E}}^{\mathcal{I}\to\mathcal{E}^{\times}}\boldsymbol{r}+\omega_{Et}^{\times}(\boldsymbol{r}+\boldsymbol{D}|_{\mathcal{I}}^{\mathcal{E}}\tilde{\boldsymbol{r}})\right)^{T}\frac{\partial\left(\boldsymbol{D}(\boldsymbol{q}\oplus\tilde{\boldsymbol{q}})\boldsymbol{n}_{2,A}\right)}{\partial \boldsymbol{q}}\right]\right\} \tag{4.33}$$

$$\frac{\partial\, \boldsymbol{a}_{a,2}\big|_{\mathcal{I}}}{\partial \boldsymbol{\omega}} = 0 \tag{4.34}$$

$$\begin{aligned}\frac{\partial\, \boldsymbol{a}_{a,2}\big|_{\mathcal{I}}}{\partial \tilde{\boldsymbol{r}}} = {} & \frac{1}{2}\frac{C_{D,2}A_{d,i}}{m_2}\Big\{(\boldsymbol{D}(\boldsymbol{q}\oplus\tilde{\boldsymbol{q}})\boldsymbol{n}_{2,A})^{T}(\boldsymbol{v}+\boldsymbol{D}|_{\mathcal{I}}^{\mathcal{E}}\tilde{\boldsymbol{v}}|_{\mathcal{E}}+\Omega|_{\mathcal{E}}^{\mathcal{I}\to\mathcal{E}^{\times}}\boldsymbol{r}+\omega_{Et}^{\times}(\boldsymbol{r}+\boldsymbol{D}|_{\mathcal{I}}^{\mathcal{E}}\tilde{\boldsymbol{r}})) \\ & \left(\boldsymbol{v}+\boldsymbol{D}|_{\mathcal{I}}^{\mathcal{E}}\tilde{\boldsymbol{v}}|_{\mathcal{E}}+\Omega|_{\mathcal{E}}^{\mathcal{I}\to\mathcal{E}^{\times}}\boldsymbol{r}+\omega_{Et}^{\times}(\boldsymbol{r}+\boldsymbol{D}|_{\mathcal{I}}^{\mathcal{E}}\tilde{\boldsymbol{r}})\right) \\ & \rho(h_i)\exp\left(\frac{h_i-|\boldsymbol{r}+\boldsymbol{D}|_{\mathcal{I}}^{\mathcal{E}}\tilde{\boldsymbol{r}}}{H_m}\right)\left(\frac{(\boldsymbol{r}+\boldsymbol{D}|_{\mathcal{I}}^{\mathcal{E}}\tilde{\boldsymbol{r}})^{T}}{|\boldsymbol{r}+\boldsymbol{D}|_{\mathcal{I}}^{\mathcal{E}}\tilde{\boldsymbol{r}}|H_m}\boldsymbol{D}|_{\mathcal{I}}^{\mathcal{E}}\right)+ \\ & \rho(\boldsymbol{r}+\boldsymbol{D}|_{\mathcal{I}}^{\mathcal{E}}\tilde{\boldsymbol{r}})\Big[\Big((\boldsymbol{D}(\boldsymbol{q}\oplus\tilde{\boldsymbol{q}})\boldsymbol{n}_{2,A})^{T}(\boldsymbol{v}+\boldsymbol{D}|_{\mathcal{I}}^{\mathcal{E}}\tilde{\boldsymbol{v}}|_{\mathcal{E}}+\Omega|_{\mathcal{E}}^{\mathcal{I}\to\mathcal{E}^{\times}}\boldsymbol{r}+\omega_{Et}^{\times}(\boldsymbol{r}+\boldsymbol{D}|_{\mathcal{I}}^{\mathcal{E}}\tilde{\boldsymbol{r}}))\Big) \\ & \left(\omega_{Et}^{\times}\,\boldsymbol{D}|_{\mathcal{I}}^{\mathcal{E}}\right)+(\boldsymbol{v}+\boldsymbol{D}|_{\mathcal{I}}^{\mathcal{E}}\tilde{\boldsymbol{v}}|_{\mathcal{E}}+\Omega|_{\mathcal{E}}^{\mathcal{I}\to\mathcal{E}^{\times}}\boldsymbol{r}+\omega_{Et}^{\times}(\boldsymbol{r}+\boldsymbol{D}|_{\mathcal{I}}^{\mathcal{E}}\tilde{\boldsymbol{r}}))(\boldsymbol{D}(\boldsymbol{q}\oplus\tilde{\boldsymbol{q}})\boldsymbol{n}_{2,A})^{T} \\ & \left(\omega_{Et}^{\times}\,\boldsymbol{D}|_{\mathcal{I}}^{\mathcal{E}}\right)\Big]\Big\}\end{aligned} \tag{4.35}$$

$$\frac{\partial\, \boldsymbol{a}_{a,2}\big|_{\mathcal{I}}}{\partial \tilde{\boldsymbol{v}}} = \frac{1}{2}\frac{C_{D,2}A_{d,i}}{m_2}\rho(\boldsymbol{r}+\boldsymbol{D}|_{\mathcal{I}}^{\mathcal{E}}\tilde{\boldsymbol{r}}) \left\{\left((\boldsymbol{D}(\boldsymbol{q}\oplus\tilde{\boldsymbol{q}})\boldsymbol{n}_{2,A})^{T}(\boldsymbol{v}+\boldsymbol{D}|_{\mathcal{I}}^{\mathcal{E}}\tilde{\boldsymbol{v}}|_{\mathcal{E}}+\Omega|_{\mathcal{E}}^{\mathcal{I}\to\mathcal{E}^{\times}}\boldsymbol{r}+\omega_{Et}^{\times}(\boldsymbol{r}+\boldsymbol{D}|_{\mathcal{I}}^{\mathcal{E}}\tilde{\boldsymbol{r}}))\right)\boldsymbol{D}|_{\mathcal{I}}^{\mathcal{E}}+ \left(\boldsymbol{v}+\boldsymbol{D}|_{\mathcal{I}}^{\mathcal{E}}\tilde{\boldsymbol{v}}|_{\mathcal{E}}+\Omega|_{\mathcal{E}}^{\mathcal{I}\to\mathcal{E}^{\times}}\boldsymbol{r}+\omega_{Et}^{\times}(\boldsymbol{r}+\boldsymbol{D}|_{\mathcal{I}}^{\mathcal{E}}\tilde{\boldsymbol{r}})\right)(\boldsymbol{D}(\boldsymbol{q}\oplus\tilde{\boldsymbol{q}})\boldsymbol{n}_{2,A})^{T}\,\boldsymbol{D}|_{\mathcal{I}}^{\mathcal{E}}\right\} \tag{4.36}$$

$$\frac{\partial\, \boldsymbol{a}_{a,2}\big|_{\mathcal{I}}}{\partial \tilde{\boldsymbol{q}}} = \frac{1}{2}\frac{C_{D,2}A_{d,i}}{m_2}\rho(\boldsymbol{r}+\boldsymbol{D}|_{\mathcal{I}}^{\mathcal{E}}\tilde{\boldsymbol{r}}) \left\{\left(\boldsymbol{v}+\boldsymbol{D}|_{\mathcal{I}}^{\mathcal{E}}\tilde{\boldsymbol{v}}|_{\mathcal{E}}+\Omega|_{\mathcal{E}}^{\mathcal{I}\to\mathcal{E}^{\times}}\boldsymbol{r}+\omega_{Et}^{\times}(\boldsymbol{r}+\boldsymbol{D}|_{\mathcal{I}}^{\mathcal{E}}\tilde{\boldsymbol{r}})\right) \left(\boldsymbol{v}+\boldsymbol{D}|_{\mathcal{I}}^{\mathcal{E}}\tilde{\boldsymbol{v}}|_{\mathcal{E}}+\Omega|_{\mathcal{E}}^{\mathcal{I}\to\mathcal{E}^{\times}}\boldsymbol{r}+\omega_{Et}^{\times}(\boldsymbol{r}+\boldsymbol{D}|_{\mathcal{I}}^{\mathcal{E}}\tilde{\boldsymbol{r}})\right)^{T}\frac{\partial(\boldsymbol{D}(\boldsymbol{q}\oplus\tilde{\boldsymbol{q}})\boldsymbol{n}_{2,A})}{\partial\tilde{\boldsymbol{q}}}\right\} \tag{4.37}$$

$$\frac{\partial\, \boldsymbol{a}_{a,2}\big|_{\mathcal{J}}}{\partial \tilde{\boldsymbol{\omega}}} = \mathbf{0} \tag{4.38}$$

### Differential Atmospheric Drag Torque

Taking the expression for the atmospheric drag torque projected in the $\mathcal{B}$ frame, repeated here for convenience

$$\begin{aligned}\boldsymbol{\tau}_{a,2}\big|_{\mathcal{B}} = & \frac{1}{2} C_{D,2} A_{d,i} \rho(\boldsymbol{r} + \boldsymbol{D}|_{\mathcal{J}}^{\mathcal{E}} \tilde{\boldsymbol{r}}) \left(\boldsymbol{n}_{2,A}^{T} (\boldsymbol{D}(\tilde{\boldsymbol{q}} \oplus \boldsymbol{q})(\boldsymbol{D}|_{\mathcal{J}}^{\mathcal{E}} \tilde{\boldsymbol{v}} + \boldsymbol{v} + \omega_{Et}^{\times}(\boldsymbol{r} + \boldsymbol{D}|_{\mathcal{J}}^{\mathcal{E}} \tilde{\boldsymbol{r}})))\right) \\ & \left(\boldsymbol{d}_{2,A}^{\times} (\boldsymbol{D}(\tilde{\boldsymbol{q}} \oplus \boldsymbol{q})(\boldsymbol{D}|_{\mathcal{J}}^{\mathcal{E}} \tilde{\boldsymbol{v}} + \boldsymbol{v} + \omega_{Et}^{\times}(\boldsymbol{r} + \boldsymbol{D}|_{\mathcal{J}}^{\mathcal{E}} \tilde{\boldsymbol{r}})))\right).\end{aligned} \tag{4.39}$$

Then, we get

$$\begin{aligned}\frac{\partial \boldsymbol{\tau}_{a,2}}{\partial \boldsymbol{r}} = & \frac{1}{2} C_{D,2} A_{d,i} \left\{ \left(\boldsymbol{n}_{2,A}^{T} (\boldsymbol{D}(\tilde{\boldsymbol{q}} \oplus \boldsymbol{q})(\boldsymbol{D}|_{\mathcal{J}}^{\mathcal{E}} \tilde{\boldsymbol{v}} + \boldsymbol{v} + \omega_{Et}^{\times}(\boldsymbol{r} + \boldsymbol{D}|_{\mathcal{J}}^{\mathcal{E}} \tilde{\boldsymbol{r}}))) \right) \right. \\ & \left(\boldsymbol{d}_{2,A}^{\times} (\boldsymbol{D}(\tilde{\boldsymbol{q}} \oplus \boldsymbol{q})(\boldsymbol{D}|_{\mathcal{J}}^{\mathcal{E}} \tilde{\boldsymbol{v}} + \boldsymbol{v} + \omega_{Et}^{\times}(\boldsymbol{r} + \boldsymbol{D}|_{\mathcal{J}}^{\mathcal{E}} \tilde{\boldsymbol{r}}))) \right) \\ & \rho(h_i) \exp\left(\frac{h_i - |\boldsymbol{r} + \boldsymbol{D}|_{\mathcal{J}}^{\mathcal{E}} \tilde{\boldsymbol{r}}|}{H_m}\right) \left(\frac{\boldsymbol{r}^{T}}{|\boldsymbol{r}| H_m} + \frac{1}{H_m} \frac{\partial\, \boldsymbol{D}|_{\mathcal{J}}^{\mathcal{E}} \tilde{\boldsymbol{r}}}{\partial \boldsymbol{r}}\right) + \\ & \rho(\boldsymbol{r} + \boldsymbol{D}|_{\mathcal{J}}^{\mathcal{E}} \tilde{\boldsymbol{r}}) \left(\boldsymbol{d}_{2,A}^{\times} (\boldsymbol{D}(\tilde{\boldsymbol{q}} \oplus \boldsymbol{q})(\boldsymbol{D}|_{\mathcal{J}}^{\mathcal{E}} \tilde{\boldsymbol{v}} + \boldsymbol{v} + \omega_{Et}^{\times}(\boldsymbol{r} + \boldsymbol{D}|_{\mathcal{J}}^{\mathcal{E}} \tilde{\boldsymbol{r}}))) \right) \\ & (\boldsymbol{n}_{2,A}^{T} \boldsymbol{D}(\tilde{\boldsymbol{q}} \oplus \boldsymbol{q})(\frac{\partial\, \boldsymbol{D}|_{\mathcal{J}}^{\mathcal{E}} \tilde{\boldsymbol{v}}}{\partial \boldsymbol{r}} + \omega_{Et}^{\times} + \omega_{Et}^{\times} \frac{\partial\, \boldsymbol{D}|_{\mathcal{J}}^{\mathcal{E}} \tilde{\boldsymbol{r}}}{\partial \boldsymbol{r}})) + \\ & \rho(\boldsymbol{r} + \boldsymbol{D}|_{\mathcal{J}}^{\mathcal{E}} \tilde{\boldsymbol{r}}) \left(\boldsymbol{n}_{2,A}^{T} (\boldsymbol{D}(\tilde{\boldsymbol{q}} \oplus \boldsymbol{q})(\boldsymbol{D}|_{\mathcal{J}}^{\mathcal{E}} \tilde{\boldsymbol{v}} + \boldsymbol{v} + \omega_{Et}^{\times}(\boldsymbol{r} + \boldsymbol{D}|_{\mathcal{J}}^{\mathcal{E}} \tilde{\boldsymbol{r}}))) \right) \\ & \left. (\boldsymbol{d}_{2,A}^{\times} \boldsymbol{D}(\tilde{\boldsymbol{q}} \oplus \boldsymbol{q})(\frac{\partial\, \boldsymbol{D}|_{\mathcal{J}}^{\mathcal{E}} \tilde{\boldsymbol{v}}}{\partial \boldsymbol{r}} + \omega_{Et}^{\times} + \omega_{Et}^{\times} \frac{\partial\, \boldsymbol{D}|_{\mathcal{J}}^{\mathcal{E}} \tilde{\boldsymbol{r}}}{\partial \boldsymbol{r}})) \right\}\end{aligned} \tag{4.40}$$

$$\begin{aligned}\frac{\partial \boldsymbol{\tau}_{a,2}}{\partial \boldsymbol{v}} = & \frac{1}{2} C_{D,2} A_{d,i} \rho(\boldsymbol{r} + \boldsymbol{D}|_{\mathcal{J}}^{\mathcal{E}} \tilde{\boldsymbol{r}}) \left\{ \left(\boldsymbol{d}_{2,A}^{\times} (\boldsymbol{D}(\tilde{\boldsymbol{q}} \oplus \boldsymbol{q})(\boldsymbol{D}|_{\mathcal{J}}^{\mathcal{E}} \tilde{\boldsymbol{v}} + \boldsymbol{v} + \omega_{Et}^{\times}(\boldsymbol{r} + \boldsymbol{D}|_{\mathcal{J}}^{\mathcal{E}} \tilde{\boldsymbol{r}}))) \right) \right. \\ & \left(\boldsymbol{n}_{2,A}^{T} \boldsymbol{D}(\tilde{\boldsymbol{q}} \oplus \boldsymbol{q})(\frac{\partial\, \boldsymbol{D}|_{\mathcal{J}}^{\mathcal{E}} \tilde{\boldsymbol{v}}}{\partial \boldsymbol{v}} + I_3 + \boldsymbol{\omega}_{E}^{\times} \frac{\partial\, \boldsymbol{D}|_{\mathcal{J}}^{\mathcal{E}} \tilde{\boldsymbol{r}}}{\partial \boldsymbol{v}}) \right) + \\ & \left(\boldsymbol{n}_{2,A}^{T} (\boldsymbol{D}(\tilde{\boldsymbol{q}} \oplus \boldsymbol{q})(\boldsymbol{D}|_{\mathcal{J}}^{\mathcal{E}} \tilde{\boldsymbol{v}} + \boldsymbol{v} + \omega_{Et}^{\times}(\boldsymbol{r} + \boldsymbol{D}|_{\mathcal{J}}^{\mathcal{E}} \tilde{\boldsymbol{r}}))) \right) \\ & \left. \left(\boldsymbol{d}_{2,A}^{\times} \boldsymbol{D}(\tilde{\boldsymbol{q}} \oplus \boldsymbol{q})(\frac{\partial\, \boldsymbol{D}|_{\mathcal{J}}^{\mathcal{E}} \tilde{\boldsymbol{v}}}{\partial \boldsymbol{v}} + I_3 + \boldsymbol{\omega}_{E}^{\times} \frac{\partial\, \boldsymbol{D}|_{\mathcal{J}}^{\mathcal{E}} \tilde{\boldsymbol{r}}}{\partial \boldsymbol{v}}) \right) \right\}\end{aligned} \tag{4.41}$$

$$\frac{\partial \boldsymbol{\tau}_{a,2}}{\partial \boldsymbol{q}} = \frac{1}{2} C_{D,2} A_{d,i} \rho(\boldsymbol{r} + \boldsymbol{D}|_J^{\mathcal{E}} \tilde{\boldsymbol{r}}) \left\{ \left( \boldsymbol{d}_{2,A}^{\times} (\boldsymbol{D}(\tilde{\boldsymbol{q}} \oplus \boldsymbol{q})(\boldsymbol{D}|_J^{\mathcal{E}} \tilde{\boldsymbol{v}} + \boldsymbol{v} + \omega_{Et}^{\times}(\boldsymbol{r} + \boldsymbol{D}|_J^{\mathcal{E}} \tilde{\boldsymbol{r}}))) \right) \left( \boldsymbol{n}_{2,A}^{T} (\boldsymbol{D}(\tilde{\boldsymbol{q}}) \sum_{j=1}^{3} \frac{\partial \boldsymbol{D}(\boldsymbol{q})_{[:,j]}}{\partial \boldsymbol{q}} (\boldsymbol{D}|_J^{\mathcal{E}} \tilde{\boldsymbol{v}} + \boldsymbol{v} + \omega_{Et}^{\times}(\boldsymbol{r} + \boldsymbol{D}|_J^{\mathcal{E}} \tilde{\boldsymbol{r}})))_{[j]} \right) + \left( \boldsymbol{n}_{2,A}^{T} (\boldsymbol{D}(\tilde{\boldsymbol{q}} \oplus \boldsymbol{q})(\boldsymbol{D}|_J^{\mathcal{E}} \tilde{\boldsymbol{v}} + \boldsymbol{v} + \omega_{Et}^{\times}(\boldsymbol{r} + \boldsymbol{D}|_J^{\mathcal{E}} \tilde{\boldsymbol{r}}))) \right) \left( \boldsymbol{d}_{2,A}^{\times} (\boldsymbol{D}(\tilde{\boldsymbol{q}}) \sum_{j=1}^{3} \frac{\partial \boldsymbol{D}(\boldsymbol{q})_{[:,j]}}{\partial \boldsymbol{q}} (\boldsymbol{D}|_J^{\mathcal{E}} \tilde{\boldsymbol{v}} + \boldsymbol{v} + \omega_{Et}^{\times}(\boldsymbol{r} + \boldsymbol{D}|_J^{\mathcal{E}} \tilde{\boldsymbol{r}})))_{[j]} \right) \right\} \tag{4.42}$$

4

$$\begin{aligned} \frac{\partial \boldsymbol{\tau}_{a,2}}{\partial \tilde{\boldsymbol{r}}} = \frac{1}{2} C_{D,2} A_{d,i} \Big\{ & \left( \boldsymbol{n}_{2,A}^{T} (\boldsymbol{D}(\tilde{\boldsymbol{q}} \oplus \boldsymbol{q})(\boldsymbol{D}|_J^{\mathcal{E}} \tilde{\boldsymbol{v}} + \boldsymbol{v} + \omega_{Et}^{\times}(\boldsymbol{r} + \boldsymbol{D}|_J^{\mathcal{E}} \tilde{\boldsymbol{r}}))) \right) \\ & \left( \boldsymbol{d}_{2,A}^{\times} (\boldsymbol{D}(\tilde{\boldsymbol{q}} \oplus \boldsymbol{q})(\boldsymbol{D}|_J^{\mathcal{E}} \tilde{\boldsymbol{v}} + \boldsymbol{v} + \omega_{Et}^{\times}(\boldsymbol{r} + \boldsymbol{D}|_J^{\mathcal{E}} \tilde{\boldsymbol{r}}))) \right) \\ & \rho(h_i) \exp\left( \frac{h_i - |\boldsymbol{r} + \boldsymbol{D}|_J^{\mathcal{E}} \tilde{\boldsymbol{r}}}{H_m} \right) \left( \frac{(\boldsymbol{r} + \boldsymbol{D}|_J^{\mathcal{E}} \tilde{\boldsymbol{r}})^T}{|\boldsymbol{r} + \boldsymbol{D}|_J^{\mathcal{E}} \tilde{\boldsymbol{r}}| H_m} \boldsymbol{D}|_J^{\mathcal{E}} \right) + \\ & \rho(\boldsymbol{r} + \boldsymbol{D}|_J^{\mathcal{E}} \tilde{\boldsymbol{r}}) \left( \boldsymbol{d}_{2,A}^{\times} (\boldsymbol{D}(\tilde{\boldsymbol{q}} \oplus \boldsymbol{q})(\boldsymbol{D}|_J^{\mathcal{E}} \tilde{\boldsymbol{v}} + \boldsymbol{v} + \omega_{Et}^{\times}(\boldsymbol{r} + \boldsymbol{D}|_J^{\mathcal{E}} \tilde{\boldsymbol{r}}))) \right) \\ & \left( \boldsymbol{n}_{2,A}^{T} (\boldsymbol{D}(\tilde{\boldsymbol{q}} \oplus \boldsymbol{q})(\boldsymbol{\omega}_E^{\times} \boldsymbol{D}|_J^{\mathcal{E}})) \right) + \\ & \rho(\boldsymbol{r} + \boldsymbol{D}|_J^{\mathcal{E}} \tilde{\boldsymbol{r}}) \left( \boldsymbol{n}_{2,A}^{T} (\boldsymbol{D}(\tilde{\boldsymbol{q}} \oplus \boldsymbol{q})(\boldsymbol{D}|_J^{\mathcal{E}} \tilde{\boldsymbol{v}} + \boldsymbol{v} + \omega_{Et}^{\times}(\boldsymbol{r} + \boldsymbol{D}|_J^{\mathcal{E}} \tilde{\boldsymbol{r}}))) \right) \\ & \left( \boldsymbol{d}_{2,A}^{\times} (\boldsymbol{D}(\tilde{\boldsymbol{q}} \oplus \boldsymbol{q})(\boldsymbol{\omega}_E^{\times} \boldsymbol{D}|_J^{\mathcal{E}})) \right) \Big\} \end{aligned} \tag{4.43}$$

$$\frac{\partial \boldsymbol{\tau}_{a,2}}{\partial \tilde{\boldsymbol{v}}} = \frac{1}{2} C_{D,2} A_{d,i} \rho(\boldsymbol{r} + \boldsymbol{D}|_J^{\mathcal{E}} \tilde{\boldsymbol{r}}) \left\{ \left( \boldsymbol{d}_{2,A}^{\times} (\boldsymbol{D}(\tilde{\boldsymbol{q}} \oplus \boldsymbol{q})(\boldsymbol{D}|_J^{\mathcal{E}} \tilde{\boldsymbol{v}} + \boldsymbol{v} + \omega_{Et}^{\times}(\boldsymbol{r} + \boldsymbol{D}|_J^{\mathcal{E}} \tilde{\boldsymbol{r}}))) \right) \left( \boldsymbol{n}_{2,A}^{T} (\boldsymbol{D}(\tilde{\boldsymbol{q}} \oplus \boldsymbol{q}) \boldsymbol{D}|_J^{\mathcal{E}}) \right) + \left( \boldsymbol{n}_{2,A}^{T} (\boldsymbol{D}(\tilde{\boldsymbol{q}} \oplus \boldsymbol{q})(\boldsymbol{D}|_J^{\mathcal{E}} \tilde{\boldsymbol{v}} + \boldsymbol{v} + \omega_{Et}^{\times}(\boldsymbol{r} + \boldsymbol{D}|_J^{\mathcal{E}} \tilde{\boldsymbol{r}}))) \right) \left( \boldsymbol{d}_{2,A}^{\times} (\boldsymbol{D}(\tilde{\boldsymbol{q}} \oplus \boldsymbol{q}) \boldsymbol{D}|_J^{\mathcal{E}}) \right) \right\} \tag{4.44}$$

$$\frac{\partial \boldsymbol{\tau}_{a,2}}{\partial \tilde{\boldsymbol{q}}} = \frac{1}{2} C_{D,2} A_{d,i} \rho(\boldsymbol{r} + \boldsymbol{D}|_J^{\mathcal{E}} \tilde{\boldsymbol{r}}) \left\{ \left( \boldsymbol{d}_{2,A}^{\times} (\boldsymbol{D}(\tilde{\boldsymbol{q}} \oplus \boldsymbol{q})(\boldsymbol{D}|_J^{\mathcal{E}} \tilde{\boldsymbol{v}} + \boldsymbol{v} + \omega_{Et}^{\times}(\boldsymbol{r} + \boldsymbol{D}|_J^{\mathcal{E}} \tilde{\boldsymbol{r}}))) \right) \left( \boldsymbol{n}_{2,A}^{T} \sum_{j=1}^{3} \frac{\partial \boldsymbol{D}(\tilde{\boldsymbol{q}})_{[:,j]}}{\partial \tilde{\boldsymbol{q}}} (\boldsymbol{D}(\boldsymbol{q})(\boldsymbol{D}|_J^{\mathcal{E}} \tilde{\boldsymbol{v}} + \boldsymbol{v} + \omega_{Et}^{\times}(\boldsymbol{r} + \boldsymbol{D}|_J^{\mathcal{E}} \tilde{\boldsymbol{r}})))_{[j]} \right) + \left( \boldsymbol{n}_{2,A}^{T} (\boldsymbol{D}(\tilde{\boldsymbol{q}} \oplus \boldsymbol{q})(\boldsymbol{D}|_J^{\mathcal{E}} \tilde{\boldsymbol{v}} + \boldsymbol{v} + \omega_{Et}^{\times}(\boldsymbol{r} + \boldsymbol{D}|_J^{\mathcal{E}} \tilde{\boldsymbol{r}}))) \right) \left( \boldsymbol{d}_{2,A}^{\times} \sum_{j=1}^{3} \frac{\partial \boldsymbol{D}(\tilde{\boldsymbol{q}})_{[:,j]}}{\partial \tilde{\boldsymbol{q}}} (\boldsymbol{D}(\boldsymbol{q})(\boldsymbol{D}|_J^{\mathcal{E}} \tilde{\boldsymbol{v}} + \boldsymbol{v} + \omega_{Et}^{\times}(\boldsymbol{r} + \boldsymbol{D}|_J^{\mathcal{E}} \tilde{\boldsymbol{r}})))_{[j]} \right) \right\} \tag{4.45}$$

where

$$\frac{\partial \boldsymbol{D}(\tilde{\boldsymbol{q}})_{[:,1]}}{\partial \tilde{\boldsymbol{q}}} = 2\begin{bmatrix} \tilde{q}_1 & \tilde{q}_2 & -\tilde{q}_3 & -\tilde{q}_4 \\ -\tilde{q}_4 & \tilde{q}_3 & \tilde{q}_2 & -\tilde{q}_1 \\ \tilde{q}_3 & \tilde{q}_4 & \tilde{q}_1 & \tilde{q}_2 \end{bmatrix} \tag{4.46}$$

$$\frac{\partial \boldsymbol{D}(\tilde{\boldsymbol{q}})_{[:,2]}}{\partial \tilde{\boldsymbol{q}}} = 2\begin{bmatrix} \tilde{q}_4 & \tilde{q}_3 & \tilde{q}_2 & \tilde{q}_1 \\ \tilde{q}_1 & -\tilde{q}_2 & \tilde{q}_3 & -\tilde{q}_4 \\ -\tilde{q}_2 & -\tilde{q}_1 & \tilde{q}_3 & \tilde{q}_4 \end{bmatrix} \tag{4.47}$$

$$\frac{\partial \boldsymbol{D}(\tilde{\boldsymbol{q}})_{[:,3]}}{\partial \tilde{\boldsymbol{q}}} = 2\begin{bmatrix} -\tilde{q}_3 & \tilde{q}_4 & -\tilde{q}_1 & \tilde{q}_2 \\ \tilde{q}_2 & \tilde{q}_1 & \tilde{q}_4 & \tilde{q}_3 \\ \tilde{q}_1 & -\tilde{q}_2 & -\tilde{q}_3 & \tilde{q}_4 \end{bmatrix} \tag{4.48}$$



### 4.3.3. Matrix Multiplication Partial Derivative

The linearization of the dynamics of the relative attitude of spacecraft requires the derivation of the partial derivatives of matrices that are included in the state for which the linearization is done. This section describes the way to obtain the partial derivatives that depend on the variable to be derived when it is multiplied with a vector. This method was derived for this work, since no equivalent methods were found. This is useful to derive rotation matrices that depend directly on the states.

Assume the existence of vectors $\boldsymbol{x} \in \mathbb{R}^n$, $\boldsymbol{v} \in \mathbb{R}^m$ and a matrix $\boldsymbol{M}(\boldsymbol{x}) \in \mathbb{R}^{p\times m}$. If the derivative of, e.g.

$$\frac{\partial\,(\boldsymbol{M}(\boldsymbol{x})\boldsymbol{v})}{\partial \boldsymbol{x}}, \tag{4.49}$$

is needed, the use of the chain rule is not straightforward. Due to the fact that $\boldsymbol{M}(\boldsymbol{x})\boldsymbol{v} \in \mathbb{R}^n$ , so the result needs to be an element of $\mathbb{R}^{n\times n}$.

The problem can be solved in two different ways presented here for reference.

### 4.3.4. Method 1: Row operations method

Model the matrix multiplication as a series of vector multiplications in each row

$$\boldsymbol{M}(\boldsymbol{x})\boldsymbol{v} = \begin{bmatrix} \boldsymbol{M}(\boldsymbol{x})_{[1,:]}\boldsymbol{v} \\ \boldsymbol{M}(\boldsymbol{x})_{[2,:]}\boldsymbol{v} \\ .. \\ \boldsymbol{M}(\boldsymbol{x})_{[p,:]}\boldsymbol{v} \end{bmatrix} \in \mathbb{R}^p \tag{4.50}$$

with $\boldsymbol{M}_{[i,:]}$ being the $i$-th row of matrix $\boldsymbol{M}(\boldsymbol{x})$. This means that each element $\boldsymbol{M}_{[i,:]}\boldsymbol{v}$ is a scalar. Then

$$\frac{\partial (M_{[i,:]}\boldsymbol{v})}{\partial \boldsymbol{x}} = \boldsymbol{v}\frac{\partial \boldsymbol{M}(\boldsymbol{x})^T_{[i,:]}}{\partial \boldsymbol{x}}, \tag{4.51}$$

where $\partial \boldsymbol{M}^T_{[i,:]}/\partial \boldsymbol{x}$ has the form of a typical vector partial derivative. Therefore,

$$\frac{\partial \boldsymbol{M}(\boldsymbol{x})\boldsymbol{v}}{\partial \boldsymbol{x}} = \begin{bmatrix} \boldsymbol{v}^T \frac{\partial \boldsymbol{M}(\boldsymbol{x})^T_{[1,:]}}{\partial \boldsymbol{x}} \\ \boldsymbol{v}^T \frac{\partial \boldsymbol{M}(\boldsymbol{x})^T_{[2,:]}}{\partial \boldsymbol{x}} \\ .. \\ \boldsymbol{v}^T \frac{\partial \boldsymbol{M}(\boldsymbol{x})^T_{[n,:]}}{\partial \boldsymbol{x}} \end{bmatrix}. \tag{4.52}$$

### 4.3.5. Method 2: Column operations method

The matrix-vector multiplication can be also expressed as

$$\boldsymbol{M}(\boldsymbol{x})\boldsymbol{v} = v_1\boldsymbol{M}(\boldsymbol{x})_{[:,1]} + v_2\boldsymbol{M}(\boldsymbol{x})_{[:,2]} + ... + v_m\boldsymbol{M}(\boldsymbol{x})_{[:,m]}, \tag{4.53}$$



with $\boldsymbol{M}(\boldsymbol{x})_{[:,i]}$ being the $i$ column of matrix $\boldsymbol{M}(\boldsymbol{x})$. Then, it is clear that for each element

$$\frac{\partial v_i\boldsymbol{M}(\boldsymbol{x})_{[:,i]}}{\partial \boldsymbol{x}} = v_i \frac{\partial \boldsymbol{M}(\boldsymbol{x})_{[:,i]}}{\partial \boldsymbol{x}}. \tag{4.54}$$

This leads to

$$\frac{\partial \boldsymbol{M}(\boldsymbol{x})\boldsymbol{v}}{\partial \boldsymbol{x}} = v_1 \frac{\partial \boldsymbol{M}(\boldsymbol{x})_{[:,1]}}{\partial \boldsymbol{x}} + v_2 \frac{\partial \boldsymbol{M}(\boldsymbol{x})_{[:,2]}}{\partial \boldsymbol{x}} + ... + v_m \frac{\partial \boldsymbol{M}(\boldsymbol{x})_{[:,m]}}{\partial \boldsymbol{x}}. \tag{4.55}$$

Clearly, both methods are identical in their final result. Nevertheless, one may be more convenient than than the other depending on the case. Both of them are used to arrive at the partial derivatives derivations presented in this chapter.

## 4.4. Verification

Due to the error-prone analytical derivation of the partial derivatives, their verification is fundamental. In order to do this, the analytic results of the partial derivatives are propagated and compared with the results from a numerical propagation. The method for the numerical propagation is described here.

### 4.4.1. Difference Quotient Approximations

The analytical calculation of partial derivatives in this chapter is prone to errors due to their complexity. The method of difference quotient approximation is presented here to determine the partial derivatives numerically.

For a given initial state $\boldsymbol{y}_0$ and a nominal coefficient $\alpha$, the dynamic equation partial derivative is obtained from the first-order different quotient [41]

$$\frac{\partial \boldsymbol{y}(t)}{\partial \alpha} \approx \frac{\boldsymbol{y}(t, \boldsymbol{y}_0, \alpha + \Delta\alpha) - \boldsymbol{y}(t, \boldsymbol{y}_0, \alpha)}{\Delta\alpha}, \tag{4.56}$$

where the parameter $\alpha + \Delta\alpha$ is used to vary the trajectory of $\boldsymbol{y}$. As the authors of [41] describe, the major drawback of the approach lies in the difficulty of choosing a proper value for the parameter increment $\Delta\alpha$. In this work, its selection is considered sufficient if it leads to a relative error of less than 0.1%.

Table 4.8: Initial conditions for the dynamics of the system under study. for an along-track separation ($R_A$) of 1000 km. Two initial rotation rate cases will be used for comparison purposes. The angular separation between the two spacecraft, given that they are in the same orbit, is their difference in true anomaly, a function of $R_A$ (here Earth radius $R_E = 6,371$ km ).

| State | S/C 1 | S/C 2 |
|---|---|---|
| Position [km] | $[300 + R_E, 0, 0]$ | $(300 + R_E)[\cos\theta_2, \sin\theta_2, 0]$ |
| Velocity [km/s] | $[0, 7.7142, 0]$ | $7.7142[-\sin\theta_2, \cos\theta_2, 0]$ |
| Attitude quaternion | $[0, 0, 0, 1]$ | $[0, 0, 0, 1]$ |
| Rotation rate for the rotating case [rad/s] | $[0, \pi/18, 0]$ | $[0, 0, \pi/18]$ |
| True anomaly $\theta$ [rad] | 0 | $\frac{R_A}{R_E+R_A}$ |

Table 4.9: Increment parameters for the numerical integration of the partial derivatives. These incremented parameters are used for both the absolute and the relative states

| Absolute and Relative State | Value |
|---|---|
| $\Delta\boldsymbol{r}$,$\Delta\tilde{\boldsymbol{r}}$ (m) | 1 |
| $\Delta\boldsymbol{v}$,$\Delta\tilde{\boldsymbol{v}}$ (m/s) | 0.01 |
| $\Delta\boldsymbol{q}$,$\Delta\tilde{\boldsymbol{q}}$ | 0.01 |
| $\Delta\boldsymbol{\omega}$,$\Delta\tilde{\boldsymbol{\omega}}$ (rad/s) | 0.001 |



### 4.4.2. Verification Scenario

The scenario selected is based on two spacecraft flying in formation, with an along track separation of 1000 km at a 300 km altitude circular and equatorial orbit. Their complete initial dynamics are described in Table 4.8.

The calculation of the numeric partial derivatives is done using the difference quotient approximation presented in the previous section. The selection of the increment parameter for the numerical integration is presented in Table 4.9.

### 4.4.3. Sample Results of the Verification

In Figure 4.1 the numerically and the analytically propagated derivatives for $\partial\dot{\boldsymbol{v}}/\partial\boldsymbol{r}$ are shown and the difference between the symbolic and the numerical propagation. Clearly, in this case, the error is six orders of magnitude smaller than the magnitude of both the numeric and symbolic propagation. For this reason, the verification is consider satisfactory.

The atmospheric drag partial derivatives obtained here were also verified using numerical propagation. The acceleration due to the atmospheric drag in the $\mathcal{I}$ frame is given by

$$\boldsymbol{a}_a = -\frac{1}{2}\frac{\rho(\boldsymbol{r})}{m}\sum_{i=1}^{s} C_i A_i \left\{\left(D^T(\boldsymbol{q})\boldsymbol{n}_i\right)^T (\boldsymbol{v} - \boldsymbol{\omega}_E^{\times}\boldsymbol{r})\right\}(\boldsymbol{v} - \boldsymbol{\omega}_E^{\times}\boldsymbol{r}). \tag{4.57}$$

The variation of atmospheric drag with respect to the velocity is given by

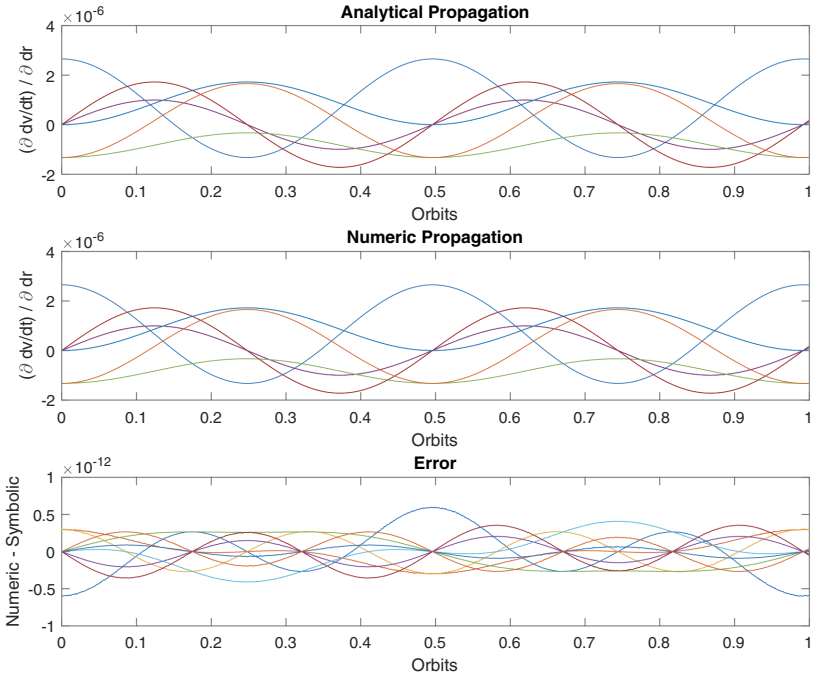


Figure 4.1: Propagation of the analytical and numeric partial derivative $\partial\dot{\boldsymbol{v}}/\partial\boldsymbol{r}$ as an example of the verification

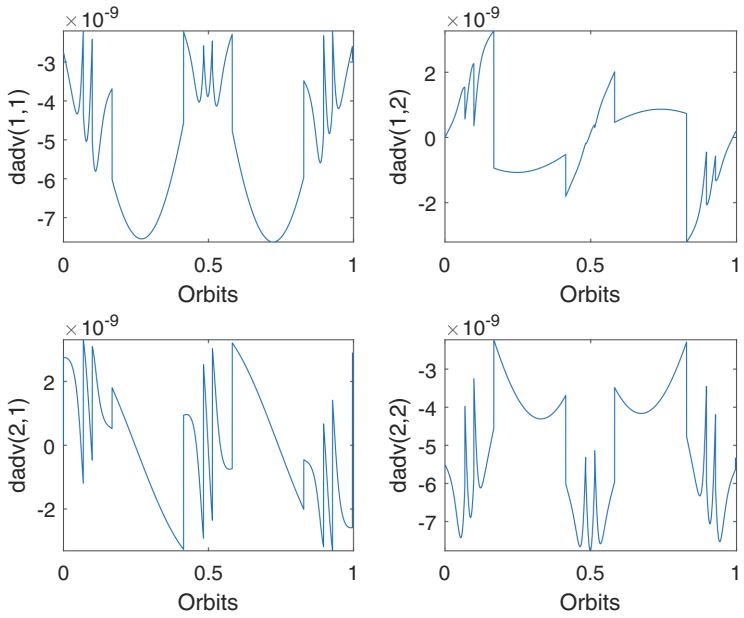


Figure 4.2: Propagation of the numerical variation of the atmospheric drag force with respect to the velocity. The derivation of the third component is not shown due to the fact that the propagation is done in an equatorial orbit.

$$\frac{\partial \boldsymbol{a}_a}{\partial \boldsymbol{v}} = -\frac{\rho(\boldsymbol{r})}{2m}\sum_{i=1}^{k} C_i A_i \left(((\boldsymbol{v}-\boldsymbol{\omega}_E^{\times}\boldsymbol{r})^T \boldsymbol{D}(\boldsymbol{q})\boldsymbol{n}_i) I_3 + (\boldsymbol{v}-\boldsymbol{\omega}_E^{\times}\boldsymbol{r})(\boldsymbol{D}(\boldsymbol{q})\boldsymbol{n}_i)^T\right). \quad (4.58)$$

The propagation of the numerical variation and the analytical expressions of this partial derivative of atmospheric drag acceleration is shown in Fig. 4.2 and 4.3. The difference between the analytical and the numerical propagations is then shown in Figure 4.4. The error is nine order of magnitude smaller than the magnitude of the propagation of the partial derivatives. Hence the verification is consider satisfactory. Here, the propagation is shown in two coordinates, due to the fact that the both the atmospheric drag force and the velocity are zero in the axis that is perpendicular to the spacecraft orbit, for an equatorial orbit.

For a more general verification of the atmospheric drag partial derivatives expressions, Figure 4.5 shows for example the results of the numerical and analytical propagation of the partial derivatives with respect to the orbit absolute states, and the differences between both of them. Here, it is clear that in the worst-case scenario, the error is six orders of magnitude smaller than the magnitude of the partial derivatives propagations, proving one more time that the verification is sucessful.

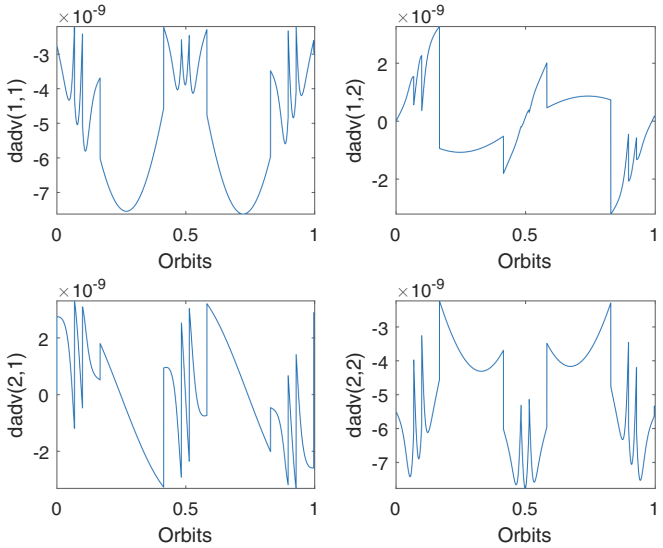


Figure 4.3: Propagation of the symbolic variation of the atmospheric drag force with respect to the velocity.The derivation of the third component is not shown due to the fact that the propagation is done in an equatorial orbit.

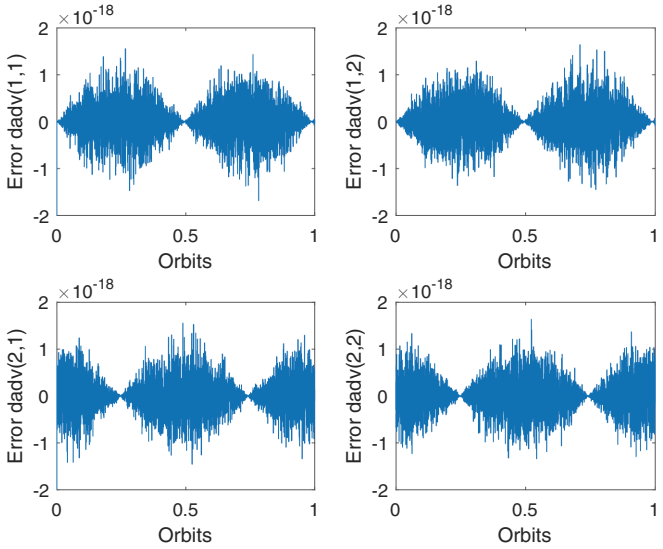


Figure 4.4: Differences in the analytical and numerical results of the of the atmospheric drag force with respect to the velocity. The derivation of the third component is not shown due to the fact that the propagation is done in an equatorial orbit.

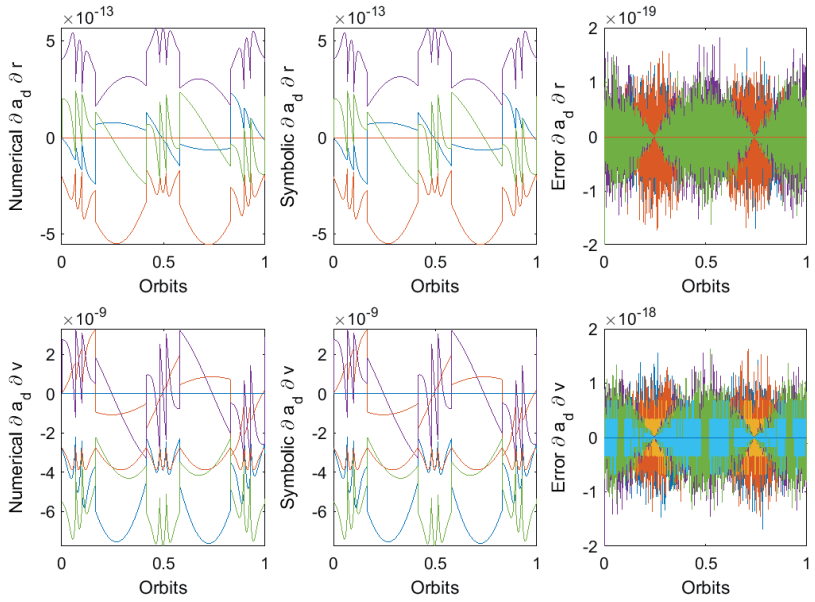


Figure 4.5: Verification result of the atmospheric drag force acceleration partial derivatives with respect to the absolute orbit state.

# 5

# Observability of Coupled Orbit and Attitude Dynamics

*In this chapter, the Observability Gramian is used as a tool to determine how the consideration of coupling between position and attitude influences the observability of absolute and relative states of the spacecraft attitude and orbital dynamics. Scenarios where observability of all states is only possible by taking into account coupling are of special interest in the analysis presented here.*

## 5.1. Introduction

The answer of the first research question of this work "How can the coupling between attitude and orbit dynamics affect the observability of the relative dynamics of spacecraft?" leads to the necessity to determine how different environmental factors affect the observability of the dynamic states of two spacecraft in the formation. Answering *how* these factors affect observability by the use of methods that would only lead to the conclusion on whether a system is observable or not would be unsatisfactory.

Nevertheless, the application of the OG method offers an evaluation that does not only allow to conclude whether a system is observable or not, but also shows the observability level of any analyzed system, and enables the comparison of two observable systems. This is enabled by the fact that the ratio between the highest and the lowest eigenvalue of the OG is a numerical quantity that indicates the observability level of a system. Take for example two systems that are both observable. The highest/lowest eigenvalue ratio indicates numerically which of the two systems is better observable, thus helping to conclude, as it is shown in one case in this chapter, if the rotation of the satellite improves the observability of the system with limited measurement conditions. Nonlinear methods such as the use of Lie Algebra to determine the observability of the system only lead to the conclusion of whether a system is observable or not, with no possibility to compare the observability of two or more systems. Such comparisons are not possible, to the best knowledge of the author, with any known nonlinear observability method.



## 5.2. Observability Analysis of Spacecraft Dynamics

When working on estimation problems, it is important to assess how the observability of spacecraft relative dynamics is affected by factors like the geometry of the formation or the sensor configuration or the mathematical model of a system dynamics.

For this purpose, different methods of system theory have been used for the evaluation of the observability of spacecraft dynamics. For example, a linear time invariant (LTI) method is used in [79]. In [80] and [81] the nonlinear relative dynamics are directly evaluated via the Lie algebraic observability method.

However, these methods only determine if the system is observable or not. They do not provide any information indicating how observable a system is.

To overcome this shortcoming, one possible solution is the use of the Observability Gramian (OG) method. The OG is a linear time variant method. Here, we make use of the linearized time-variant version of the nonlinear system to make use of the OG. This methodology enables the possibility to determine the level of observability of a system under evaluation. The use of the Observability Gramian for spacecraft dynamics observability evaluation is not new, but is limited to few publications like [79] and [82]. Here the focus is given on how the sensor design and positioning affect the observability level of the estimation system.

It is important to notice that the value of the Observability Gramian resides on the fact that it does not only provide a numerical ratio of the observability level of a

system under evaluation. Instead, as shown in [80], the inverse of the Observability Gramian is directly related to the highest bound of the covariance of the error via the dilution of precision (DOP) based covariance forecast.

Achieving full observability of spacecraft dynamics systems under limited sensing configurations is an area of increasing interest for researchers. In [63] it is presented how full observability of the orbital elements of a single spacecraft is achieved by using magnetometers and sun sensor data only. In [83], the authors show how the orbital elements of a relative spacecraft configuration can be observed by using only relative position measurements. In these cases, observability is demonstrated by directly showing the estimation results. This method, however, provides limited information about the level of observability of such cases, since the improvement in estimation is not only constrained by observability itself, but also to the performance of the estimation method itself.

The present chapter evaluates the observability of spacecraft relative position and attitude. The contribution of this research consists in investigating, using the OG as a tool, to what extend the coupling effects between orbit and attitude dynamics can be advantageously exploited for estimation purposes. We use a simple yet common configuration of two spacecraft in along track formation flying in low Earth Orbit (LEO) as a case study defined in Chapter 2. Here the atmospheric drag perturbation presented in Chapter 3 constitutes the source of dynamic coupling between orbital and attitude absolute and relative dynamics.

We are able to show that in constrained sensing configurations, this consideration may not only enable full observability, but reveals how the observability level varies with respect to the area of the spacecraft and the initial dynamics conditions due to the coupling effect caused by the atmospheric drag.

The proposed system can easily be extended to any number of spacecraft, and as such, constitutes a tool for the evaluation of how the coupling between relative attitude and orbital dynamics can improve the performance of the estimation of their dynamics.

## 5.3. The Observability Gramian

Take a linear time-variant system (LTV) with the form

$$\dot{\boldsymbol{x}}(t) = \boldsymbol{A}(t)\boldsymbol{x}(t), \tag{5.1}$$

$$\boldsymbol{z}(t) = \boldsymbol{H}(t)\boldsymbol{x}(t) + \boldsymbol{\nu}_{\boldsymbol{z}}(t), \tag{5.2}$$

where $\boldsymbol{x} \in \mathbb{R}^n$ is the state, $\boldsymbol{z} \in \mathbb{R}^m$ is the output resulting from the measurements, $\boldsymbol{\nu}_{\boldsymbol{z}}(t) \sim N(0, \mathbf{R}(t))$ with $\mathbf{R}(t) \in \mathbb{R}^m$ its variance matrix , and time-variant matrices $\mathbf{A}(t) \in \mathbb{R}^{nxn}, \mathbf{H}(t) \in \mathbb{R}^{mxn}$. The solution for the state has the form $\boldsymbol{x}(t) = \boldsymbol{\Phi}(t, t_0)\boldsymbol{x}(t_0)$, with $\boldsymbol{\Phi}(t, t_0)$ being the state transition matrix.

For this system, the Observability Gramian (OG) $\mathfrak{I}(t, t_0) \in \mathbb{R}^{n\times n}$ is defined as [77, Ch. 7]

$$\mathfrak{I}(t, t_0) = \int_{t_0}^{t} \boldsymbol{\Phi}(\tau, t)^T \boldsymbol{H}^T(\tau)\boldsymbol{R}^{-1}(\tau)\boldsymbol{H}(\tau)\boldsymbol{\Phi}(\tau, t)d\tau. \tag{5.3}$$

An LTV system is observable if $\mathfrak{I}(t, t_0)$ is positive definite. According to [104], the magnitude of each eigenvalue of the OG gives an indication of the degree of observability of the system. The ratio between the largest and the smallest eigenvalue is defined as the observability index, also known as condition number. The observability degree refers to the fact that some states yield higher output norms from the output signal than others [105, Ch.4].

With $\mathfrak{I}(t, t_0)$ defined, the linear time-variant observability condition results in the definition [80]:

**Definition:** The $n^{th}$ order, linear time-varying version of the system of Equation 5.3 is said to be locally observable if, and only if, the matrix $\mathfrak{I}(t, t_0)$ is rank $n$.

### 5.3.1. Determination of the Observability Grammian

In this thesis, the state space representation of the dynamics given by equation 2.30 has the general form



$$\dot{\boldsymbol{x}} = \mathbf{f}(\boldsymbol{x}, t). \tag{5.4}$$

With $\delta\boldsymbol{x} = \boldsymbol{x} - \boldsymbol{x}^*$ we have the discretized perturbation state-variable model associated with the linearized version of the nonlinear system (5.4) as described in detail in Chapter 4.

$$\delta\dot{\boldsymbol{x}} = \boldsymbol{F}_x(\boldsymbol{x}^*, t)\delta\boldsymbol{x}, \tag{5.5}$$

where $\boldsymbol{F}_x$ is a $n \times n$ Jacobian matrix; i.e.

$$\boldsymbol{F}_x(\boldsymbol{x}^*, t) = \begin{bmatrix} \frac{\partial f_1(\boldsymbol{x}^*)}{\partial x_1} & \cdots & \frac{\partial f_1(\boldsymbol{x}^*)}{\partial x_n} \\ \vdots & \ddots & \vdots \\ \frac{\partial f_n(\boldsymbol{x}^*)}{\partial x_1} & \cdots & \frac{\partial f_n(\boldsymbol{x}^*)}{\partial x_n} \end{bmatrix}, \tag{5.6}$$

and $\mathbf{x}^*$ represents the nominal trajectory. In this work, the gradient of the nonlinear system is numerically propagated in order to obtain a local linearized representation of the dynamics, enabling the use of the Observability Gramian for observability analysis purposes. Chapter 4 of this work details the derivation of the gradient of the nonlinear system under analysis. These results are used in this chapter for the propagation of the Observability Gramian.

### 5.3.2. Coupling Elements in the Transition Matrix

In order to determine the Observability Gramian, it is necessary to compute the transition matrix of the nonlinear system described in the previous section. When coupling between orbital and attitude dynamics is taken into account, the gradient matrix of the system in equation [2.30] has the form

$$\frac{\partial \dot{\boldsymbol{x}}}{\partial \boldsymbol{x}} = \begin{bmatrix} 0 & \frac{\partial \dot{\boldsymbol{r}}}{\partial \boldsymbol{v}} & 0 & 0 & 0 & 0 & 0 & 0 \\ \frac{\partial \dot{\boldsymbol{v}}}{\partial \boldsymbol{r}} & \frac{\partial \dot{\boldsymbol{v}}}{\partial \boldsymbol{v}} & \boxed{\frac{\partial \dot{\boldsymbol{v}}}{\partial \boldsymbol{q}}} & 0 & 0 & 0 & 0 & 0 \\ 0 & 0 & \frac{\partial \dot{\boldsymbol{q}}}{\partial \boldsymbol{q}} & \frac{\partial \dot{\boldsymbol{q}}}{\partial \boldsymbol{\omega}} & 0 & 0 & 0 & 0 \\ \boxed{\frac{\partial \dot{\boldsymbol{\omega}}}{\partial \boldsymbol{r}}} & \boxed{\frac{\partial \dot{\boldsymbol{\omega}}}{\partial \boldsymbol{v}}} & \frac{\partial \dot{\boldsymbol{\omega}}}{\partial \boldsymbol{q}} & \frac{\partial \dot{\boldsymbol{\omega}}}{\partial \boldsymbol{\omega}} & 0 & 0 & 0 & 0 \\ 0 & 0 & 0 & 0 & 0 & \frac{\partial \dot{\tilde{\boldsymbol{r}}}}{\partial \tilde{\boldsymbol{v}}} & 0 & 0 \\ \frac{\partial \dot{\tilde{\boldsymbol{v}}}}{\partial \boldsymbol{r}} & \frac{\partial \dot{\tilde{\boldsymbol{v}}}}{\partial \boldsymbol{v}} & \boxed{\frac{\partial \dot{\tilde{\boldsymbol{v}}}}{\partial \boldsymbol{q}}} & 0 & \frac{\partial \dot{\tilde{\boldsymbol{v}}}}{\partial \tilde{\boldsymbol{r}}} & \frac{\partial \dot{\tilde{\boldsymbol{v}}}}{\partial \tilde{\boldsymbol{v}}} & \boxed{\frac{\partial \dot{\tilde{\boldsymbol{v}}}}{\partial \tilde{\boldsymbol{q}}}} & 0 \\ 0 & 0 & 0 & 0 & 0 & 0 & \frac{\partial \dot{\tilde{\boldsymbol{q}}}}{\partial \tilde{\boldsymbol{q}}} & \frac{\partial \dot{\tilde{\boldsymbol{q}}}}{\partial \tilde{\boldsymbol{\omega}}} \\ \boxed{\frac{\partial \dot{\tilde{\boldsymbol{\omega}}}}{\partial \boldsymbol{r}}} & \boxed{\frac{\partial \dot{\tilde{\boldsymbol{\omega}}}}{\partial \boldsymbol{v}}} & \frac{\partial \dot{\tilde{\boldsymbol{\omega}}}}{\partial \boldsymbol{q}} & \frac{\partial \dot{\tilde{\boldsymbol{\omega}}}}{\partial \boldsymbol{\omega}} & \boxed{\frac{\partial \dot{\tilde{\boldsymbol{\omega}}}}{\partial \tilde{\boldsymbol{r}}}} & \boxed{\frac{\partial \dot{\tilde{\boldsymbol{\omega}}}}{\partial \tilde{\boldsymbol{v}}}} & \frac{\partial \dot{\tilde{\boldsymbol{\omega}}}}{\partial \tilde{\boldsymbol{q}}} & \frac{\partial \dot{\tilde{\boldsymbol{\omega}}}}{\partial \tilde{\boldsymbol{\omega}}} \end{bmatrix}. \tag{5.7}$$

In this expression, the elements marked by boxes are the coupling terms between orbital and attitude dynamics. Hence, if there is a change of the degree of observability of the system, it means that the relative values of these elements are significant with respect to the elements that already existed when the coupling was not taken into account.

An example is the variation of the relative acceleration with respect to the relative orientation $\partial \dot{\tilde{\boldsymbol{v}}}/\partial \tilde{\boldsymbol{q}}$. As explained before, the atmospheric drag is the strongest nonlinear acceleration affecting spacecraft in formation in orbits as low as 300 km altitude. This drag is a linear function of the effective area of each spacecraft (eq. 4.57). If there is a variation of the relative orientation $\tilde{\boldsymbol{q}}$, in cases where both spacecraft are of non-spherical shape, this implies that at least one of the spacecraft effective areas has changed, thus varying the total differential acceleration affecting the formation.

## 5.4. Scenario

We consider a two-spacecraft system orbiting the Earth with dynamics described in equation (2.30). These two spacecraft follow a circular equatorial orbit with an initial altitude of 300 km in an along-track configuration with a relative distance of 1000 km. The use of this orbit is justified by its applicability in distributed space systems (DSS) missions ranking from Earth-observation to gravity measurement. This orbit is of use also for future DSS missions to limit the debris density.

The conditions of the dynamics and the spacecraft mechanical characteristics used in the propagation are given in Table 5.1. Two different initial conditions are used in the simulations for the rotation rate: one with no initial rotation for any of the spacecraft, and one with an initial rotation for both of them. They are used to asses the impact of the rotating conditions on the observability when coupling is taken into account.

Given that the spacecraft are in a circular orbit, it will be assumed that the atmospheric density is known and constant, and is given by its value at solar radiation



544941-L-bw-Jimenez
Processed on: 16-6-2020

Table 5.1: Configuration of the dynamics of the system under study.

| **Initial Conditions** | | |
|---|---|---|
| Spacecraft | **S/C 1** | **S/C 2** |
| Position (km) | $[300 + R_E, 0, 0]$ | $(300 + R_E)[\cos\theta_2, \sin\theta_2, 0]$ |
| Velocity (km/s) | $[0, 7.7142, 0]$ | $7.7142[-\sin\theta_2, \cos\theta_2, 0]$ |
| Attitude quaternion | $[0, 0, 0, 1]$ | $[0, 0, 0, 1]$ |
| Rotation rate for the rotating case (rad/s) | $[0, \pi/18, 0]$ | $[0, 0, \pi/18]$ |
| Initial along-track separation ($R_A$) | 1000 km | |
| **Spacecraft mechanical characteristics.** | | |
| Mass (m) | 3.6 kg | 3.6 kg |
| Inertia matrix ($\boldsymbol{I}$) | $\begin{bmatrix} 0.055 & 0 & 0 \\ 0 & 0.055 & 0 \\ 0 & 0 & 0.017 \end{bmatrix}$ kg m$^2$ | $\begin{bmatrix} 0.055 & 0 & 0 \\ 0 & 0.055 & 0 \\ 0 & 0 & 0.017 \end{bmatrix}$ kg m$^2$ |
| Drag coefficient ($C_D$) | 2.3 | 2.3 |

Table 5.2: Values of maximum Atmospheric density as a function of the altitude (see [36], inside its rear cover, for complete table).

| Altitude (km) | 300 | 350 | 400 | 450 |
|---|---|---|---|---|
| Maximum atmospheric density (kg/m$^3$) | $3.96x10^{-11}$ | $1.66x10^{-11}$ | $7.55x10^{-12}$ | $3.61x10^{-12}$ |

5

maximum (see Table5.2).

The gradient matrix (eq. 5.7) of the system under study is numerically propagated. With this it is possible to obtain the transition matrix of the linearized system $\boldsymbol{\Phi}(t, t_0)$ used in the OG propagation (eq. 5.3). The linearization is done in every evaluation step, emulating a linear-time-variant system.

Given that the present work focuses on the impact of the dynamics model on observability, a simple measurement model is used: direct measurements of the states with no noise. It is assumed that this scenario has no noise for a better understanding of the coupling effect itself without other effects affecting the Gramian results. In order to do this, the **R** matrix is assumed to be an identity matrix of proper size. Nevertheless, when the accuracy of sensors has to be taken into account, accounting for the noise level of the sensors is mandatory. Modifications of these assumptions, such as more complex sensor scenarios may be added easily by modifying the matrix **H** and **R** of Eq. 5.2.

Different measurements scenarios are defined to evaluate their impact in the observability (Table 5.3). Here, the first two cases (1 and 2) are the extreme cases where only one sensor is measuring a single relative state, in order to evaluate the impact of that single state measurement on the complete observability result. Case 3 is a case where it is assumed that the system has position sensors (absolute and relative). In this case, all observability results related to attitude are attributed to coupling. In analogy to case 3, case 4 only includes absolute and relative attitude measurements. Case 5 includes only relative measurements, in order to evaluate as well the observability of the absolute states with this indirect measurement. Case 6 includes all sensors considered in the previous cases.

In this work, we focus on cases like 1 from Table 5.4 instead of more typical measuring configurations like case 6, because the former shows clearly the effect

Table 5.3: Measurement configurations. An "x" indicates a measurement of the state.

| Case | $\boldsymbol{r}$ | $\boldsymbol{v}$ | $\boldsymbol{q}$ | $\boldsymbol{\omega}$ | $\tilde{\boldsymbol{r}}$ | $\tilde{\boldsymbol{v}}$ | $\tilde{\boldsymbol{q}}$ | $\tilde{\boldsymbol{\omega}}$ | Description |
|---|---|---|---|---|---|---|---|---|---|
| 1 | | | | | x | | | | Only relative position |
| 2 | | | | | | | x | | Only relative attitude |
| 3 | x | | | | x | | | | All position measurements |
| 4 | | | x | | | | x | | All attitude measurements |
| 5 | | | | | x | | x | | All relative measurements |
| 6 | x | | x | | x | | x | | All available measurements |

Table 5.4: Variation of the area of the spacecraft for sensitivity analysis.

| Area Configuration | size [cm$^3$] |
|---|---|
| 1 | 30x 10 x 10 |
| 2 | 60 x 20 x 20 |
| 3 | 120 x 30 x 30 |
| 4 | 240 x 40 x40 |

of coupling in observability while in the latter the effect is marginal. For example, when $\tilde{\boldsymbol{q}}$ is directly measured, both $\tilde{\boldsymbol{q}}$ and $\tilde{\boldsymbol{\omega}}$ are fully observable. Instead, when the only measurement available is $\tilde{\boldsymbol{r}}$, only $\tilde{\boldsymbol{r}}$ and $\tilde{\boldsymbol{v}}$ are fully observable, and the only way $\tilde{\boldsymbol{q}}$ may become observable is through the coupling (see the related explanation about the element $\partial\dot{\tilde{\boldsymbol{v}}}/\partial\tilde{\boldsymbol{q}}$ in section 5.3.2), thus revealing the magnitude of how the coupling consideration affects the observability.

Different spacecraft areas are used as a parameter to see how the observability is influenced by the consideration of coupling. Cuboid-shaped spacecraft are used with areas shown in Table 5.4.

To properly interpret the results of this work, it is necessary to normalize the states [106]. This normalization is done based on the work of [104, p.84]. In it, in equation 3.39, the author describes that the dimensional system may be related to the nondimensional system via

$$\mathrm{A} = C\mathrm{X} = diag\left(\frac{1}{L}, \frac{1}{L}, \frac{1}{L}, \frac{1}{V}, \frac{1}{V}, \frac{1}{V}, \ldots\right)\mathrm{X} \tag{5.8}$$

with $\mathrm{X}$ describing the state of the dimensional system, and $\mathrm{A}$ the resulting nondimensional system state vector. Here, $L$ is given in position units, and $V$ in velocity units, and so on. The factors used to normalize the states in this work are summarized in Table 5.5

Different normalizers have been used for orbital relative states compared to the

Table 5.5: Normalization factors. The quaternion states do not require normalization.

| State | Normalization divisor | Representation |
|---|---|---|
| $\boldsymbol{r}$ | Semimajor Axis of the orbit | $a$ |
| $\boldsymbol{v}, \tilde{\boldsymbol{v}}$ | Magnitude of maximum velocity | $\sqrt{\mu/a}$ |
| $\boldsymbol{\omega}, \tilde{\boldsymbol{\omega}}$ | Maximum assumed rotation rate | $\pi/18$ rad/s |
| $\tilde{\boldsymbol{r}}$ | Initial distance between spacecraft | $1000$ km |

orbital absolute states due to their difference in magnitude in this work.

## 5.5. Results and Analysis

### 5.5.1. Gradient Variation under Coupled Dynamics

The origin of the influence of the coupling between the attitude and the orbital dynamics of the system, reflected in the Observability Gramian (OG) results, can be traced to the elements of the gradient matrix of the nonlinear system that would not exist if the coupling consideration is not present, as described in section 5.3.2. Thus, before using the OG, the gradient matrix of the system under consideration (Eq. 5.7) provides a tool to explore the influence of the coupling between orbital and attitude dynamics of the system.

For a first approach to illustrate the coupling between orbital and attitude dynamics, the result of the gradient matrix both using coupling and no-coupling in the dynamics model is propagated for one orbit. When the coupling is taken into account, the atmospheric drag model described in Chapter 3 is used. When coupling is not taken into account, it is assumed that the effective areas of the spacecraft are constant and their values are assumed to be the maximum possible given the spacecraft configurations (see Table 5.4). Due to the fact that the magnitude of the atmospheric drag torque depends on the altitude (a direct dependency on the orbital states), we assume no atmospheric drag torque for the non-coupling case.

The first propagation is done using two spacecraft with the dimensions of a 3-unit CubeSat (Configuration 1 of Table 5.4) and an initial non-zero rotating rate (as defined in Table 5.1). These results are shown in Figure 5.1 (no coupling) and Figure 5.2 (with coupling). In the second propagation, a spacecraft with a larger surface area is used (Configuration 4 of Table 5.4 for both satellites). The result of these propagations for the uncoupled and coupled case is illustrated in Figure 5.3 and Figure 5.4 respectively . In it is shown the approximately largest value of the propagation of the gradient matrix of the system when the coupling consideration is not taken into account and when it is taken into account, respectively. These graphics give visually an idea of how the coupling affects the magnitude of the gradient elements, how new elements appear in the gradient, and the magnitude of such elements. With this, we can get insight of the influence of the coupling in the system.

In both cases, it can be observed that taking into account coupling does not alter significantly the maximum values of the elements of the gradient that already existed for the non-coupling case. This is caused by the difference of magnitude between the gravitational attraction force, that is at least five orders of magnitude larger than the atmospheric perturbation. Nevertheless, the coupling consideration does create new elements that influence the observability degree of the system, like $\partial\dot{\boldsymbol{q}}/\partial\boldsymbol{r}$. These elements explain the differences in the observability evaluations of next section.

When the results of area configurations 1 and 4 are compared, it can be observed that all the elements that only exist when coupling is used, increase their magnitude linearly as a function of the increase of the areas of the spacecraft (all

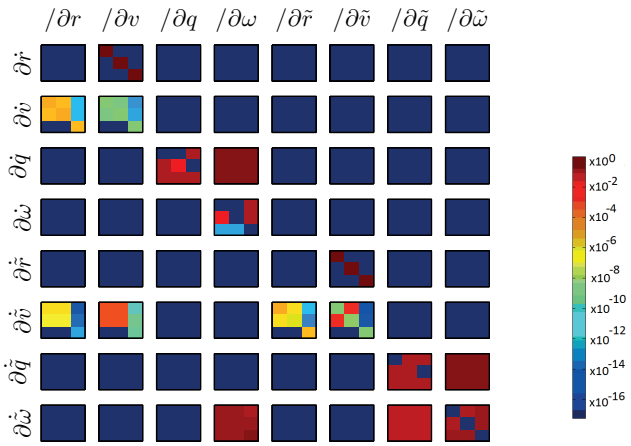


Figure 5.1: Maximum value of the gradiant matrix of the space state system under study for case 1, area configuration 1, rotating, when coupling is not taken into account. Values are shown in a logarithm scale.

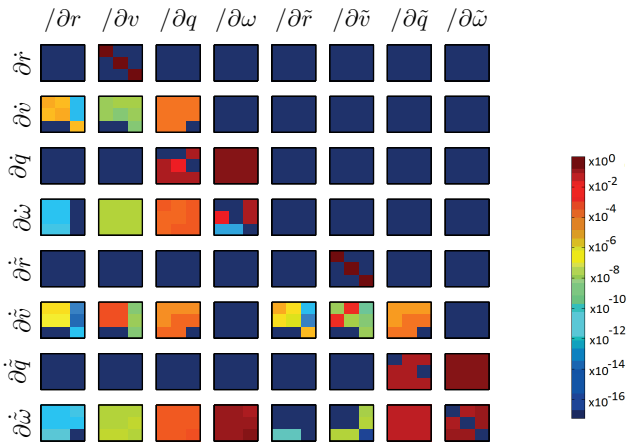


Figure 5.2: Maximum value of the gradiant matrix of the space state system under study for case 1, area configuration 1,rotating when coupling is taken into account. Values are shown in a logarithm scale.

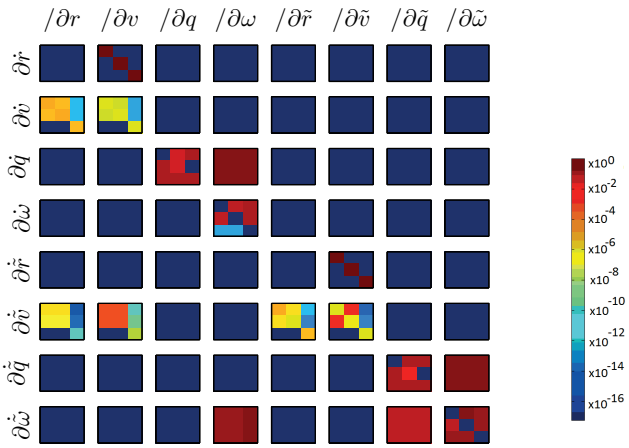


Figure 5.3: Maximum value of the gradiant matrix of the space state system under study for case 1, area configuration 4, rotating, when coupling is not taken into account. Values are shown in a logarithm scale.

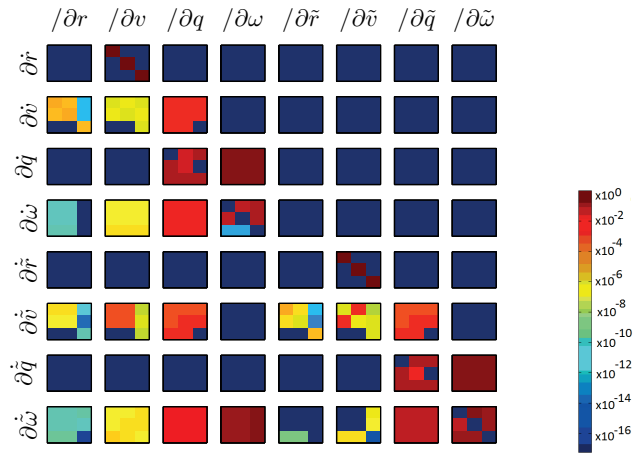


Figure 5.4: Maximum value of the gradiant matrix of the space state system under study for case 1, area configuration 4, rotating when coupling is taken into account. Values are shown in a logarithm scale.

these elements are 32 times larger for area configuration 4 compared to area configuration 1), leading to the conclusion that for the scenario under analysis, only the ratio $A/m$ influences the coupling components propagation results. This linear dependency was verified for all area configurations on Table 5.4. This is expected because the magnitude of the increment of the coupling elements, depending on the requirements of a mission, may create a non negligible influence on the observability results, as it will be shown in the next section.

To illustrate how the gradients vary in detail, take as an example the propagation of $\partial\dot{\tilde{\boldsymbol{v}}}/\partial\tilde{\boldsymbol{q}}$. This element is only present in the gradient matrix, and hence in the observability analysis, if coupling is considered. In Fig. 5.5 and 5.6 the propagation of this elements is shown for one orbit with and without an initial rotation rate. It is important to notice that this element is not zero even when the initial conditions of rotation are null for both spacecraft due to the influence of the atmospheric drag torque. It can be observed that if the maximum value in both cases does not vary significantly it does not imply that their behavior is the same.

Let us compare the case of area configuration 1 with the case where we use area configuration 4 illustrated for the component $\partial\dot{\tilde{\boldsymbol{v}}}/\partial\tilde{\boldsymbol{q}}$ in fig. 5.7 and 5.8. The maximum value of the result is linearly dependent on the maximum possible value of the effective area (a factor of 32), as explained before. In this scenario, this coupling element may be considered significant with respect to the other elements of the gradient for estimation purposes.



### 5.5.2. Observability using Observability Gramian Eigenvalues

As mentioned in Section 5.3, the ratio between the highest and the lowest eigenvalues of the OG provides a direct measurement of the degree of observability of a system. Using this property, the eigenvalues of the system under study under different measurement scenarios are determined. The results are normalized with respect to the highest eigenvalue, to ease the interpretation of the results.

First, an analysis is done with only one element of the state observable (either $\tilde{\boldsymbol{r}}$ or $\tilde{\boldsymbol{q}}$) to investigate the impact of coupling. Later, we compare the impact of the different measurement cases and the orbit altitude on the observability.

#### Evaluation 1: Relative Position or Relative Attitude Measurement Only

First, let us assume a scenario where only the relative position ($\tilde{\boldsymbol{r}}$) or the relative attitude ($\tilde{\boldsymbol{q}}$) between the two spacecraft are directly measured, and the other elements of the state are estimated from there. Clearly, it is impossible to have a fully observable system unless the coupling is taken into account.

Fig. 5.9 and 5.10, show the results of the normalized eigenvalues when the system is initially not rotating and when it is initially rotating for different spacecraft area configurations at an altitude of 300 km. It is obvious that the observability is increased as a direct function of the spacecraft area.

Now, take the eigenvalue with the lowest magnitude (eigenvalue 24). For both cases, this eigenvalue is related to the absolute position of the leader spacecraft. Its magnitude is low due to the fact that the dependency of $\boldsymbol{r}$ with respect to $\tilde{\boldsymbol{r}}$ in a nearly-circular orbit (it is important to remember that the orbit is not perfectly

circular due to the perturbation of drag) is very small.

Presumably, other scenarios with a non-circular orbit, causing that the variation of the atmospheric perturbation with respect to $\boldsymbol{r}$ increases, would increase the observability of this state. This result is out of the scope of this study, and will be explored in the future.

For the propagation of measurement case 2, with results shown in Fig. 5.10, the lowest eigenvalues are related to the relative position $\tilde{\boldsymbol{r}}$ (the lowest one), the absolute position $\boldsymbol{r}$, the relative velocity $\tilde{\boldsymbol{v}}$ and the velocity of the spacecraft $\tilde{\boldsymbol{v}}$, in that order. This is expected since the measurements of $\tilde{\boldsymbol{q}}$ tell little about the absolute and relative position and velocity.

It is visible that in the left case of Fig. 5.9, that we call "Case A" most eigenvalues increase considerably as a result of the increase in spacecraft area.

### Evaluation 2: Changes in Measurements Configuration

It has been shown in previous works, like [82], that the measurement configuration influences the degree of observability of the relative dynamics of spacecraft. Nevertheless, a complex dynamics model with coupling between orbit and attitude has never been considered in these analyses. To determine its effect in this scenario, the OG has been propagated with the different measurement configurations described in Table 5.3, using Area Configuration 4 and with both spacecraft initially rotating for various altitudes. The results are shown in Fig. 5.11.

Clearly, given the fact that drag is the perturbing agent generating the coupling, when coupling affects observability (all cases but case 6), the observability is better for lower altitudes. This effect is analyzed in more detail in the next subsection.

In this scenario, the altitude measurements cases (cases 2 and 4), both absolute and relative provide better observability results than the position measurements cases (cases 1 and 3). This is given due to the fact that in each propagation altitude does not vary significantly (initial circular orbit), but the effective area also varies constantly, thus giving more elements for observability evaluation. Nevertheless, checking if this is the case in a highly elliptical orbit may be a result of a future evaluation.

For measurement case 6, where there is no necessity to take into account the coupling effect to guarantee full observability, the condition number of the OG shows that there is no variation in the level of observability with respect to the variation of the altitude. This happens because the elements in the gradient that enable observability in this case are very large (gravity force), and the contributions of the coupling-generating elements to increase the observability (perturbations) are negligible in comparison.

### Evaluation 3: Observability Sensitivity with Respect to Altitude

To have a more accurate notion on how the observability is affected by altitude, an evaluation of the variation of the eigenvalues with respect to different altitudes is done (Fig. 5.12). This example shows that for the limited observability conditions of measurement case 1 (Table 5.3), the rotation of the spacecraft does increase the level of observability of the system. Taking into account that the atmospheric density at 300 km altitude is only one order of magnitude larger than its value at 450 km

(see Table 5.2), other elements have to be considered to explain the difference in magnitude of the smallest eigenvalue. The orbital velocity is not the factor affecting either, because it is not even one order of magnitude larger (approximately 7.73 at 300 km altitude versus 7.64 km/s at 450 km altitude). The increase in the lowest eigenvalue is even more pronounced when the spacecraft is rotating. What is the relation between the physical factors and the increase in observability may be the subject to future research.

## 5.6. Remarks

The OG has been employed as a tool to evaluate the dependency of the observability on the dynamics of relative dynamics of spacecraft. It has been shown that the coupling, created by the atmospheric drag for spacecraft in formation in LEO, enables observability of the complete state not possible without such coupling. Furthermore, the sensitivity of the degree of observability has been analyzed with changing altitude and spacecraft mechanical characteristics. As a result, new elements on the gradient of the dynamics are appearing, creating a significant change on the observability of the system.

The cases of limited observability, where only the relative position of the spacecraft or the relative attitude of the spacecraft are measured, are of special interest in this work. They show that full observability is achieved, not possible in the scenario under study without such coupling.

Although this effect has been presented in previous publications, in this research a method was proposed that allows to quantitatively compare how different conditions may change the observability in a methodical way. This contrasts to the use of the propagated estimating results as a comparison method, where other elements (as the performance of the selected estimator itself) may have an influence on the result.

The OG method also helps to determine in the design phase of missions which sensor scenario benefits the most from this coupling. This information is therefore very valuable for the relative spacecraft dynamics estimation implementation, as well as the design of sensor suites for formation flying missions.

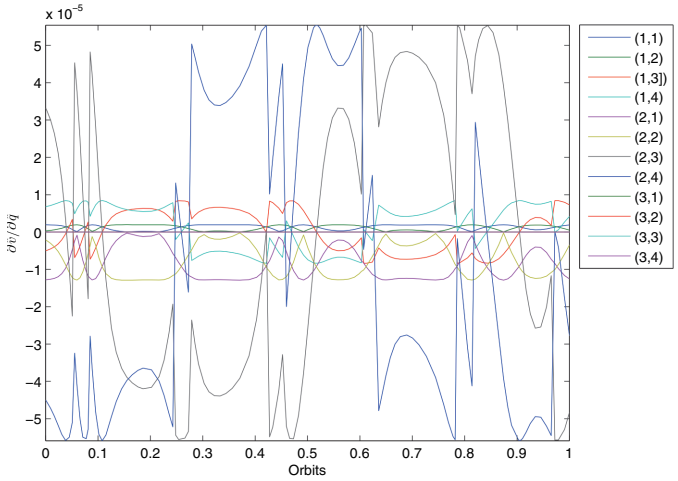


Figure 5.5: Variation of $\partial\dot{\tilde{\boldsymbol{v}}}/\partial\tilde{\boldsymbol{q}}$ when the system is not initially rotating for one orbit on a spacecraft system with area configuration 1 (smallest)

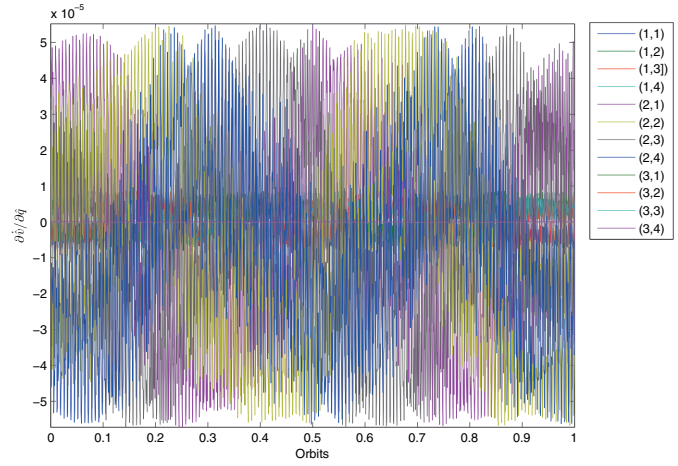


Figure 5.6: Variation of $\partial\dot{\tilde{\boldsymbol{v}}}/\partial\tilde{\boldsymbol{q}}$ when the system is initially rotating for one orbit on a spacecraft system with area configuration 1 (smallest).

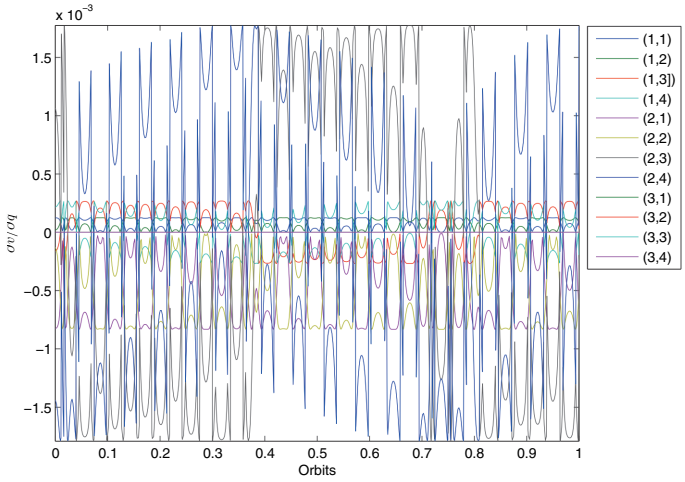


Figure 5.7: Variation of $\partial\dot{\boldsymbol{v}}/\partial\tilde{\boldsymbol{q}}$ when the system is initially not rotating for one orbit on a spacecraft system with area configuration 4 (largest)

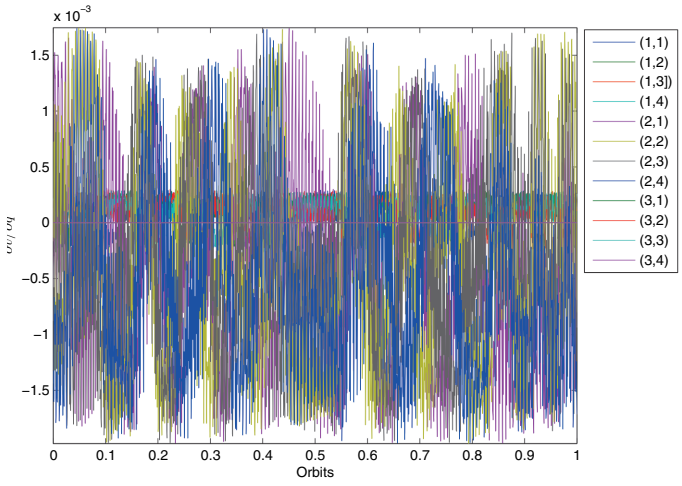


Figure 5.8: Variation of $\partial\dot{\boldsymbol{v}}/\partial\tilde{\boldsymbol{q}}$ when the system is initially rotating for one orbit on a spacecraft system with area configuration 4 (largest)

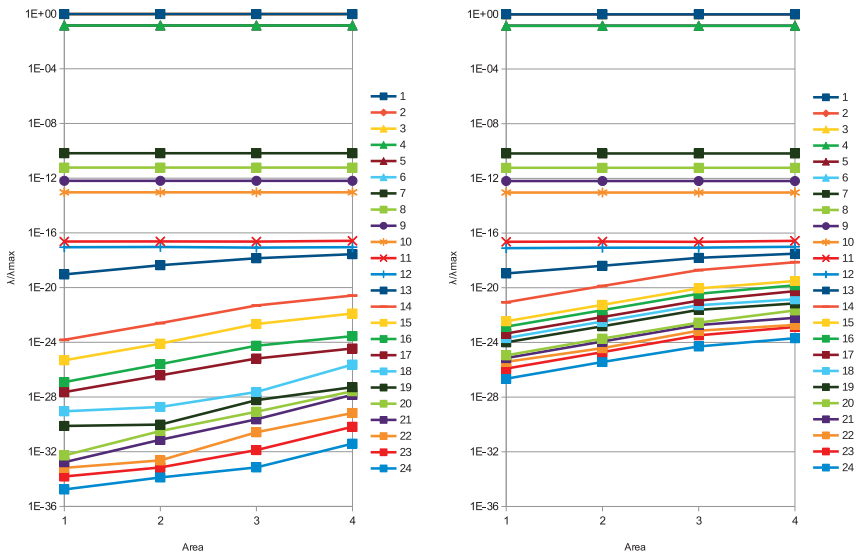


Figure 5.9: Variation of the eigenvalues with respect to spacecraft area for measurement case 1 (only relative position) at an altitude of 300 km. Left: with no initial rotation. Right: with initial rotation.

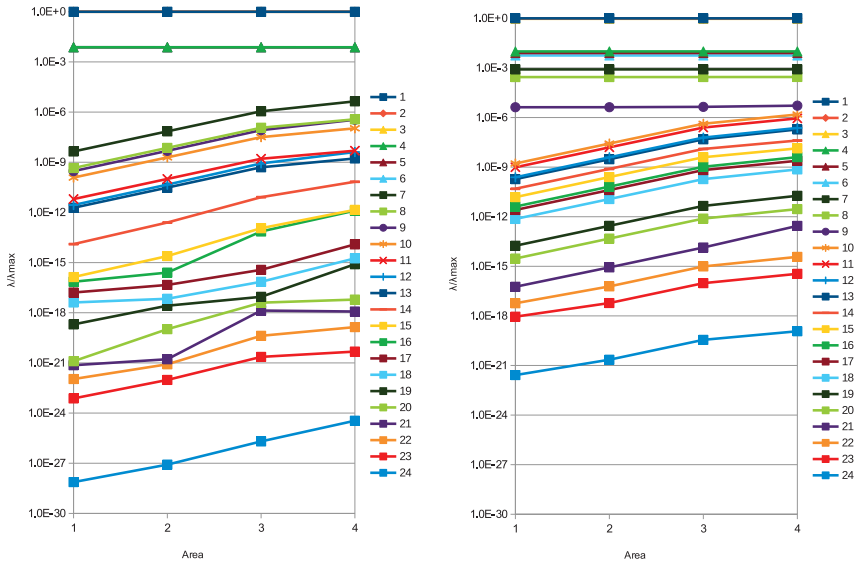


Figure 5.10: Variation of the eigenvalues with respect to spacecraft area. Measurement case 2 (only relative attitude) at an altitude of 300 km. Left: with no initial rotation. Right: with initial rotation.

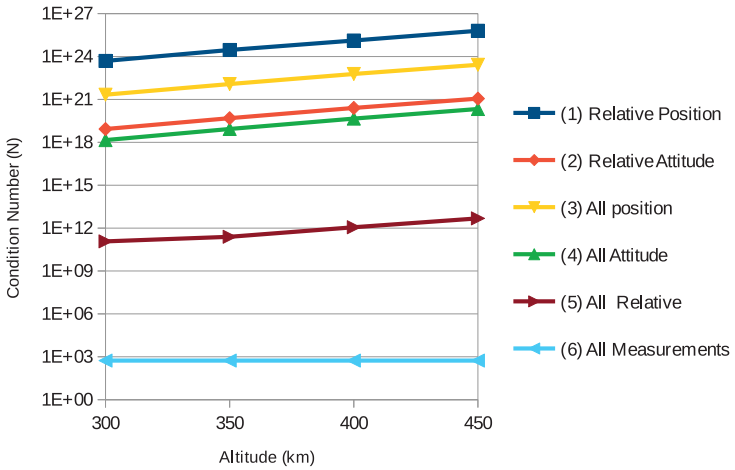


Figure 5.11: Observability degree vs to altitude for measurements described on Table 5.3

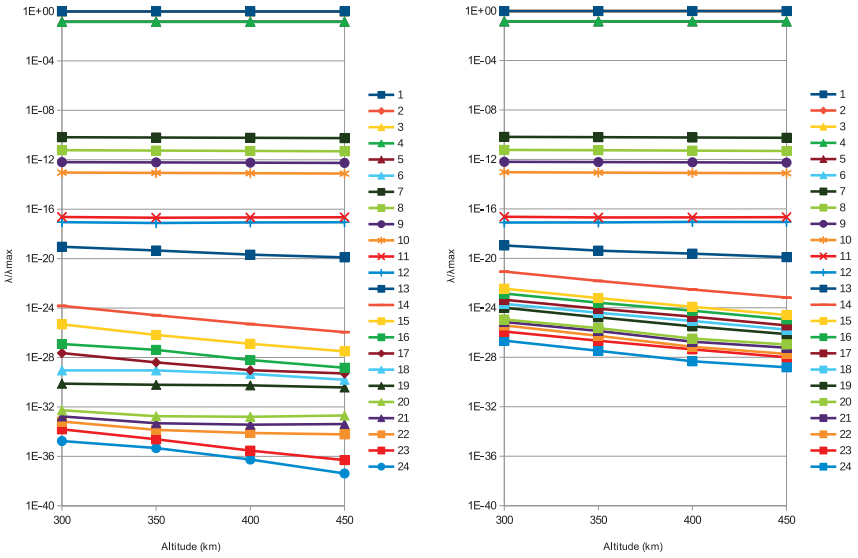


Figure 5.12: Eigenvalues variation vs altitude. Measurement case 1 (only relative position), Area Configuration 1 (30x10x10 cm). Left: with no initial rotation. Right: with initial rotation.

# 6

# Estimation of Coupled Orbit and Attitude Dynamics

*In this chapter, the Extended Kalman Filter is used as a tool to determine how drag-induced coupling between position and attitude influences the observability of the spacecraft relative attitude and orbital dynamics.*



544941-L-bw-Jimenez
Processed on: 16-6-2020

In previous years the assumption that relative spacecraft orbital and attitude dynamics are not coupled has been deemed accurate enough for estimation and control purposes [43, 45–47]. Nevertheless, recent works are taking into account the joint representation of attitude and orbital dynamics for improved guidance, navigation and control performance.

In [48, 49] the gravity-induced mutual coupling between orbital and attitude dynamics is taken into account when solving a spacecraft relative dynamics tracking problem using nonlinear control techniques. In [50] the coupling effect generated by the gravity gradient and the solar pressure is considered in the spacecraft formation control system for a space interferometry mission. Similarly, in [51] it is described how the gravity gradient, solar pressure and atmospheric drag are a source of coupling between attitude and orbital dynamics. Later, this dynamics model is applied for control purposes in [52]. Furthermore, the coupling effect generated by actuation is considered in [53–57]. The modeling of dynamics affected by coupling in deep space missions is reported in [58, 59].

A joint relative orbital and attitude dynamics representation for estimation purposes is not new [64, 70, 107]. However, unlike the cited control application examples, none of these took the coupling between orbital and attitude dynamics into account. This simplification is typically well justified when the magnitude of this coupling effect is negligible.



Nevertheless, the dynamic coupling between orbit and attitude dynamics for estimation purposes was considered as early as 1982 [1]. In this work, a dynamic coupling given by both the gravity gradient and the atmospheric perturbation for a single spacecraft with very high area to mass ratio in a very low orbit (a low-eccentricity orbit at 250 km altitude) was considered.

Since this time, most of the focus of research between orbit and attitude dynamics for estimation purposes was focused on measurement-related coupling, such as vision-based navigation (VISNAV). For example, in [71] the $J_2$-term in the Earth's gravitational potential is taken into account to estimate the relative pose using an Unscented Kalman Filter, and in [72] a similar work is done using a Cubature Predictive Filter. In these papers, the dynamics are estimated using an arbitrary reference center within the satellite. A similar assumption of measurements from an arbitrary feature point of the spacecraft is done in [73]. Due to the fact that this coupling is not related to any force, it is considered a kinematic coupling. Multiple works take a similar approach in considering the measurement model as the source of coupling between orbit and attitude relative dynamics [64, 65, 67–69, 108, 109].

Another example of objects in orbit where the coupling is taken into account for purposes of estimation is the tracking of Space-Debris with High Area-to-Mass ratio from terrestrial telescopes [62]. In this work, an Unscented Kalman Filter is used for the observation of the orbit and attitude of objects near the Geostationary orbit (GEO), where the effect of the solar pressure is not negligible.

Nevertheless, to the best of our knowledge, no work has been published yet where the coupling between the attitude and orbital dynamics caused by external perturbations is adopted in spacecraft relative dynamics models to improve their estimation accuracy, in a similar fashion as it has been used for control purposes.

There are many estimation methods for states. The Least-Squares (LSQ) Estimators, or Kalman Filters, named after R. Kalman who developed it in 1959 [102], are some of the best known.

The present chapter evaluates how such coupling affects the spacecraft relative position and attitude estimation, in order to answer the second research question "How can the coupling between attitude and orbit dynamics be used to improve the performance of estimation for relative dynamics of spacecraft?" This work presents a similar objective as [1] but this time in the realm of relative pose dynamics. The contribution of this research consists in investigating, using a spacecraft dynamics estimator, to what extent the coupling effects between orbit and attitude dynamics can be advantageously exploited for estimation purposes. The focus of this research is the evaluation of the coupled relative pose physical model, and for this reason, a very well known Extended Kalman Filter (EKF) method is the estimator of choice. The selection of the EKF is justified by the fact that its use is very common for spacecraft dynamics. As such, it provides a representative well-known tool to determine and analyze the results when coupling is taken into account in order to improve the spacecraft relative orbit and attitude estimation.

We use a simple yet common configuration of two spacecraft in along track formation flying in low Earth Orbit (LEO) as a case study. Here the atmospheric drag perturbation constitutes the source of coupling between orbital and attitude absolute and relative dynamics. The proposed system can easily be extended to any amount of spacecraft, and as such, constitutes a tool for the evaluation of whether and how the coupling between relative attitude and orbital dynamics can improve the performance of the state estimation. It is investigated if the estimation convergence is improved and to which extent when the coupling consideration is taken into account. The approach of this work, where an improvement of the dynamics model is proposed, may be seen as complementary to the approach where new mathematical methods are proposed in order to improve the relative dynamics of spacecraft.



## 6.1. States Observation Modeling

Due to the fact that we want to study the impact of coupling on the estimation of spacecraft relative dynamics, it is necessary to define which measurements will be used to estimate the spacecraft states. The most simple assumption that may be used for this purpose would be that "pseudo-measurements" of the states are available, i.e. it is possible to measure the states directly. Actual sensors exist that provide comparable measurements, for example, GPS or relative GPS in the case of position dynamics.

There are two reasons for this assumption. First of all, a more complex measurement model may interfere with the estimation results, thus not allowing to focus only on the effects of the estimation performance given by the better dynamical model. A second reason is to reduce to a minimum the sources of error in the results not related to the simulation itself that may appear if a more realistic measurement model is used. Implementation of more sophisticated measurement models to use with the proposed model may be done both for an EKF as well as for

any other filtering algorithm to be used with the coupled dynamics model.

In this work, the measurement model $\boldsymbol{z}(t)$ assumes that the position and attitude states are directly measured, so that

$$\boldsymbol{z}(t) = \begin{bmatrix} \mathbf{1}_3 & \mathbf{0}_{3\times3} & \mathbf{0}_{3\times4} & \mathbf{0}_{3\times3} & \mathbf{0}_{3\times3} & \mathbf{0}_{3\times3} & \mathbf{0}_{3\times4} & \mathbf{0}_{3\times3} \\ \mathbf{0}_{4\times3} & \mathbf{0}_{4\times3} & \mathbf{1}_4 & \mathbf{0}_{4\times3} & \mathbf{0}_{4\times3} & \mathbf{0}_{4\times3} & \mathbf{0}_{4\times4} & \mathbf{0}_{4\times3} \\ \mathbf{0}_{3\times3} & \mathbf{0}_{3\times3} & \mathbf{0}_{3\times4} & \mathbf{0}_{3\times3} & \mathbf{1}_3 & \mathbf{0}_{3\times3} & \mathbf{0}_{3\times4} & \mathbf{0}_{3\times3} \\ \mathbf{0}_{4\times3} & \mathbf{0}_{4\times3} & \mathbf{0}_{4\times4} & \mathbf{0}_{4\times3} & \mathbf{0}_{4\times3} & \mathbf{0}_{4\times3} & \mathbf{1}_4 & \mathbf{0}_{4\times3} \end{bmatrix} \begin{bmatrix} \boldsymbol{r} \\ \boldsymbol{v} \\ \boldsymbol{q} \\ \boldsymbol{\omega} \\ \tilde{\boldsymbol{r}} \\ \tilde{\boldsymbol{v}} \\ \tilde{\boldsymbol{q}} \\ \tilde{\boldsymbol{\omega}} \end{bmatrix} + \boldsymbol{\nu}_{\boldsymbol{z}}(t), \tag{6.1}$$

leading to a direct measurement of the states $\boldsymbol{r}, \boldsymbol{q}, \tilde{\boldsymbol{r}}, \tilde{\boldsymbol{q}}$ with noise $\boldsymbol{\nu}_{\boldsymbol{z}}(t) \sim N(0, R)$, with a covariance $R \in \mathbb{R}^{14x14}$ matrix.

## 6.2. The Extended Kalman Filter

In this work, an EKF is used to test the effect of coupling in spacecraft relative dynamics estimation. Since our focus is on the improvement of state estimation using the dynamic coupling, the use of newer estimators is not necessary and we focus on the standard EKF.

Take a model of the dynamics based on equation 2.30 and a measurement model based on equation 6.1

$$\dot{\boldsymbol{x}} = f(\boldsymbol{x}, t) + \boldsymbol{\nu}_x(t), \tag{6.2}$$
$$\boldsymbol{z}(t) = \boldsymbol{h}(\boldsymbol{x}(t), t) + \boldsymbol{\nu}_{\boldsymbol{z}}(t), \tag{6.3}$$

where $\boldsymbol{x} \in \mathbb{R}^n$ is the state, $\boldsymbol{z} \in \mathbb{R}^m$ is the output resulting from the measurements, $\boldsymbol{\nu}_x(t) \sim N(0, Q(t))$ the process noise, representing the deviation of the model to the truth. The linearization of this equation is done around a nominal state $\boldsymbol{x}^*$ where $\boldsymbol{x} \in \mathbb{R}$ with $\delta\boldsymbol{x} = \boldsymbol{x} - \boldsymbol{x}^*$ lead us to a discretized perturbation state-variable model associated with the linearized version of the nonlinear system 2.30 as described in [102].

$$\delta\dot{\boldsymbol{x}} = \boldsymbol{F}_x(\boldsymbol{x}^*, t)\delta\boldsymbol{x} + \boldsymbol{\nu}_x(t), \tag{6.4}$$
$$\delta\boldsymbol{z} = \boldsymbol{H}_x(\boldsymbol{x}^*, t)\delta\boldsymbol{x} + \boldsymbol{\nu}_{\boldsymbol{z}}(t), \tag{6.5}$$

where $\boldsymbol{F}_x$ is an $n \times n$ Jacobian matrix and $\boldsymbol{H}_x$ an $m \times n$ matrix ; i.e.

$$\boldsymbol{F}_x(\boldsymbol{x}^*, t) = \begin{bmatrix} \frac{\partial f_1(\boldsymbol{x}^*)}{\partial x_1} & \cdots & \frac{\partial f_1(\boldsymbol{x}^*)}{\partial x_n} \\ \vdots & \ddots & \vdots \\ \frac{\partial f_n(\boldsymbol{x}^*)}{\partial x_1} & \cdots & \frac{\partial f_n(\boldsymbol{x}^*)}{\partial x_n} \end{bmatrix}, \boldsymbol{H}_x(\boldsymbol{x}^*, t) = \begin{bmatrix} \frac{\partial \boldsymbol{h}_1(\boldsymbol{x}^*)}{\partial x_1} & \cdots & \frac{\partial \boldsymbol{h}_1(\boldsymbol{x}^*)}{\partial x_n} \\ \vdots & \ddots & \vdots \\ \frac{\partial \boldsymbol{h}_n(\boldsymbol{x}^*)}{\partial x_1} & \cdots & \frac{\partial \boldsymbol{h}_n(\boldsymbol{x}^*)}{\partial x_n} \end{bmatrix} \tag{6.6}$$

Here, no input forces are taken into account. If necessary, the linearization should also be done around the corresponding input.

The implementation of a discrete (EFK) for the nonlinear system of equations 6.2 and 6.3 using the linearization of equations 5.5 and 6.5 is based on two processes: prediction and measurement update.

### 6.2.1. Prediction

Prediction uses the last estimated state $\hat{\boldsymbol{x}}(k,k)$ to obtain a prediction of the value of the state $\boldsymbol{x}$ in time $k+1$ by using the analytical model of the state. The predicted state is called $\hat{\boldsymbol{x}}(k+1,k)$

$$\hat{\boldsymbol{x}}(k+1,k) = \hat{\boldsymbol{x}}(k,k) + \int_{t_k}^{t_{k+1}} \boldsymbol{f}(\hat{\boldsymbol{x}}(k+1,k), \boldsymbol{u}^*(t), t)dt. \tag{6.7}$$

### 6.2.2. Measurement Update

Correction uses the measurements of the state at time $k+1$ to update the prediction and finally arrive at the estimated state $\hat{\boldsymbol{x}}(k+1,k+1)$ and its covariance matrix $\boldsymbol{P}(k+1,k+1)$ . The weight of the prediction and the correction is determined by the gain matrix $\boldsymbol{K}(k+1)$.

$$\hat{\boldsymbol{x}}(k+1,k+1) = \hat{\boldsymbol{x}}(k+1,k) + \boldsymbol{K}(k+1)\{\boldsymbol{z}(k+1) - \boldsymbol{h}(\hat{\boldsymbol{x}}(k+1,k),k+1)\} \tag{6.8}$$

$$\boldsymbol{P}(k+1,k+1) = [\boldsymbol{1}_n - \boldsymbol{K}(k+1)\boldsymbol{H}_{\boldsymbol{x}}(k+1,k)]\,\boldsymbol{P}(k+1,k) \tag{6.9}$$

where

$$\boldsymbol{K}(k+1) = \boldsymbol{P}(k+1,k)\left[\boldsymbol{H}_{\boldsymbol{x}}(k+1,k)\boldsymbol{P}(k+1,k)\boldsymbol{H}_{\boldsymbol{x}}{}^{T}(k+1,k) + \boldsymbol{R}(k+1)\right]^{-1} \tag{6.10}$$

$$\boldsymbol{P}(k+1,k) = \boldsymbol{\Phi}(t,t_0)\boldsymbol{P}(k,k)\boldsymbol{\Phi}^{\boldsymbol{T}}(t,t_0) + \boldsymbol{Q}(k+1,k) \tag{6.11}$$

$$\boldsymbol{\Phi}(t,t_0) = e^{\boldsymbol{F}_x(t-t_0)} \tag{6.12}$$

and $\boldsymbol{R}(k+1), \boldsymbol{Q}(k+1,k)$ and $\boldsymbol{H}_{\boldsymbol{x}}(k+1,k)$ are the linearized versions of $\boldsymbol{R}(t), \boldsymbol{Q}(t)$ and $\boldsymbol{H}_x(t)$. Please be aware that the equations here do not include an input function. For the most general form of the equation and details about the derivation of the linearized version of the matrices $\boldsymbol{R}(k+1), \boldsymbol{Q}(k+1,k)$ and $\boldsymbol{H}_{\boldsymbol{x}}(k+1,k)$ we refer the reader to [102].

## 6.3. Spacecraft Relative Dynamics Estimator

### 6.3.1. Scenario

Take two spacecraft orbiting the Earth with dynamics described in equation 2.30. These two spacecraft follow a circular equatorial orbit with an initial altitude of 300 km in an along-track configuration with a relative distance of 1000 km. An equatorial orbit is selected in order to avoid taking into account the $J_2$ effects on

Table 6.1: Configuration of the dynamics of the system under study.

| **Initial Conditions** | | |
|---|---|---|
| Spacecraft | **S/C 1** | **S/C 2** |
| Position (km) | $[300 + R_E, 0, 0]$ | $(300 + R_E)[\cos\theta_2, \sin\theta_2, 0]$ |
| Velocity (km/s) | $[0, 7.7142, 0]$ | $7.7142[-\sin\theta_2, \cos\theta_2, 0]$ |
| Attitude quaternion | $[0, 0, 0, 1]$ | $[0, 0, 0, 1]$ |
| Rotation rate for the rotating case (rad/s) | $[0, \pi/18, 0]$ | $[0, 0, \pi/18]$ |
| Initial along-track separation ($R_A$) | 1000 km | |
| **Spacecraft mechanical characteristics.** | | |
| Mass (m) | 3.6 kg | 3.6 kg |
| Inertia matrix ($\boldsymbol{I}$) | $\begin{bmatrix} 0.055 & 0 & 0 \\ 0 & 0.055 & 0 \\ 0 & 0 & 0.017 \end{bmatrix}$ kg m$^2$ | $\begin{bmatrix} 0.055 & 0 & 0 \\ 0 & 0.055 & 0 \\ 0 & 0 & 0.017 \end{bmatrix}$ kg m$^2$ |
| Drag coefficient ($C_D$) | 2.3 | 2.3 |

Table 6.2: Sensors accuracy

| Sensor | Noise variance |
|---|---|
| Relative position | $\pm 100\ m$ |
| Attitude quaternion | $\pm 0.1$ |

6

the dynamics model. This altitude is selected because in this orbit a strong signal of the coupling due to the atmospheric drag is obtained. Its use is justified by its applicability in distributed space systems (DSS) missions ranking from Earth-observation to gravity missions. This orbit is of use also for future DSS missions that may avoid debris by best placed in very low orbits. The drag coefficients ($C_D$) of both spacecraft are equal and assumed to have the same dimensions as the ones used in the simulation of the formation flying mission proposed by TU Delft in the framework of the QB50 mission [99].

The parameters used in the scenario are given in Table 6.1. It is assumed that the atmospheric density is known, and is given by its values at solar radiation maximum (see [36]).

The accuracy of the pseudo-measurements is defined on Table 6.2.

In order to demonstrate the effect of coupling, two EKF are used: one that includes the coupling dynamics in the model described by equation 2.30. This estimator is called for now on the "Coupled Estimator". Another estimator was implemented for comparison purposes. In this one, the model assumes that the areas of the spacecraft are constant, equal to the largest possible facing area of both satellites, and no dynamic coupling is considered. This estimator is called here the "Uncoupled Estimator".

Two different kinds of satellites, by size, are used on this research. The first kind of spacecraft is a 3-unit Cubesat, one of the smallest forms proposed for co-operative missions, for example in the QB-50 mission [99]. These satellites have a 30x10x10 cm cuboid form. For comparison purposes, another "large spacecraft" is used. The size of the "large spacecraft" is defined as a cuboid with the same ratio between sides of the CubeSat configuration, while at the same time having a size comparable to a large spacecraft used for formation flying missions. With this

Table 6.3: Test cases area configuration for the spacecraft

| **Configuration** | **size** $(cm^3)$ |
|---|---|
| CubeSat (3U) | 30 x 10 x 10 |
| Large Spacecraft | 240 x 40 x 40 |

Table 6.4: Process noise configuration for the coupled and uncoupled estimator.

| | | | |
|---|---|---|---|
| $n_{\boldsymbol{r}}$ | $10^{-9}$ | $n_{\tilde{\boldsymbol{r}}}$ | $10^{-9}$ |
| $n_{\boldsymbol{v}}$ | $10^{-9}$ (Calibrated) | $n_{\tilde{\boldsymbol{v}}}$ | $10^{-9}$ (Calibrated) |
| $n_{\boldsymbol{q}}$ | $10^{-7}$ | $n_{\tilde{\boldsymbol{q}}}$ | $10^{-7}$ |
| $n_{\boldsymbol{\omega}}$ | $10^{-5}$ | $n_{\tilde{\boldsymbol{\omega}}}$ | $10^{-5}$ |

purpose, the "large spacecraft" is set up as a cuboid where each side is 8 times larger than every side of the CubeSat configuration. Under these assumptions, the "large spacecraft" size is similar in size to the spacecraft used for the Grace mission (length = 312.2 cm, height = 72 cm, bottom width = 194.2 cm, top width = 69.3 cm) [110]. For reference, their sizes are described on Table 6.3.

The process noise to be used in the implementation of the EKF is fundamental for the proper performance of both estimators. The noise matrix to be used in the model $\boldsymbol{Q}(k)$ is given as

$$\boldsymbol{Q}(k+1) = \left[\begin{array}{cccc:cccc} \boldsymbol{Q_r} & \boldsymbol{0}_{3\times3} & \boldsymbol{0}_{3\times4} & \boldsymbol{0}_{3\times3} & \boldsymbol{0}_{3\times3} & \boldsymbol{0}_{3\times3} & \boldsymbol{0}_{3\times4} & \boldsymbol{0}_{3\times3} \\ \boldsymbol{0}_{3\times3} & \boldsymbol{Q_v} & \boldsymbol{0}_{3\times4} & \boldsymbol{0}_{3\times3} & \boldsymbol{0}_{3\times3} & \boldsymbol{0}_{3\times3} & \boldsymbol{0}_{3\times4} & \boldsymbol{0}_{3\times3} \\ \boldsymbol{0}_{4\times3} & \boldsymbol{0}_{4\times3} & \boldsymbol{Q_q} & \boldsymbol{0}_{4\times16} & \boldsymbol{0}_{3\times3} & \boldsymbol{0}_{3\times3} & \boldsymbol{0}_{3\times4} & \boldsymbol{0}_{3\times3} \\ \boldsymbol{0}_{3\times3} & \boldsymbol{0}_{3\times3} & \boldsymbol{0}_{3\times3} & \boldsymbol{Q_\omega} & \boldsymbol{0}_{3\times3} & \boldsymbol{0}_{3\times3} & \boldsymbol{0}_{3\times4} & \boldsymbol{0}_{3\times3} \\ \hdashline \boldsymbol{0}_{3\times3} & \boldsymbol{0}_{3\times3} & \boldsymbol{0}_{3\times4} & \boldsymbol{0}_{3\times3} & \boldsymbol{Q_{\tilde{r}}} & \boldsymbol{0}_{3\times3} & \boldsymbol{0}_{3\times4} & \boldsymbol{0}_{3\times3} \\ \boldsymbol{0}_{3\times3} & \boldsymbol{0}_{3\times3} & \boldsymbol{0}_{3\times4} & \boldsymbol{0}_{3\times3} & \boldsymbol{0}_{3\times3} & \boldsymbol{Q_{\tilde{v}}} & \boldsymbol{0}_{3\times4} & \boldsymbol{0}_{3\times3} \\ \boldsymbol{0}_{3\times3} & \boldsymbol{0}_{3\times3} & \boldsymbol{0}_{3\times4} & \boldsymbol{0}_{3\times3} & \boldsymbol{0}_{4\times3} & \boldsymbol{0}_{4\times3} & \boldsymbol{Q_{\tilde{q}}} & \boldsymbol{0}_{4\times3} \\ \boldsymbol{0}_{3\times3} & \boldsymbol{0}_{3\times3} & \boldsymbol{0}_{3\times4} & \boldsymbol{0}_{3\times3} & \boldsymbol{0}_{3\times3} & \boldsymbol{0}_{3\times3} & \boldsymbol{0}_{3\times4} & \boldsymbol{Q_{\tilde{\omega}}} \end{array}\right] \tag{6.13}$$

where $\boldsymbol{Q}_\alpha = n_\alpha^2 \boldsymbol{1}_3$ with $\alpha = \{\boldsymbol{r}, \boldsymbol{v}, \boldsymbol{q}, \boldsymbol{\omega}, \tilde{\boldsymbol{r}}, \tilde{\boldsymbol{v}}, \tilde{\boldsymbol{q}}, \tilde{\boldsymbol{\omega}}\}$ and $\boldsymbol{Q}_\beta = n_\alpha^2 \boldsymbol{1}_4$ with $\beta = \{\boldsymbol{q}, \tilde{\boldsymbol{q}}\}$. The values for each of these process noises used for this simulation are given in Table 6.4.

For spacecraft estimation purposes, incorporating the non-modeled perturbation effects in the dynamics model as part of the process noise is a common practice (this is done for example in [64]). For this reason, in order to know if, and to what extend the "Coupled Estimator" leads to a better estimation, the magnitude of the velocity process noise of the uncoupled estimator is adjusted until the estimation reaches its best performance. In this way, the process noise is used to simulate the atmospheric drag for the "Uncoupled Estimator". This is the reason why the velocity process noise is indicated in Table 6.4 as "Calibrated". The best possible uncoupled estimator is defined as the one that leads to the lowest average estimation error after five orbits. The estimation error $\Delta\tilde{\boldsymbol{r}}_u$ is defined as the error between the real dynamics and the dynamics predicted by the Uncoupled Estimator.

In order to determine the "calibrated" magnitude of the velocity noise, the following procedure is used:

1. The initial value for both $n_{\boldsymbol{v}}, n_{\tilde{\boldsymbol{v}}}$ is set to be the largest magnitude of the atmospheric drag force $\boldsymbol{a}_a$ at the evaluating altitude. For example, on the 300 km orbit propagation, for the largest spacecraft, the largest absolute value of the atmospheric drag force was calculated to be $9.9170 \cdot 10^{-4}$ N.
2. The estimator is propagated for five orbits.
3. The magnitude of $\Delta\tilde{\boldsymbol{r}}_u$ is calculated.
4. The magnitudes of $n_{\boldsymbol{v}}, n_{\tilde{\boldsymbol{v}}}$ is incremented and decremented in steps of $10\%$ of their initial value until the minimum value of the average of $\Delta\tilde{\boldsymbol{r}}_u$ for the fifth orbit is obtained. For example, in this case, for the incremented process noise, we use $n_{\boldsymbol{v}} = 10.9087$, that constitutes 10% more than the initial process noise use.
5. This increment and decrement continues until the lowest value for $\Delta\tilde{\boldsymbol{r}}_u$ is found. For this example, the value of the process noise that lead to the lowest error was $6.9419 \cdot 10^{-4}$ (a 30% decrement from the initial value).



Hence, the calibration procedure is based on the minimization of $\Delta\tilde{\boldsymbol{r}}_u$ via the calibration of the velocities process noise. This calibration is done every time the area or the altitude is changed.

The objective of this procedure is to compare the Coupled Estimator with the best possible Uncoupled Estimator. With this, it is shown that even in the best possible assumption of the perturbation as a white-Gaussian noise, the Coupled Estimator shows a better performance in terms of convergence and precision.

### 6.3.2. Results and Analysis

In this section, it will be shown how the model taking into account the coupling between relative position and attitude impacts the performance of the estimation of orbital relative dynamics. For this, two variables are evaluated: the change in the spacecraft effective area and the change in the spacecraft set altitude. Take into account the fact that the mass of the spacecraft is not changed for any of the simulations, the change of area may be interpreted here also as the change of the area-mass ratio.

Here, the improvement on the estimation results is shown via the difference of the estimation error between the coupled and the uncoupled estimator, and also by showing the accumulated variance of both estimators, via the accumulative effect of the estimation convergence. This simulation is carried out over five orbits, showing clearly the best convergence of the coupled estimator.

#### Scenario 1: Variation of the spacecraft effective area

In order to evaluate the effect of the effective area of the spacecraft in formation, this work uses four different area configurations, all with a rectangular form,

Table 6.5: Variation of the area of the spacecraft for sensitivity analysis

| Area Configuration | Area $[cm^3]$ |
|---|---|
| 1 | 30 x 10 x 10 |
| 2 | 60 x 20 x 20 |
| 3 | 120 x 30 x 30 |
| 4 | 240 x 40 x 40 |

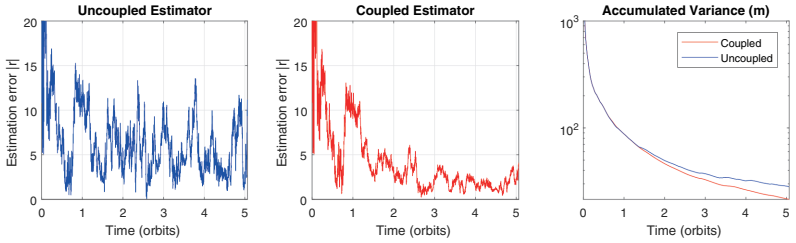


Figure 6.1: Relative position estimation results for a 2-spacecraft formation with 3-unit Cubesat configuration.

starting from a 3-unit Cubesat configuration (30x10x10 cm), one of the smallest area configurations proposed for formation flying missions. This base configuration was selected due to its popular use in spacecraft constellation projects like Planet Labs constellation [18]. From here, areas are incremented to determine the sensitivity between its variation and the estimation performance. The areas used are summarized on Table 6.5.

Results using the smallest satellite (a 3 unit Cubesat configuration) are shown in Figure 6.1, and the largest in Figure 6.2, both in a circular orbit with an altitude of 300 km. Here it is shown that even in the smallest spacecraft area case, coupled estimator outperforms the ”Best Uncoupled Estimator”.

Figure 6.3 shows how the variance after the fifth orbit differs for the uncoupled and the coupled case, and its variability with the spacecraft area, as a parameter of the performance of the estimator with respect to the spacecraft area. For reference, the values shown in this figure are the values after five orbits of the ”accumulated variance” value shown on Figure 6.2 and Figure 6.3. Here, as expected, it is clear

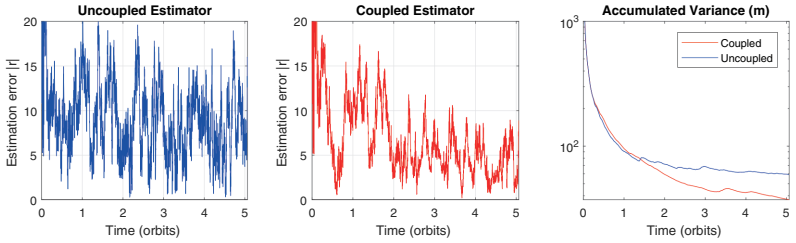


Figure 6.2: Relative position estimation results for the large spacecraft case.

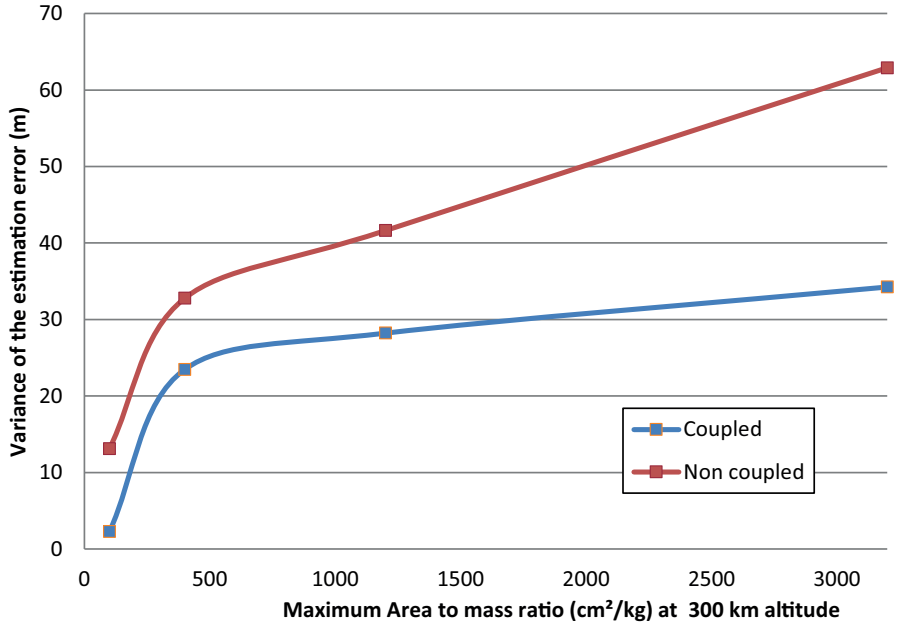




Figure 6.3: Variance of the error after five orbit with respect to the spacecraft area at a 300 km altitude.

that with a larger area, the difference between the coupled and the uncoupled estimator is higher. With an increment of about 32 times between the smallest and the largest area, the difference between variances for the smallest spacecraft is $10.849$ m, but for the largest spacecraft it is $28.651$ m, a factor of about three.

Here it is also shown that even for the smallest spacecraft evaluated, the coupled estimator shows an improvement on the estimation performance. These differences are significant for most Earth Observation missions proposed in present times.

### Scenario 2: Variation of the spacecraft altitude

In order to study the effect of coupling for different spacecraft, the orbits of the two-satellites, both with the largest spacecraft area (Area 4 of Table 6.5) are propagated in circular orbits with different altitudes. The estimation performance of this configuration in a 300 km altitude orbit was already illustrated in the first scenario in Figure 6.2.

Take now the results of increasing the spacecraft altitude, shown in Figure 6.4 for 350 km altitude and in Figure 6.5 for 650 km altitude. Both figures show that even for a 650 km orbit, the coupled estimator leads to non-negligible improvements on the estimation performance of the dynamics.

Figure 6.6 shows the result of the final value of the accumulated variance after five orbits for the coupled and the uncoupled estimator with respect to the altitude. It is evident that even at 650 km altitude, the coupled estimator leads to better re-

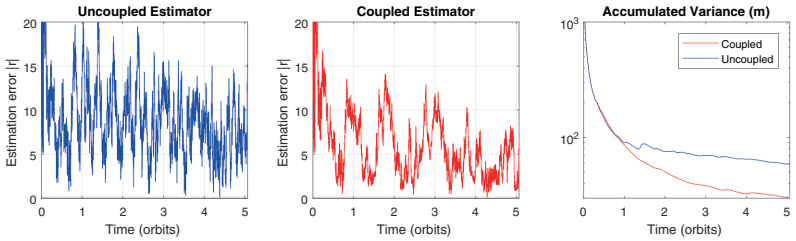


Figure 6.4: Variance of the error after five orbit at 350 km altitude.

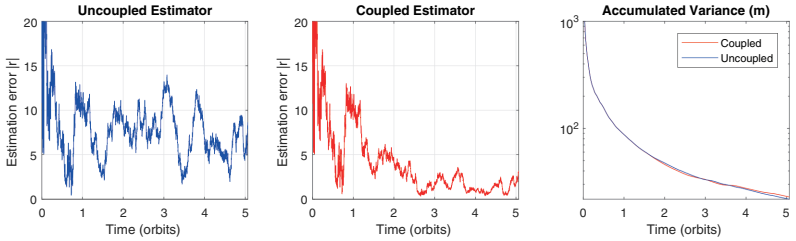


Figure 6.5: Variance of the error after five orbits at 650 km altitude.



sults. Nevertheless, the difference between both estimator considerably diminishes at this altitude.

The main variable affecting here the estimation performance is the atmospheric density, that changes from a value of $3.96 \cdot 10^{-11}$ kg/m$^3$ for the 300 km altitude to $2.64 \cdot 10^{-13}$ kg/m$^3$, a magnitude 250 times higher for the former compared to the latter. Nevertheless, this is not the only variable affecting the estimation performance. For reference, the variation of the atmospheric density is also illustrated in Figure 6.6. At a lower altitude, the velocity to remain in a circular orbit is higher, hence the effect of the atmospheric perturbation is further increased. For this, it is very difficult to compute the direct relation between the physical variables and the increment in performance due to the altitude changes. The accumulated variance after five orbits for the 300 km altitude is 34.2 m for the coupled case, and of 62.9 m for the uncoupled case, a difference of almost 30 meters in variation. Nevertheless, for the 650 km altitude evaluation, the variance is 20.8 m for the coupled case and 24.2 m for the uncoupled case. With this, it may be concluded that fundamentally for all cases evaluated here, the difference between estimators is not significant beyond 700 km altitude.

## 6.4. Remarks

The work of this chapter shows how the coupling between orbit and attitude dynamics caused by the atmospheric drag force and torque improves the estimation of relative dynamics of spacecraft. For this, the effectiveness of the ”Coupled estimator” (an estimator considering such physical effect) is shown.

For comparison purposes, another estimator where the perturbation was sim-

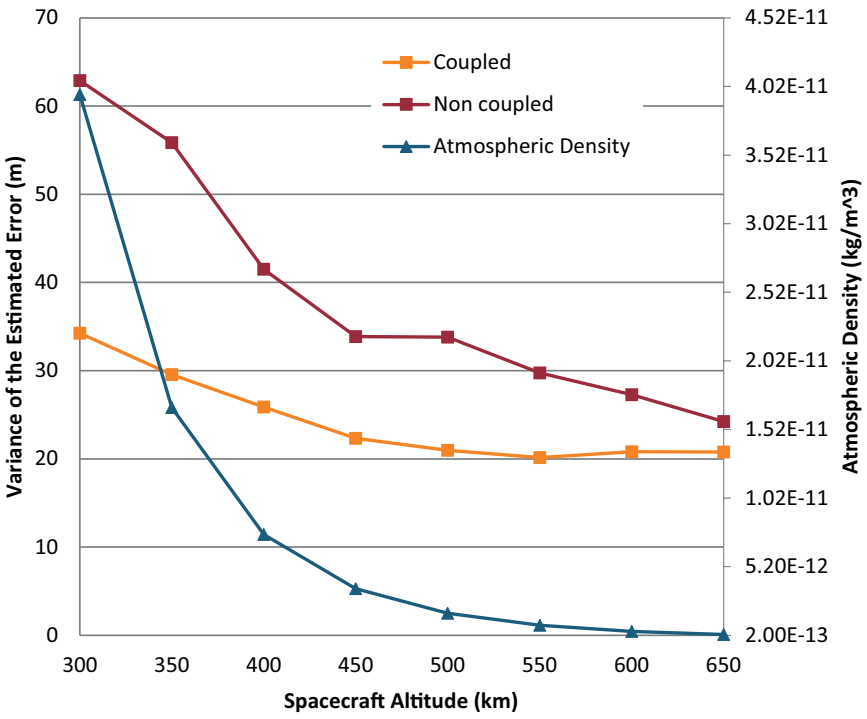


Figure 6.6: Variance of the error after five orbit with respect to the altitude.

ulated using only white-Gaussian noise, is used. Using white Gaussian noise to simulate the perturbation effect is a common practice in spacecraft dynamics estimation. Due to the fact that it may be argued that the selection of the magnitude of this noise may affect the validity of the comparison, the magnitude of the white-Gaussian noise was adjusted until the lowest average error after five orbits was obtained in the estimation process. Even under this condition, the ”Coupled Estimator” shows a better estimation performance.

For a case of a very low orbit, a 300 km altitude orbit, even with two CubeSat flying in a along-track configuration, the improvement shown by the use of the coupled estimator is significant, leading to an improvement of 6.9 m in the average position estimation compared to the ”best uncoupled estimator”.

Changes in estimation performance are even observed for altitudes of as much as 650 km, where for a 240x40x40 cm spacecraft, an improvement of 3.5 m in the average of the error in the estimation of relative position is shown. Nevertheless, when altitudes over 700 km are used in our simulations, the difference in negligible, as expected.

This work shows and quantifies the improved estimation performance of relative dynamics of spacecraft using a orbit-attitude model closer to reality, and a method to be applied to different formation flying configurations. Also, since this work uses nonlinear orbit and attitude dynamics equations is not limited to circular or near-circular orbits as would be the case when the Clohessy-Wiltshire equations ([43]) were used. The use of more complex models has been restricted in the past due to computation constraints. However, the latest improvements in electronics computing performance, both in velocity and in power consumption, lead to the possibility of using more complex spacecraft dynamics models in on-board spacecraft computers with no additional risk.

Future work may take into account other spacecraft formation flying configuration with different densities, elliptic orbits, and other effects, like the gravity gradient in different relative pose configurations, the diurnal effect of the atmosphere, as well as the use of other estimation techniques that provide a better operation performance when models of spacecraft nonlinear dynamics are used.

# 7

# Conclusions and Outlook

## 7.1. Summary

This dissertation describes the effect of a sophisticated model of spacecraft dynamics where the coupling between attitude and orbital dynamics via the atmospheric drag influences estimation of the relative states of a distributed space system. The scenario used for the analysis consist of two satellites in orbit around the Earth. The dynamics of the first satellite, known as the Chief, are described as a function of its absolute orbit and attitude. The motion of the second satellite, known as the deputy, is described using its relative dynamics with respect to the chief spacecraft. The description of the dynamics of the deputy may be used to expand the model to any number of spacecraft flying in formation, because any additional spacecraft relative dynamics can be described using the Chief as its reference.

In order to describe the atmospheric drag force and torque as the source of coupling, spacecraft geometries are described as a set of areas, and for this work, rectangular spacecraft are assumed. Despite its apparent simplicity, this model may be generalized to any spacecraft form. The atmospheric drag perturbation is described for the chief spacecraft using its absolute states, and the differential drag is described using the relative dynamic states. The expressions describing differential drag under the aforementioned conditions were not found in the scientific literature, thus they were first derived here.

The use of the Observability Gramian (OG) as a tool for the evaluation of the observability level of the system required the linearization of the absolute and relative dynamics. The linearization of the model of absolute and differential atmospheric drag force and torque was derived in Chapter 3. This tool allows to analytically determine which of the states affects the observability, specially the partial differential of the orbit states with respect to attitude states, and constitute a tool for further analysis. Chapter 4 presents the analytical linearization of all states, including the atmospheric drag perturbation. These results are necessary for the determination of the OG.

Chapter 5 and 6 describe the main results of this thesis work. In Chapter 5, the OG is used to determine the effect of coupling in spacecraft dynamics in the observability level of the system. It is shown that coupling not only enables full observability for limited sensing configurations, but reveals how the observability level of the dynamic system varies with respect to spacecraft parameters and their initial dynamics conditions. In this scenario, variation of the observability level up to three orders of magnitude are observed due to the effect of the variation of these parameters. The proposed methodology constitutes a tool to obtain a numerical evaluation on how the use of sophisticated dynamics models and sensing configurations impact the observability of relative dynamics of spacecraft.

In Chapter 6, the Extended Kalman Filter (EKF) is used to analyze how the drag-induced coupling of relative orbit and attitude affects the estimation accuracy of the relative spacecraft states. Here, a scenario is assumed that uses an equatorial low-Earth orbit (LEO), to focus on the drag-induced coupling and avoid an interplay with gravity-induced coupling, e.g. from the $J_2$ effect. The atmospheric perturbation is the largest non-gravitational perturbation affecting the spacecraft dynamics at altitudes below 700 km. An EKF accounted for the dynamic coupling, called "coupled estimator", is compared to an "uncoupled estimator", which simulates the drag perturbation as white noise only. It is shown how the uncoupled estimator can be calibrated to provide a fair comparison to the results of the coupled estimator. It is shown that even with the best calibration possible, the coupled estimator provides superior estimation errors as compared to the result of the uncoupled. A sensitivity analysis is performed with various area-to-mass ratios and spacecraft altitudes which reveals that even for small 3-U CubeSats, significant improvements can be obtained taking the dynamic coupling into account. Furthermore, improvements of the estimation errors have been shown for altitudes below 650 km.



## 7.2. Conclusions

New demands are arising for distributed space systems, where several spacecraft work together in a single mission. Examples are formations which constitute virtual instruments or rendez-vous missions with uncooperative space debris objects. These demands cause new challenges and solutions for spacecraft engineering, such as new sensor technology and improved algorithms and processors. In order to make the best use of those developments, the dynamic models that describe the relative motion of involved spacecraft need to be improved as well.

For spacecraft relative dynamics, little progress has been made in the impact of the coupling between orbit and attitude dynamics in the observability of the system. Most research focuses instead on the measurement model and technology. Also, little attention has been given to the use of the Observability Gramian in the assessment of spacecraft observability. The current work provides innovative contributions to these shortcomings of the body of knowledge.

The exploration of the effect of coupling for control purposes has been the subject of increasing attention the last years. Nevertheless, to the best knowledge of the author, no work has been published, before the thesis presented here, where the coupling between the attitude and orbital dynamics caused by external

perturbations is adopted in spacecraft relative dynamics models to improve their estimation accuracy. This simplification is typically justified, in the preparation of a mission, by assuming that the magnitude of this coupling effect is negligible.

Conclusions and key innovations of this thesis are two-fold: first, it is shown how even limited measurements scenarios may lead to full observability, if the coupling between orbit and attitude dynamics is taken into account. Secondly, it is shown via the EKF that even in full observability situations, accounting for the coupling leads to better estimation results, compared to an uncoupled estimator where the perturbations were assumed to be white-Gaussian noise and calibrated to their best possible performance.

How can the coupling between attitude and orbit dynamics affect the observability of the relative dynamics of spacecraft? (Research question 1). It has been observed in Chapter 5 that, when a fully observable system is used and perfect measurements are assumed, the dynamic model does not increase the observability of the system. Nevertheless, observability is improved under limited observable scenarios, depending on the condition of the system. The OG has been employed as a tool to evaluate the dependency of the observability on the dynamics of relative motion. It has been shown that the coupling, created by the atmospheric drag force for spacecraft in formation in LEO, enables full observability of the state, not possible without such coupling. Furthermore, the degree of observability has been analyzed for various orbits and spacecraft mechanical characteristics. As a result, new elements on the gradient of the dynamics are appearing in an analytical model of the partial derivatives, creating a significant change in the observability of the system.

The cases of limited observability, where only the relative position of the spacecraft or the relative attitude of the spacecraft are measured, are of special interest on this work. They show that full observability is achieved, not possible in the scenario under study without such coupling.



This thesis proposed the use of the OG method, allowing to compare how different scenarios change the observability conditions in a methodical way. This contrasts to the use of the propagated estimating results as a comparison method, where other elements (as the configuration and effectiveness of the selected estimator itself) may have an influence on the result.

The OG method also helps to determine during mission analysis and design which sensor scenario benefits the most from the consideration of coupling. This information is valuable for the implementation of the estimation of relative spacecraft dynamics, as well as the design of sensor suites for formation flying missions.

How can the coupling between attitude and orbit dynamics be used to improve the estimation of the relative dynamics of spacecraft? (Research question 2). The effects of the coupling elements of the system gradient are observed also when estimation is done using the Extended Kalman Filter (EKF). Here, even in full observability situations, accounting for the dynamic coupling leads to better estimation results, even when an uncoupled reference estimator is optimized for minimum errors. This means that in situations where the Observability Gramian leads to the same observability rank, especially situations of full observability, the sophisticated

model of dynamics used in the model of the estimator leads to more stable, smaller estimation errors. This is even true for CubeSat spacecraft, where the area to mass ratio is unfavorable as compared to missions using large spacecraft. The reason for this improvement in estimation performance, not visible in the OG analysis for fully-observable scenarios with coupling is that measurements have an associated noise in the EKF. It is in those cases that the more precise model improves the estimation performance.

## 7.3. Outlook

The Observability Gramian, used to evaluate the drag-induced coupling between orbit and attitude dynamics for formations, proposed in this thesis, provides a powerful tool to study any other kind of perturbation, like the $J_2$-gravity effect or solar radiation pressure. It likewise allows to study more complex mission scenarios, such as highly elliptic orbits. These effect are well known, but their influence in observability has never been analyzed using a tool with the numerical evaluation capabilities of the OG.

Also, the use of the OG may be expanded to any number of spacecraft flying in formation, by describing any additional spacecraft dynamics relative to the dynamics of a chief spacecraft using the same equations presented here for the deputy.

The present work may be further improved by using more advanced models of the variation of the atmospheric density. A more sophisticated density model may allow better estimation performance if the density is defined as a state of the system. A spacecraft geometry taking advantage of the knowledge of this physical effect to improve the estimation of density may be a direct application of the results of this work. Another use of advanced atmospheric density models is that they would enable the use of the OG analysis in cases where the orbits are highly elliptic. In those cases, the change of atmospheric drag density influences highly the differential of the attitude states with respect to the orbit states, leading to an increase in the coupling effect.

The future use of the Controllability Gramian (CG) in an analogue way as the use of the OG is considered to have high potential. Coupling in control is related directly to the effect of any actuator affecting both orbit and attitude, for example, propulsion not aligned with the center of mass or pressure. Although, this has been subject of previous studies, nevertheless, none of them made use of the advantages of the OG to assess the degree of controllability of a system. Also, the combination of the effect of the actuator when the coupling effect of the perturbation is taken into account may lead to more precise solutions for the estimation and control of spacecraft, via the analysis of both the Observability and the Controllability Gramian.

Future areas of exploration may arise from taking into account the computational and power requirements when used with sophisticated models of estimators as the one proposed in this work. Such knowledge would enable space systems engineers to make a proper trade-off analysis where the increment in performance is analyzed as a function of the use of computational resources, leading to more informed decisions about an optimized mission design.

# References


[1] P. Chodas, *Combined satellite attitude and orbit determination with dynamic coupling,* in *Astrodynamics Conference*, Vol. 1 (1982).

[2] A. Zolli, *Responding to the nepal earthquake,* https://www.planet.com/pulse/nepal/ (2015), [Online; Accessed: October 2019].

[3] NASA, *Nssdca master catalog search,* https://nssdc.gsfc.nasa.gov/nmc/spacecraftDisplay.do?id=1957-001B (2017), [Online; Accessed: December 2018].

[4] H. Jones, *The recent large reduction in space launch cost,* (48th International Conference on Environmental Systems, 2018).

[5] G. E. Moore *et al.*, *Progress in digital integrated electronics,* in *Electron Devices Meeting*, Vol. 21 (1975) pp. 11–13.

[6] B. Lal and T. Zurbuchen, *Achieving science with cubesats: Thinking inside the box,* in *AGU Fall Meeting Abstracts* (2016).

[7] S. D'Amico, O. Montenbruck, C. Arbinger, and H. Fiedler, *Formation flying concept for close remote sensing satellites,* in *Proc. 15th AAS/AIAA Space Flight Mech. Conf* (2005) pp. 831–848.

[8] J. Van Den IJssel, J. Encarnação, E. Doornbos, and P. Visser, *Precise science orbits for the swarm satellite constellation,* Advances in Space Research **56**, 1042 (2015).

[9] O. Montenbruck, S. Hackel, and A. Jäggi, *Precise orbit determination of the sentinel-3a altimetry satellite using ambiguity-fixed gps carrier phase observations,* Journal of geodesy **92**, 711 (2018).

[10] European Space Agency, *Sentinel 3,* http://www.esa.int/esl/ESA_in_your_country/Spain/Sentinel-3_Vision_panoramica_para_Copernico (2016), [Online; Accessed: December 2017].

[11] E. Gill, O. Montenbruck, and S. D'Amico, *Autonomous formation flying for the prisma mission,* Journal of Spacecraft and Rockets **44**, 671 (2007).

[12] German Aerospace Center (DLR), *The prisma formation with the main (left) and target (right) satellites,* http://www.dlr.de/rb/en/Portaldata/38/Resources/images/RB-RFT/Prisma_HighRes.jpg (2016), [Online; accessed November 28, 2016].

[13] K. Lagedec, J. Lebas, and F. Ankersen, *Precision formation flying for the darwin interferometer,* in *Proceedings of the 5th International ESA Conference on Spacecraft Guidance, Navigation and Control Systems* (2003).

[14] ESA, *Darwin: study ended, no further activities planned,* http://www.esa.int/science/darwin (2009), [Online; Accessed: November 2019].

[15] S. Engelen, C. J. Verhoeven, and M. Bentum, *OLFAR, A Radio Telescope Based on Nano-Satellites in Moon Orbit,* in *24th Annual AIAA/USU Conference on Small Satellites* (2010).

[16] E. Dekens, S. Engelen, and R. Noomen, *A satellite swarm for radio astronomy,* Acta Astronautica **102**, 321 (2014).

[17] S. I. Corporation, *Worldview-3 satellite sensor,* https://www.satimagingcorp.com/satellite-sensors/worldview-3/, [Online; Accessed: November 2019].

[18] D. Butler, *Many eyes on earth,* Nature **505**, 143 (2014).

[19] G. B. Shaw, D. Miller, and D. Hastings, *Generalized characteristics of communication, sensing, and navigation satellite systems,* Journal of Spacecraft and Rockets **37**, 801 (2000).

[20] D. Barnhart, T. Vladimirova, and M. Sweeting, *Very-Small-Satellite Design for Distributed Space Missions,* Journal of Spacecraft and Rockets **44**, 1294 (2007).

[21] C. Boshuizen, J. Mason, P. Klupar, and S. Spanhake, *Results from the planet labs flock constellation,* in *28th AIAA/USU Conference on Small Satellites* (Logan, UT, 2014).

[22] NASA, *An example of a satellite constellation: Two planet labs dove satellites being deployed from the iss in february 2014,* https://www.greenpolicy360.net/w/File:Dove_minisat_launch_Nov19,2013.jpg (2016), [Online; accessed March 15, 2017].

[23] E. Gill, *Together in space: Potentials and challenges of distributed space systems,* (2008), inaugural speech.

[24] European Space Agency (ESA), *Artist's impression showing atv docking with iss,* http://www.esa.int/spaceinimages/Images/2007/03/Artist_s_impression_showing_ATV_docking_with_ISS (2007), [Online; accessed July 26, 2019].

[25] NASA/JPL-Caltech, *Artist's concept of gravity recovery and climate experiment,* https://www.jpl.nasa.gov/spaceimages/details.php?id=PIA04236 (2002), [Online; accessed July 26, 2019].

[26] S. Bandyopadhyay, G. P. Subramanian, R. Foust, D. Morgan, S.-J. Chung, and F. Y. Hadaegh, *A Review of Impending Small Satellite Formation Flying Missions,* Proceedings of the 53rd AIAA Aerospace Sciences Meeting , 1 (2015).

[27] G. Crowley, C. Fish, C. Swenson, R. Burt, E. Stromberg, T. Neilsen, S. Burr, A. Barjatya, G. Bust, and M. Larsen, *Dynamic ionosphere cubesat experiment (dice),* in *AIAA/USU Conference on Small Satellites* (Logan, UT, 2011).

[28] T. Kuiper, L. Clare, J. Gao, W. Majid, D. Meier, C. Norton, and N. Renno, *Cubesat constellation for communications and mars radio monitoring,* in *Concepts and Approaches for Mars Exploration*, Vol. 1679 (2012).

[29] M. Bentum, C. Verhoeven, A.-J. Boonstra, A. J. van der Veen, and E. K. A. Gill, *A novel astronomical application for formation flying small satellites,* International Astronautical Congress (IAC) , 09.A3.4.3 (2009).

[30] National Aeronautics and Space Administration, *Nasa heliophysics,* https://science.nasa.gov/heliophysics.

[31] Keck Institute for Space Studies, *Update for low-frequency astronomy: Missions enabled by an interplanetary cubesat architecture,* http://kiss.caltech.edu/workshops/cubesat/presentations/staehle-interplanetary-cubesat-missions.pdf, [Online; accessed November, 2019].

[32] V. Chirayath and B. Mahlstedt, *Himarc 3d-high-speed, multispectral, adaptive resolution stereographic cubesat imaging constellation,* in *AIAA/USU Conference on Small Satellites* (Logan, UT, 2012).

[33] Space Dynamics Laboratory, Utah State University Research Foundation, *Dice (dynamic ionosphere cubesat experiment), dice-1 and dice-2,* http://www.sdl.usu.edu/downloads/dice.pdf, [Online; accessed November, 2019].

[34] Delfi Space, Delft University of Technology, *The olfar mission,* http://www.delfispace.nl/advanced-concepts/olfar-mission (2017), [Online; accessed December, 2017].

[35] B. Yost, *State of the Art of Small Spacecraft Technology*, Tech. Rep. (National Aeronautics and Space Administration (NASA), 2017).

[36] W. J. Larson and J. R. Wertz, *Space mission analysis and design*, Tech. Rep. (Microcosm, Inc., Torrance, CA (US), 1992).

[37] G. K. Skinner, B. R. Dennis, J. F. Krizmanic, and E. P. Kontar, *Science Enabled by High Precision Inertial Formation Flying,* International Journal of Space Science and Engineering **1**, 331 (2013), arXiv:1311.6955 .

[38] NASA, *Maxim science,* https://bhi.gsfc.nasa.gov/docs/science/science.html (2017), [Online; accessed December, 2017].

[39] J. R. Wertz, ed., *Spacecraft Attitude Determination and Control* (D. Reidel, Dordrecht, The Netherlands, 1984).

[40] J. L. Junkins and H. Schaub, *Analytical Mechanics of Aerospace Systems* (American Institute of Aeronautics and Astronautics, 2009).

[41] O. Montenbruck and E. Gill, *Satellite orbits: models, methods and applications* (Springer, 2005).

[42] R. Sun, D. Maessen, J. Guo, and E. Gill, *Enabling inter-satellite communication and ranging for small satellites,* in *9th Symposium on Small Satellites Systems and Services, Funchal, Portugal*, Vol. 31 (2010).

[43] W. Clohessy and R. Wiltshire, *Terminal guidance system for satellite rendezvous,* Journal of the Aerospace Sciences **27**, 653 (1960).

[44] K. Alfriend and H. Yan, *Evaluation and comparison of relative motion theories,* Journal of Guidance, Control, and Dynamics **28**, 254 (2005).

[45] J. Tschauner, *Elliptic orbit rendezvous,* AIAA Journal **6**, 87 (1967).

[46] C. McInnes, *Autonomous Ring Formation for a Planar Constellation of Satellites,* AIAA Journal of Guidance, Control and Dynamics **5**, 1215 (1995).

[47] K. Alfriend, H. Yan, and S. Vadali, *Nonlinear Considerations in Satellite Formation Flying,* in *Proceedings of the 2002 AIAA/AAS Astrodynamics Specialist Conference* (Monterey CA, 2002).

[48] H. Pan and V. Kapila, *Adaptive nonlinear control for spacecraft formation flying with coupled translational and attitude dynamics,* in *Decision and Control, 2001. Proceedings of the 40th IEEE Conference on*, Vol. 3 (IEEE, 2001) pp. 2057–2062.

[49] H. Pan, H. Wong, and V. Kapila, *Output feedback control for spacecraft with coupled translation and attitude dynamics,* in *43th IEEE Conference on Decision and Control* (2004).

[50] S. Gaulocher, *Modeling the Coupled Translational and Rotational Relative Dynamics for Formation Flying Control,* in *AIAA Guidance, Navigation and Control Conference* (2005) pp. 1–6.

[51] R. Kristiansen, E. Grotli, P. J. Nicklasson, and J. T. Gravdahl, *A model of relative translation and rotation in leader-follower spacecraft formations,* Modeling, Identification and Control **28**, 3 (2007).

[52] R. Kristiansen, P. J. Nicklasson, and J. T. Gravdahl, *Spacecraft Coordination Control in 6DOF: Integrator Backstepping vs Passivity-Based Control,* Automatica , 2896 (2008).

[53] W. Lu, Y. Geng, X. Chen, and F. Zhang, *Relative position and attitude coupled control for autonomous docking with a tumbling target,* International Journal of Control and Automation **4**, 1 (2011).

[54] L. Sun and W. Huo, *Robust adaptive relative position tracking and attitude synchronization for spacecraft rendezvous,* Aerospace Science and Technology **41**, 28 (2015).

[55] F. Zhang, G. Duan, and M. Hou, *Integrated relative position and attitude control of spacecraft in proximity operation missions with control saturation,* International Journal of Innovative Computing, Information and Control **8**, 3537 (2012).

[56] S. Gong, H. Baoyin, and J. Li, *Coupled attitude–orbit dynamics and control for displaced solar orbits,* Acta Astronautica **65**, 730 (2009).

[57] M. Huo, J. Zhao, S. Xie, and N. Qi, *Coupled attitude-orbit dynamics and control for an electric sail in a heliocentric transfer mission,* PLOS ONE **10**, 1 (2015).

[58] G. Misra, M. Izadi, A. Sanyal, and D. Scheeres, *Coupled orbit-attitude dynamics and relative state estimation of spacecraft near small solar system bodies,* Advances in Space Research (2015).

[59] A. J. Knutson, D. Guzzetti, K. C. Howell, and M. Lavagna, *Attitude responses in coupled orbit-attitude dynamical model in earth–moon lyapunov orbits,* Journal of Guidance, Control, and Dynamics , 1 (2015).

[60] B. Kumar, A. Ng, K. Yoshihara, and A. De Ruiter, *Differential drag as a means of spacecraft formation control,* Aerospace and Electronic Systems, IEEE Transactions on **47**, 1125 (2011).

[61] P. W. Chodas, *Combined orbit/attitude determination for low-altitude satellites,* NASA STI/Recon Technical Report N **87** (1986).

[62] S. A. Chee and J. R. Forbes, *Norm-constrained unscented kalman filter with application to high area-to-mass ratio space-debris tracking,* in *AIAA Guidance, Navigation, and Control Conference* (2016) p. 1856.

[63] M. L. Psiaki, *Autonomous low-earth-orbit determination from magnetometer and sun sensor data,* Journal of Guidance, Control, and Dynamics **22**, 296 (1999).

[64] S. Kim, J. Crassidis, and Y. Cheng, *Kalman filtering for relative spacecraft attitude and position estimation,* Journal of Guidance, Control, and Dynamics **30**, 133 (2007).

[65] X. Tang, J. Yan, and D. Zhong, *Square-root sigma-point kalman filtering for spacecraft relative navigation,* Acta Astronautica **66**, 704 (2010).

[66] L. Zhang, H. Yang, S. Zhang, H. Cai, and S. Qian, *Kalman filtering for relative spacecraft attitude and position estimation: a revisit,* Journal of Guidance, Control, and Dynamics **37**, 1706 (2014).

[67] L. Zhang, T. Li, H. Yang, S. Zhang, H. Cai, and S. Qian, *Unscented kalman filtering for relative spacecraft attitude and position estimation,* Journal of Navigation **68**, 528 (2015).

[68] L. Zhang, S. Zhang, H. Yang, H. Cai, and S. Qian, *Relative attitude and position estimation for a tumbling spacecraft,* Aerospace Science and Technology **42**, 97 (2015).

[69] Z. Zhu and Y. Yan, *Real-time relative orbit estimation of noncooperative space target based on nonlinear filtering,* Journal of Aerospace Engineering , 1 (2016).

[70] Y. Xing, X. Cao, S. Zhang, H. Guo, and F. Wang, *Relative position and attitude estimation for satellite formation with coupled translational and rotational dynamics,* Acta Astronautica **67**, 455 (2010).

[71] L. Cao, X. Chen, and A. K. Misra, *A novel unscented predictive filter for relative position and attitude estimation of satellite formation,* Acta Astronautica **112**, 140 (2015).

[72] L. Cao and H. Li, *Novel cubature predictive filter for relative position and attitude estimation of satellite formation considering j 2,* Journal of Aerospace Engineering **29**, 04015049 (2015).

[73] H. Yu, X. Zhang, L. Liu, S. Wang, and S. Song, *Relative dynamics estimation of non-cooperative spacecraft with unknown orbit elements and inertial tensor,* Chinese Journal of Aeronautics **29**, 479 (2016).

[74] L. Dell, G. Kerschen, *et al.*, *Optimal propellantless rendez-vous using differential drag,* Acta Astronautica **109**, 112 (2015).

[75] A. C. Long, J. Cappellari Jr, C. Velez, and A. Fuchs, *Mathematical Theory of the Goddard Trajectory Determination System (GTDS) (revision 1)* (1989).

[76] D. A. Vallado and D. Finkleman, *A critical assessment of satellite drag and atmospheric density modeling,* Acta Astronautica **95**, 141 (2014).

[77] A. H. Jazwinski, *Stochastic Processes and Filtering Theory* (Courier Corporation, 2007).

[78] H. Khalil, *Nonlinear Systems*, Always learning (Pearson Education Limited, 2013).

[79] P. J. Huxel and R. H. Bishop, *Navigation algorithms and observability analysis for formation flying missions,* Journal of guidance, control, and dynamics **32**, 1218 (2009).

[80] P. J. Huxel, *Navigation Algorithms and Observability Analysis for Formation Flying Missions*, Ph.D. thesis, The University of Texas at Austin (2006).

[81] Z. Yu, P. Cui, and S. Zhu, *Observability-based beacon configuration optimization for mars entry navigation,* Journal of Guidance, Control, and Dynamics , 1 (2014).

[82] D. Maessen and E. Gill, *Relative state estimation and observability analysis for formation flying satellites,* Journal of Guidance, Control, and Dynamics **35**, 321 (2012).

[83] Y. He, M. Xu, and X. Chen, *Distance-based relative orbital elements determination for formation flying system,* Acta Astronautica **118**, 109 (2016).

[84] L. Cao and A. K. Misra, *Linearized j2 and atmospheric drag model for satellite relative motion with small eccentricity,* Proceedings of the Institution of Mechanical Engineers, Part G: Journal of Aerospace Engineering **229**, 2718 (2015).

[85] J. Sullivan, S. Grimberg, and S. D'Amico, *Comprehensive survey and assessment of spacecraft relative motion dynamics models,* Journal of Guidance, Control, and Dynamics **40**, 1837 (2017).

[86] K. Alfriend, S. R. Vadali, P. Gurfil, J. How, and L. Breger, *Spacecraft Formation Flying: Dynamics, Control and Navigation*, Vol. 2 (Butterworth-Heinemann, 2009).

[87] S. A. Schweighart and R. J. Sedwick, *High-fidelity linearized j model for satellite formation flight,* Journal of Guidance, Control, and Dynamics **25**, 1073 (2002).

[88] K. Yamanaka and F. Ankersen, *New state transition matrix for relative motion on an arbitrary elliptical orbit,* Journal of Guidance, Control, and Dynamics **25**, 60 (2002).

[89] G. Gaias, J.-S. Ardaens, and O. Montenbruck, *Model of $j_2$ perturbed satellite relative motion with time-varying differential drag,* Celestial Mechanics and Dynamical Astronomy **123**, 411 (2015).

[90] D.-W. Gim and K. T. Alfriend, *State transition matrix of relative motion for the perturbed noncircular reference orbit,* Journal of Guidance, Control, and Dynamics **26**, 956 (2003).

[91] A. W. Koenig, T. Guffanti, and S. D'Amico, *New state transition matrices for relative motion of spacecraft formations in perturbed orbits,* in *AIAA/AAS Astrodynamics Specialist Conference* (2016) p. 5635.

[92] K. Alfriend, *Nonlinear considerations in satellite formation flying,* in *AIAA/AAS Astrodynamics Specialist Conference and Exhibit* (2002) p. 4741.

[93] A. D. Biria and R. P. Russell, *A satellite relative motion model including $j_2$ and $j_3$ via vinti's intermediary,* Celestial Mechanics and Dynamical Astronomy **130**, 23 (2018).

[94] J. Wang, H. Liang, and Z. Sun, *Relative Coupled Dynamics and Control Using Dual Number,* in *Systems and Control in Aeronautics and Astronautics (ISSCAA), 2010 3rd International Symposium on*, 2 (2010) pp. 277–282.

[95] M. J. Sidi, *Spacecraft Dynamics and Control: a Practical Engineering Approach*, Vol. 7 (Cambridge university press, 1997).

[96] F. L. Markley and J. L. Crassidis, *Fundamentals of spacecraft attitude determination and control*, Vol. 33 (Springer, 2014).

[97] J. L. Crassidis, F. L. Markley, and Y. Cheng, *Survey of nonlinear attitude estimation methods,* Journal of Guidance, Control, and Dynamics **30**, 12 (2007).

[98] P. C. Hughes, *Spacecraft Attitude Dynamics* (J. Wiley (New York), 1986).

[99] E. Gill, P. Sundaramoorthy, J. Bouwmeester, B. Zandbergen, and R. Reinhard, *Formation flying within a constellation of nano-satellites: The qb50 mission,* Acta Astronautica , (2012).

[100] S. D'Amico, *Autonomous Formation Flying in Low Earth Orbit*, Ph.D. thesis, Faculty of Aerospace Engineering, Delft University of Technology, Kluyverweg 1, Delft (2010).

[101] A. Noureldin, T. Karamat, and J. Georgy, *Basic navigational mathematics, reference frames and the earth's geometry,* in *Fundamentals of Inertial Navigation, Satellite-based Positioning and their Integration* (Springer Berlin Heidelberg, 2013) pp. 21–63.

[102] J. M. Mendel, *Lessons in estimation theory for signal processing, communications, and control* (Pearson Education, 1995).

[103] J. L. Crassidis and J. L. Junkins, *Optimal estimation of dynamic systems* (Chapman and Hall/CRC, 2004).

[104] J. R. Yim, *Autonomous spacecraft orbit navigation*, Ph.D. thesis, Texas A&M University (2002).

[105] G. E. Dullerud and F. Paganini, *A course in robust control theory: a convex approach*, Vol. 36 (Springer Science & Business Media, 2013).

[106] F. M. Ham and R. G. Brown, *Observability, eigenvalues, and kalman filtering,* IEEE Transactions on Aerospace and Electronic Systems **AES-19**, 269 (1983).

[107] X. Tang, J. Yan, and D. Zhong, *Square-root sigma-point Kalman filtering for spacecraft relative navigation,* Acta Astronautica **66**, 704 (2010).

[108] J. L. Crassidis, R. Alonso, and J. L. Junkins, *Optimal attitude and position determination from line-of-sight measurements.* Journal of Astronautical Sciences **48**, 391 (2000).

[109] J. M. Galante, J. Van Eepoel, C. D'Souza, and B. Patrick, *Fast kalman filtering for relative spacecraft position and attitude estimation for the raven iss hosted payload,* in *39th AAS Guidance and Control Conference (DISC, Elche, Spain, September 2009)* (2016).

[110] eoPortal Directory, *Grace (gravity recovery and climate experiment),* https://directory.eoportal.org/web/eoportal/satellite-missions/g/grace, [Online; accessed November, 2017].

# Curriculum Vitæ

## Adolfo CHAVES JIMÉNEZ

11-09-1980 Born in San Ramón, Costa Rica.

## Education

1994–1999 Secondary Education
Instituto Superior Julio Acosta García, San Ramón (1994–1996)
Colegio Científico Costarricense, San Ramón (1997–1998)

1999–2004 Electronic Engineering
Instituto Tecnológico de Costa Rica

2011-2020 PhD. Space Systems Engineering
Delft University of Technology, Delft
*Thesis:* On the Coupling of Orbit and Attitude Determination of Satellite Formations from Atmospheric Drag. Observability and Estimation Performance
*Promotor:* Prof. dr. E.K.A. Gill

# List of Publications

2. **A. Chaves-Jimenez**, J. Guo, E.K.A. Gill , *Impact of dynamic coupling between relative orbit and attitude on the estimation of relative dynamics of spacecraft*, Acta Astronautica **152**, 891 (2018).

1. **A. Chaves-Jimenez**, J. Guo, E.K.A. Gill , *Impact of Atmospheric Coupling Between Orbit and Attitude in Relative Dynamics Observability*, Journal of Guidance Control and Dynamics **40**, 12 (2017).